THERMAL DESIGN CONSIDERATIONS FOR A SEASONALLY FROZEN CAPILLARY BARRIER DIVERSION COVER SYSTEM

A Thesis Submitted to the College of

Graduate Studies and Research

In Partial Fulfillment of the Requirements

For the Degree of Master of Science

In the Department of Civil and Geological Engineering

University of Saskatchewan

Saskatoon

By

Joel Timothy Steeves

PERMISSION TO USE

In presenting this thesis in partial fulfilment of the requirements for a Postgraduate degree from the University of Saskatchewan, I agree that the Libraries of this University may make it freely available for inspection. I further agree that permission for copying of this thesis in any manner, in whole or in part, for scholarly purposes may be granted by the professor or professors who supervised my thesis work or, in their absence, by the Head of the Department or the Dean of the College in which my thesis work was done. It is understood that any copying or publication or use of this thesis or parts thereof for financial gain shall not be allowed without my written permission. It is also understood that due recognition shall be given to me and to the University of Saskatchewan in any scholarly use which may be made of any material in my thesis.

Requests for permission to copy or to make other use of material in this thesis in whole or part should be addressed to:

Head of the Department of Civil and Geological Engineering
University of Saskatchewan
Engineering Building
57 Campus Drive
Saskatoon, Saskatchewan
Canada, S7N 5A9

ABSTRACT

Soil covers on mining waste are typically designed for temperate climates and often rely on fine-grained soils to limit net percolation. Mine sites in cold regions, such as Northern Canada, have limited fine-grained materials and have climates that reduce the effectiveness of designs utilized in more temperate climates. A new cover system that harnesses the cold climate and available coarse textured materials has been proposed. The cover system, a seasonally frozen capillary barrier diversion cover system, relies on the ability of frozen soils with high levels of water saturation, to divert infiltrating meltwater downslope and away from the underlying mine waste.

The thermal effects of flowing water on heat transfer in the frozen soil were studied in this research. The potential for early thaw due to the convection and conduction associated with water flow was examined through the use of a numerical model to simulate several case studies and cover geometries. Vertical forced convection was investigated through a case study of frozen column experiments. Lateral convection was investigated through a case study of a natural analogue at Wolf Creek, Yukon, while conduction was investigated through a case study of ponding water and increased conduction. Illustrative cover design models incorporated climate data and idealized materials from a representative mine site into several different geometries, each representing a potential thermal failure mode.

These simulations reveal that no one thermal process dominates in frozen soil. Lateral convection can dominate in sloped high hydraulic conductivity soil, given enough water is available to generate large lateral water flows. Under low flow conditions, the influence of lateral convection drops. Vertical convection will result when large amounts of water percolate vertically, causing greater thaw rates throughout the slope than by conduction alone. Conduction will occur regardless of water flow, but increased rates of conductive heat transfer can occur when water ponds on the ground surface, which results in increased rates of thaw leading to preferential infiltration of water below ponded areas. In finer layers of low hydraulic conductivity, conduction will always dominate, as water cannot achieve the flow rates necessary for convection to dominate. This research has shown that the proposed cover design is a viable

alternative to the current practice. Further modelling, laboratory and field studies are recommended for future research.

ACKNOWLEDGMENTS

A task of this undertaking is not accomplished by one person. There are many people who help out along the way. I wish to thank everyone that has made this research possible.

First and foremost, I would like to thank my supervisors, Dr. Lee Barbour and Dr. Grant Ferguson, for all their help, guidance and patience in seeing this project through to completion. I would like to thank the members of my committee Dr. Andrew Ireson, Bonnie Dobchuk and Mike O'Kane, along with my committee chairs Dr. Ian Fleming and Dr. Christopher Hawkes and external examiner, Dr. Cherie Westbrook. I would also like to thank my undergraduate thesis advisor, Dr. Masaki Hayashi, for nudging me toward the University of Saskatchewan in the first place and his continued guidance and expertise.

Additional thanks is due to Mike O'Kane for his support and guidance and for making the resources of O'Kane Consultants available to me. I also wish to thank the rest of the O'Kane Consultants crew, both in Saskatoon and Calgary, for providing a welcoming environment and place to work. Thanks also to GEO-SLOPE International Ltd. for providing access to their software and to Dr. Chris Kelln and Dr. Curtis Kelln for software technical support. Thank you also to Dr. Sean Carey for providing observational field data.

I also wish to thank my fellow graduate students for the discussions, conversations and insights they provided, specifically Mike Amos, Bryan Koehler, Kathryn Dompierre and Thomas Baer.

Finally, thanks to my family for all their support throughout my time in academia. I would not be where I am today without the financial and emotional support from my parents and the rest of my family. Thanks also to Josh Ramirez for his encouragement and for all those late nights editing page after page.

Financial support for this research was provided by the Natural Sciences and Engineering Research Council of Canada and O'Kane Consultants Inc. through the NSERC IPS program, additional support from O'Kane Consultants, the Saskatchewan Innovation and Opportunity Scholarship program, the Department of Civil and Geological Engineering at the University of

Saskatchewan and the estate of the late Mr. Russell William Haid. I greatly appreciate all the financial contributions that made this research possible.

TABLE OF CONTENTS

LIST OF TABLES

LIST OF FIGURES

1 INTRODUCTION

1.1 Background

The Canadian federal government, through the Northern Contaminated Sites Program of Indigenous and Northern Affairs Canada (INAC), has a current estimated liability of $1.7 billion for the cleanup of contaminated sites in the north (INAC 2010). In total, there are 114 sites awaiting remediation, many of which are abandoned mines. A cover system is an integral part of the closure and remediation of mine waste, generally designed and built to limit net percolation of water or to control oxygen ingress (MEND 1.61.5c 2012).

Mine closure designs in Northern Canada and other cold regions face several challenges that require a re-evaluation of the traditional methods of cover design developed primarily for more temperate environments. The soils in northern regions are often relatively immature, with soil development delayed by the cold climate, frost action and slow weathering (Tedrow and Cantlon 1958, Munroe and Bockheim 2001). Large volumes of highly weathered fine-grained material are scarce. Where this material does exist, it is heavily disturbed by cryoperturbation (Rykaart and Hockley 2010). Typical mine closure cover designs often rely on finer-grained soil to limit water movement or to store water for release back to the atmosphere by transpiration, thereby limiting the ingress of water into the underlying mine waste (MEND 1.61.5c 2012).

The majority of precipitation in northern climates and other cold regions falls as snow, which accumulates over the winter and is released by snowmelt. Melt occurs over a relatively short period of time in the spring, releasing large amounts of water from storage (Hayashi et al. 2003). This spring freshet is often the most significant hydrological event in cold climates (Marsh 1990), especially for cover design. This large influx can overwhelm the cover system, causing ingress and ultimately, failure (MEND 1.61.5c 2012).

A new cover design has been proposed to utilize the cold climate and the available coarser textured materials to maximize snowmelt runoff. The proposed design, a seasonally frozen capillary barrier diversion (SFCBD) cover (MEND 1.61.5c 2012), is made up of a high hydraulic conductivity surface layer overlying a finer textured layer, which itself overlies a coarser layer (Figure 1.1). The SFCBD cover system relies on creating elevated levels of saturation within one layer of the cover using conventional capillary barrier cover design methods (Morris and Stormont 1997, Stormont and Morris 1997), which, when combined with seasonal soil freezing, results in enhanced surface and near surface lateral flow.

A capillary barrier cover uses a slope and a textural difference between an overlying finer soil layer, such as fine sand, and an underlying coarser soil layer, such as gravelly sand, to create elevated levels of water saturation within the finer soil layer. A frozen, saturated soil has a lower hydraulic conductivity than an unfrozen soil, as the pores are occupied by ice, preventing water from flowing through (Kane 1980). The creation of a frozen, high saturation layer will act as a barrier to vertical flow, diverting infiltrating water downslope and away from the underlying mine waste. The ability of a frozen layer to divert water has been well documented in natural settings (Kane and Stein 1983, Granger et al. 1984, Kane and Chacho 1990, Hayashi et al. 2003, Bayard et al. 2005). The frozen barrier would only be active during the spring freshet. Upon thaw in early summer, the barrier would revert to a typical capillary barrier store and release cover (MEND 1.61.5c 2012).

In order to evaluate the potential performance of the SFCBD cover design it is important to identify and evaluate potential failures modes, particularly their likelihood of occurrence, their impact on the efficacy and limitations of the design, and the possibilities for design modification to reduce the likelihood of failure. Failure of a cover system is usually defined as a set percentage of net percolation based on site conditions, for example 10% net percolation. For this research, failure is considered to have occurred when the majority of meltwater percolates through the cover. This more lenient definition of failure is useful in this case due to the nature of the research being hypothesis testing of the SFCBD cover design rather than prediction of performance.

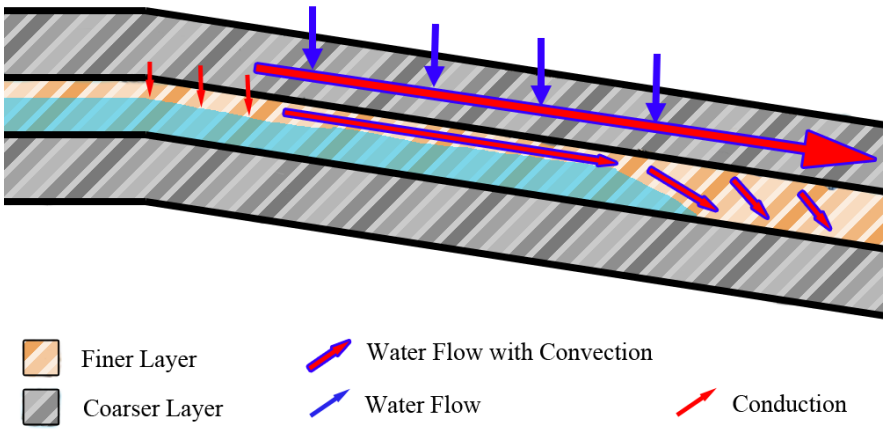

Figure 1.1 Schematic design of a SFCBD cover system showing the potential failure modes being investigated. Note that the blue region in the finer layer is representative of frozen soil.

Potential failure mechanisms for the proposed design would be the cracking of the finer layer and development of macropores and/or thawing of the frozen finer textured layer prior to diversion of the snowmelt water. This layer acts as the major barrier to net percolation during the spring snowmelt. Premature thawing of this layer could lead to water reaching the mine waste, generating contaminated effluent. Thaw of the cover system will occur as a result of conductive heat transfer but may also be influenced by some combination of conductive and convective heat transfer associated with migration of the snowmelt water. The addition of water to a soil increases the thermal conductivity and volumetric heat capacity of the soil, as water has a higher thermal conductivity and volumetric heat capacity than the soil grains and air. Water is also able to carry heat, allowing heat transfer to occur with water flow through convection. Convection, lateral and vertical, and conduction are the processes that will determine the success, or failure, of a SFCBD cover system.

1.2 Research Objectives

There are two main objectives associated with this research. The first is to determine the dominant thermal processes that are likely to have an influence on the performance of the cover

system, and consequently, are most critical to understand in the design of a SFCBD cover. The two most important processes are heat transport in response to temperature gradients (i.e. conduction) and heat transport with flowing water (i.e. convection). The aim of this study is to not only to determine which of these two heat exchange processes is dominant, but to also determine the relative importance of the non-dominant process.

The incorporation of a conventional capillary barrier design and frozen layer into the SFCBD cover system allows the current research to focus on thermal energy transfer within the cover system, as there are multiple functioning examples of the capillary barrier and natural examples of diversion by frozen layer, as noted above. As the focus of the current research is on the influence of the thermal processes on thaw and the interaction between the infiltrating meltwater and the frozen layer, this research focuses mainly on the spring freshet rather than the whole year.

The second objective is to determine the feasibility of designing a SFCBD cover designed with available materials and climatic conditions at a representative mine site in Northern Canada. The SFCBD cover is a newly proposed design that has not been tested. This study will evaluate the feasibility of constructing a SFCBD in the far north and will highlight the analyses required for design including identification of the critical properties that will need to be characterized through laboratory or field testing. It is the first step in establishing a new approach to the remediation of mine waste dumps in cold regions, specifically Northern Canada.

1.3 Scope

The scope of this project includes: the use of 1D and 2D numerical models to investigate coupled water and heat flow; typical, idealized, coarse texture materials and climate data available at a representative northern mine site; and practical cover geometries (e.g. thickness and length). The scope of this project does not include laboratory or field testing, 3D modelling or consideration of complex heterogeneity within constructed flow paths, including macropores.

1.4 Research Design

This research was carried out in phases and the thesis is divided into chapters based around each phase. The organization of the thesis and a description of each phase are summarized in this section.

Phase 1 – Literature Review and Model Benchmarking (Chapter 2 and Appendix)

The first phase of this research consisted of a literature search to identify potential modes of failure along with associated laboratory or field studies where data was available. This phase also included a review of related numerical models and their capabilities. Once GeoStudio was selected as the numerical model, benchmarking was undertaken to confirm the ability of the numerical model to accurately model the thermal processes of interest.

Phase 2 – Case Studies (Chapter 3)

The second phase of this research simplified three of the identified case studies to explore the dominant mechanisms of heat transfer based on numerical simulations of the case studies. Each case study was based around a previous study, allowing observational data to guide the numerical simulations. The first case study focused on vertical convection and was a simulation of the column experiments of Watanabe et al. (2013). The second case study focused on lateral convection and was a simulation of two slopes in the Wolf Creek basin and based on Carey and Woo (2001a, 2001b). The third case study focused on conduction and was a hypothetical example based on Hayashi et al. (2003). Results of each case study and a discussion are presented in Chapter 3.

Phase 3 – SFCBD Models (Chapter 4)

The final phase of this research incorporated the knowledge gained from the previous phases into three geometries of a SFCBD cover system at a representative mine site in northern Canada. Each SFCBD model and design was based around one thermal process that could cause failure. The first model utilized a steep slope, highlighting the potential for failure through lateral convection. The second model was a shallower slope, increasing the likelihood of failure through vertical convection. The final model was the same as the shallow slope model, but with a

depression in the middle of the slope to highlight potential failure through ponding and increased conduction. Results of each SFCBD model and a discussion of the results are contained in Chapter 4.

1.5 Publications

Portions of the work contained in the thesis, specifically the Wolf Creek case study (Section 3.3) have also been published as Steeves et al. (2016).

2 BACKGROUND

2.1 Introduction

The proposed design will couple transient, unsaturated, flow with thermal conduction and convection. In an unsaturated system, the volumetric water content and hydraulic conductivity are functions of the matric suction or the degree of saturation (Freeze and Cherry 1979, Jury and Horton 2004) and the thermal properties (thermal conductivity and specific heat) are functions of the degree of saturation (Johansen 1977, Krahn 2004a). The main objective of the cover system is to shed water from an unsaturated soil profile by generating interflow (lateral flow within the soil profile) as well as runoff.

During the spring freshet, some of the snowmelt will infiltrate into the frozen cover and be diverted by a layer of near saturated, frozen soil. Water flow within a frozen soil can influence the rate of heat transport and consequently the rate of thaw of the frozen soil (Kane and Stein 1983, Lunardini 1998, Kane et al. 2001). These processes are well documented in the literature for both laboratory and field settings. The literature describing some of the key processes controlling the behaviour of a SFCBD cover system are examined in this chapter.

2.2 Fundamental Physics

2.2.1 Water Flow in Unsaturated Soils

Water flow in the proposed cover will most likely occur under unsaturated conditions. This adds a layer of complexity due to the presence of two fluid phases in the soil; water and air. In an unsaturated soil, properties like hydraulic conductivity become a function of the negative pore-

water pressure or the degree of saturation. The proposed design takes advantage of these complexities and incorporates them into the functionality of the design.

The pore-water pressure within an unsaturated soil is negative and is often referred to in terms of matric suction, the differential air minus water pressures present within the soil pores. Flow in the unsaturated zone is governed mainly by two relationships: the relationship between volumetric water content and suction, referred to here as the water retention curve (WRC), and the relationship between hydraulic conductivity and suction. The volumetric water content varies from porosity at saturation to the residual water content (Freeze and Cherry 1979, Dingman 2008). At the residual water content it becomes increasingly difficult to reduce the water content of the soil through liquid water flow as the liquid phase becomes increasingly discontinuous (Jury and Horton 2004).

The shape of the WRC is determined by soil texture. Figure 2.1 shows the WRC for four different textured soils. Coarser grained soils are only able to store water at relatively lower values of suction since their large pores are more readily drained as suction increases (Fetter 2001). Finer grained soils, with smaller pores, remain saturated at higher suction values than coarser grained soils (Freeze and Cherry 1979, Schwartz and Zhang 2003). The suction required to initiate desaturation of the soil is often referred to as the air entry value (or height of capillary rise when suction is expressed as a pressure head). The amount of capillary rise is inversely proportional to the radius of the pore. Thus, smaller pores are able to retain water while larger pores drain (Fetter 2001).

In a saturated soil, all pores are filled with water, resulting in a constant hydraulic conductivity. As the suction increases, the volumetric water content decreases, with the larger, most conductive, pores draining first. The loss of these pores for water flow results in a reduction in the hydraulic conductivity of the soil (Jury and Horton 2004). Thus, the hydraulic conductivity is also a function of the matric suction, as shown in Figure 2.2.

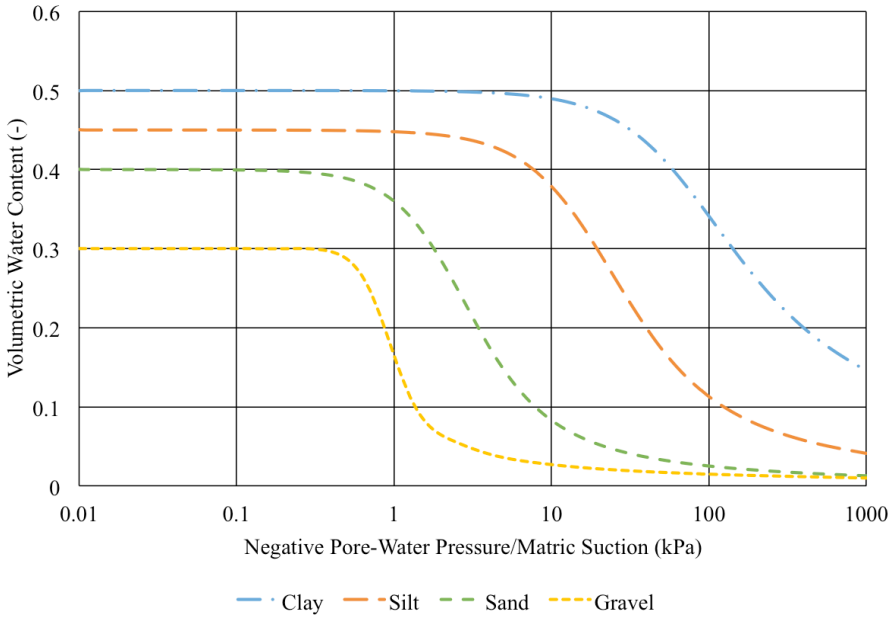

Figure 2.1 The water retention curve (WRC) for four different textured soils. The volumetric water content of the soil is a function of the matric suction due to capillarity (after Krahn 2004b).

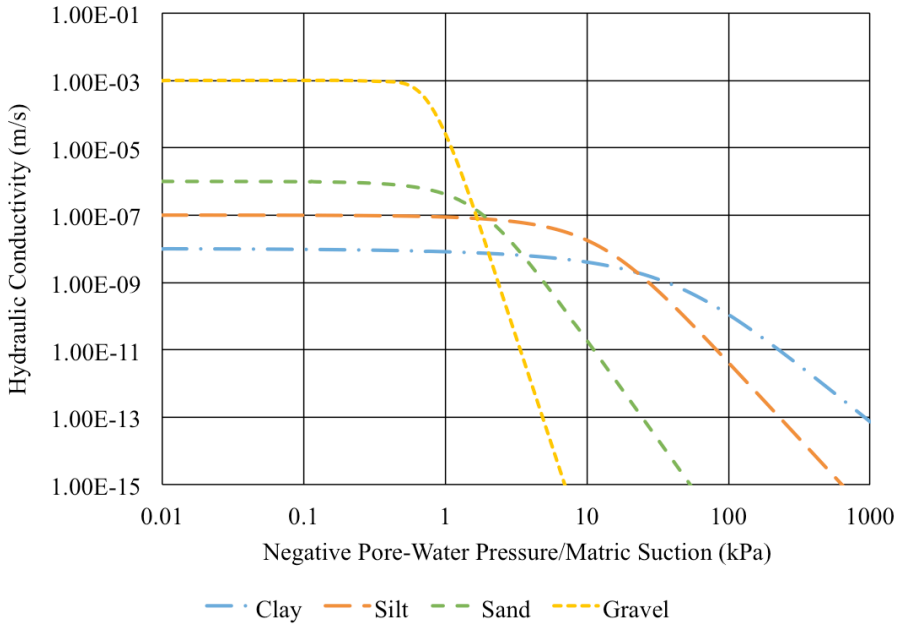

Figure 2.2 Hydraulic conductivity function for four different textured soils (after Krahn 2004b).

A capillary barrier design utilizes the differences in the WRC and hydraulic conductivity functions of two sloped layered soils to increase water storage. A capillary barrier is made up of finer textured material overlying a coarser textured material (Ross 1990, Morris and Stormont 1997, Stormont and Morris 1997, MEND 1.61.5c 2012). If the profile is drained, the lower, coarser textured soil will approach its residual water content at a relatively low value of suction. Since this suction is much lower than air entry value of the overlying finer soil, the finer soil will remain saturated. This enhanced water storage is available to plants to use through transpiration and can also enhance lateral drainage downslope.

Failure of the capillary barrier system due to breakthrough into the coarser layer will occur when the finer layer nears saturation as a result of infiltration into the profile or the accumulation of water downslope (Ross 1990). When this occurs, the suction at the base of the finer layer becomes less than the residual suction in the coarser layer and water movement into the coarser layer is initiated.

2.2.2 Infiltration and Percolation into a Frozen Soil

The infiltration of water into a frozen soil is a more complicated process than infiltration into an unfrozen soil due to the coupling that occurs between the heat and mass transfer processes and the related phase changes. At temperatures below freezing, some pore water remains unfrozen. The phase change of pore water occurs over a range of temperatures. The percentage of pore water that remains unfrozen at a given temperature is termed the unfrozen water content (UFWC) and is a function of the specific surface area of the grains and the freezing point depression (Anderson and Tice 1973). The specific surface area of a finer-grained soil is higher than that of a coarser-grained soil, causing higher UFWC at temperatures below the freezing point of bulk water (i.e. 0 ºC). Therefore, for a given volume of soil at a given temperature, the UFWC of a clay will be higher than a silt (Figure 2.3) and higher in the silt than in a sand (Kane and Chacho 1990).

Compared to an unfrozen soil, the infiltration rate into a frozen soil is typically reduced by an order of magnitude or more (Granger et al. 1984, Hayashi et al. 2003, Stähli 2006), resulting in an increase in the total runoff at the surface. The reduction in the infiltration rate is due to a

reduction in the hydraulic conductivity of the soil. Under freezing conditions, the water in the largest pores begins to freeze first (Kane and Chacho 1990). This preferential freezing of larger pores leads to a reduction in the hydraulic conductivity (Kane 1980). Water movement in the soil is then limited to the smallest liquid filled pores or to the thin film of unfrozen water that develops on the surface of the soil grains.

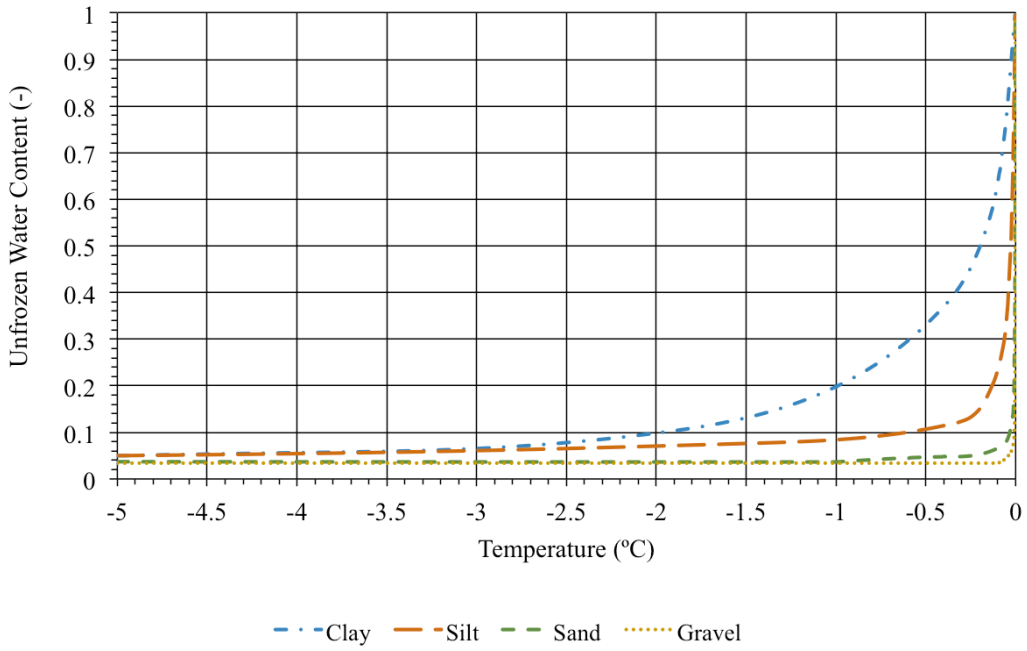

Figure 2.3 Unfrozen water contents of four different textured soils. The finer-grained soils have higher unfrozen water contents at lower temperatures. This is due to their higher specific surface areas (after Krahn 2004a).

Kane (1980) also found a link between the field total water content (both water and ice) and the infiltration rate. Soils with higher field water contents showed a lower infiltration rate. Over the winter, the freezing front propagates downward, reducing the unfrozen water content. A pressure gradient is also created, drawing water upwards toward the freezing front (Harlan 1973, Kane 1980, Kane and Stein 1983, Stähli et al. 1999, Hayashi et al. 2003). The accumulation of water near the freezing front results in higher water contents, leading to more pores being blocked with ice. Silty soils tend to have optimal properties for the migration of water to the freezing front since they have higher values of hydraulic conductivity than finer textured soils, such as a clay, but sufficient capillarity to enable water flow under negative pore pressure conditions. Soils with a higher unfrozen hydraulic conductivity and sufficient capillarity to promote flow under

negative pore pressures are able to transport greater amounts of water to the freezing front, increasing the water content and allowing more pore-ice development, and the concomitant reduction in the frozen hydraulic conductivity (Kane 1980).

Temperature can also play a role in determining the hydraulic conductivity of a soil. The viscosity of water is temperature dependent, increasing with colder temperatures (Davis and DeWiest 1966). Due to the increase in viscosity, the hydraulic conductivity of a colder saturated soil is reduced (Klock 1972 in Kane 1980). A temperature drop from 25 ºC to 0 ºC would reduce the saturated hydraulic conductivity by as much as one half (Klock 1972 in Kane 1980).

The rate of infiltration into a frozen soil is determined by a variety of factors, including the hydraulic and thermal properties of the soil. In a study of frozen Canadian Prairie soils, Granger et al. (1984) was able to group the soils into three classes based on infiltration and derive some common characteristics of each group. Soils of the unlimited class showed little to no impedance to infiltration, despite being frozen. These soils were highly organic or severely cracked soils with large macropores, allowing most, if not all, of the snow meltwater to infiltrate. The soils of the restricted class experienced little to no infiltration under frozen conditions as a result of the presence of a low hydraulic conductivity ice layer at or near the surface. Soils of this class have a high runoff potential, as the meltwater will either runoff or evaporate. Infiltration into soils of the limited class was found to be a function of the initial soil water content and the snow water equivalent (Gray et al. 1985). A higher initial soil water content resulted in more blocked pores, and therefore, less infiltration.

Soil column laboratory experiments conducted by Watanabe et al. (2013) showed that infiltration into a frozen soil occurs in three phases. The study compared infiltration into three frozen columns of volcanic ash at differing initial water contents. The columns were thermally equilibrated with an air temperature of 3.5 ºC and then exposed to a surface temperature of -2 ºC for 48 hours, resulting in freezing of the soil near the top of the column. After 48 hours of freezing conditions, 3.5 ºC water was applied to the top of the columns and infiltration was monitored over the next 48 hours.

Three phases of infiltration were observed. Very little infiltration occurred in the first phase in which the upper portion of the soil profile remained frozen. The small amount of water that did

infiltrate froze and created an ice layer at or near the surface limiting further infiltration. This process was also observed in agricultural fields by Baker and Spaans (1997).

After the development of a surface ice layer, water began to pond on the surface of the column (Watanabe et al. 2013). Once the soil had warmed to a temperature of 0 ºC, water and ice coexisted in the soil and the second phase of slow infiltration began. As the soil thawed, water began to infiltrate and moved through pores occupied by unfrozen water and air. This phase had a reduced infiltration rate, which was approximately 10% of the non-frozen rate. The third phase began when the wetting front had fully penetrated the frozen layer. A sudden increase in the infiltration rate was observed, approaching that of a non-frozen soil. The column showed an increase in the liquid water content and a decrease in ice content.

The columns with higher initial moisture contents experienced longer first and second phases. In the first phase, the higher initial water content resulted in a more pronounced ice layer, delaying infiltration. The higher initial water contents were also responsible for higher ice contents, which reduced the hydraulic conductivity, thereby increasing the length of the second phase (Watanabe et al. 2013).

The ability of a frozen layer to divert water has been well observed in nature. Pore-ice acts an impermeable boundary and prevents water from infiltrating into a frozen soil. If the frozen soil is near the surface, surface runoff will occur. If the pore-ice occurs at depth, subsurface interflow will result. In the Canadian Prairies, ice layers have been observed at or near the surface, impeding the infiltration of snowmelt and causing large amounts of surface runoff (Hayashi et al. 2003). Meltwater was then directed downslope and collected in depressions before finally infiltrating into the soil. In depression-focused recharge regimes, infiltration through the frozen soil represents less than 20% of the total snow water equivalent (Baker and Spaans 1997), indicating the potential for most of the snowmelt to be diverted under the right conditions.

In northern Canada, this phenomenon has been observed to exert a large control on the hydrology of some subalpine catchments. In studies within the Wolf Creek basin, Yukon, undertaken by Carey and Woo (1999, 2001a, 2001b), ice-rich mineral soils on the north, east and west slopes prevented infiltration, resulting in a perched saturated zone and lateral downslope flow in the organic-rich layer overlying a mineral soil. The ratio of runoff to snow water

equivalent (SWE) for the north-facing, east-facing and west-facing slopes was 0.8, 0.6 and 0.25, respectively. In contrast, the south slope had a low ice content and no organic-rich layer, allowing the infiltrating snowmelt to percolate unimpeded to the water table several metres below the surface with no runoff being generated.

The same phenomenon has also been observed at two sites in the Swiss Alps, where runoff and infiltration was tracked over two winter seasons (Bayard et al. 2005). The two winter seasons differed in that the first had an early snow and large amounts of precipitation throughout the winter, and the second experienced little snowfall except at the end of the season. The second winter had periodic melt events and significant accumulation of snow during the snow ablation period. In the first winter, the soil did not freeze at either site, due to the early snow accumulation. In the second winter, the lack of snow accumulation allowed for a deep soil frost. During the first winter, 90-100% of the snowmelt infiltrated, while during the second winter, 25-35% of the snowmelt was diverted laterally in the late winter and spring snowmelt by a basal ice sheet. The formation of the basal ice was caused from the mid-winter melt events.

Iwata et al. (2010) observed a similar relationship to snow cover in measurements of runoff from frozen soils in Japan. The paired plot experiment involved removing the snow cover from a treatment plot, while the control plot was left undisturbed. Soil under the control plot froze to a depth of 0.11 m, while the soil under the treatment plot froze to a depth of 0.43 m. A rain event during the winter caused an increase in the liquid water content below the frozen soil of the control plot. No increase was observed on the treatment plot, indicating the deep soil frost had prevented infiltration of the rainwater. Snowmelt caused a rapid increase in the liquid water content at all depths of the control plot, but increases in liquid water content under the treatment plot were slower. All of the snowmelt infiltrated into the control plot, but surface runoff was generated on the treatment plot. The plot-scale runoff ratio for the treatment plot was 0.22 and 0 for the control plot. Iwata et al. (2010) attributed the difference in runoff ratio to the difference in soil frost depth. The deeper soil frost of the treatment plot generated runoff and prolonged ground thaw relative to the control plot, in which no runoff occurred.

These natural analogues highlight how the presence of soil frost/ice can influence the soil's runoff regime. Soil frost reduces the hydraulic conductivity, which reduces the infiltration into

the soil. Ponding, surface runoff or interflow can be generated above the frozen layer due to the reduced infiltration rates.

2.2.3 Heat Flow in Unsaturated Soils

Heat transfer within a soil occurs through two main processes: conduction and convection. Heat transfer through conduction occurs when a temperature gradient exists in the soil. Heat is transferred from areas of high temperature to areas of low temperature. This occurs through all phases present in the soil: water, air, ice, and the soil grains themselves. This process is considered to be the dominant heat transfer mechanism occurring within a soil.

Smerdon et al. (2003) reconstructed two decades of surface air and subsurface temperature records for Fargo, North Dakota and showed that the propagation of the temperature signal into the soil follows the theoretical conduction simulation quite closely. Further research at multiple locations in the United States and one in Switzerland showed that the same propagation could be attributed to one-dimensional conduction (Smerdon et al. 2004).

While the assumption that conduction dominates often holds true, the addition of flowing water to a system can increase the role of convection. Two types of heat convection can occur in the fluid phase of a soil (Anderson 2005). The first type, free convection, is driven by temperature-induced density differences in the fluid. For this study, free convection was considered to be negligible, as the temperature differences, and the resulting density differences, in a thawing soil are not large enough to drive large amounts of heat transfer.

The second type is forced convection and is the only type of convection considered in this research. In this case, water flow occurs as a result of hydraulic gradients and heat is transported with flowing water (Anderson 2005). A dimensionless Peclet number can be used to determine the relative importance of forced convection with respect to conduction. It is defined as the ratio of convective heat transport to conductive heat transport (van der Kamp and Bachu 1989). A Peclet number greater than one is indicative of an environment dominated by convection, while a Peclet number less than one is indicative of an environment dominated by conduction. For groundwater-induced convection, the Peclet number (P_e) can be found by:

$$P_e = \frac{p_w c_w q l r}{k_m} \tag{2.1}$$

where ρ_w is the density of water (kg/m^3), c_w is the specific heat of water (kJ kg^{-1} K^{-1}), q is the specific discharge (m/s), l is the length scale (m), r is a length-scale ratio (-) and κ_m is the thermal conductivity of the soil (J s^{-1} m^{-1} K^{-1}) (Kane et al. 2001). This definition of the Peclet number differs from other Peclet numbers, such as the definition presented in Ferguson (2014) or the multiple definitions presented in van der Kamp and Bachu (1989), in that it incorporates a length-scale ratio, r. This allows for the comparison of convection and conduction that occur over different length scales, such as lateral convection to vertical conduction in a slope. Setting this value to 1 yields the definition presented in Ferguson (2014).

The definition of Peclet number in Equation 2.1 uses the length-scale, along with the length-scale ratio, in place of the characteristic length of other definitions. The length-scale is the order of magnitude of the length of the slope, while the length-scale ratio is the ratio of the length of interest for conduction to the length of interest for convection. Kane et al. (2001) defines these lengths as the height of the soil layer and the length of the slope, respectfully.

In reviewing geothermal systems, Ferguson (2014) found that convection began to be important in the range of Peclet numbers from 0.4 to 5.1. Despite the Peclet numbers larger than 1 at some sites, no noticeable convection was occurring. At lower values, convection may still be noticeable, but not likely important. For example, taking 0.4 as a conservative value at which convection becomes important, and using a typical well spacing of 7 to 8 m would result in a system in which heat flow can no longer be assumed to be due to conduction alone if the specific discharge was greater than 10^{-8} m/s (Ferguson 2015). These values were calculated for geothermal systems and may not be directly applicable to cover systems due to the differences in the geometry of the two problems.

2.2.4 Heat Transport in Frozen Soils

Previous studies have investigated conduction and convection in thawing frozen soils. Nixon (1975) compared vertical convection, through migration of meltwater to the soil surface, with conduction and found that the effects of convection could be neglected.

In the Imnavait Creek watershed, Alaska, Kane et al. (2001) found that for vertically infiltrating snowmelt into a frozen layer, the Peclet number was approximately 0.25 for the organic-rich soil and only 0.12 for a mineral soil. Comparing horizontal convection to vertical conduction, the Peclet number was an order of magnitude lower at 0.04 for the organic-rich soil and two orders of magnitude lower at 0.001 for the mineral soil.

Lunardini (1998) determined that vertical convection is likely to be insignificant compared to conduction if the water flux in a thawing soil is proportional to the thaw rate. This is the case when no external water is added and the water flux in the soil is from previously frozen pore water. When additional water is added to the system, such as infiltration/percolation, the effect of vertical convection can become significant. Lateral flows of released pore water at the same velocity as the vertical flow described above are half as influential as vertical convection (Lunardini 1991).

Water infiltrating into a frozen soil has the potential to freeze due to the sub-zero temperatures of the soil. The infiltration of meltwater at a temperature of 0 ºC into frozen soil at 0 °C is a special case. Since the ice and water are in equilibrium and can coexist in the soil together (Kane and Stein 1983), very little thawing of the soil will occur, regardless of the amount of ice or water present. This isothermal phase is termed the zero-curtain. Above the freezing point, the soil would begin to thaw, consuming energy for phase change while soil below the freezing point could cause the meltwater to freeze.

During refreezing, the change of state from liquid water to ice releases latent heat to the surrounding soil, which can either be conducted downward to colder soil, conducted upwards toward a cooling surface like the ground surface at night, or increase the heat content of the local soil (Baker and Spaans 1997). An increase in the local heat content can rapidly bring the soil up to 0 ºC and release frozen pore water or be transported away with any water flow (Zhao et al.

1997). This can have the effect of increasing the role of convective transport by an order of magnitude (Kane et al. 2001).

Ice accumulation due to refreezing will occur when the transport of heat away from the zone of refreezing is equal to the transport of heat with percolating water to the zone of refreezing (Baker and Spaans 1997). If the transport of heat to the refreezing zone decreases relative to the heat transport away, freezing will be directed upwards. If the heat transport to the refreezing zone increases relative to the transport away, such as an increase in convection or conduction, then remelting and downward and/or lateral water flow will occur (Baker and Spaans 1997).

The presence of water also increases the potential conduction. The thermal conductivity and volumetric heat capacity of a soil increases as the water content increases, as seen in Figure 2.4 and Figure 2.5. The ratio of thermal conductivity to volumetric heat capacity is termed the thermal diffusivity and is a measure of the rate of transmission of a temperature change in a material. A saturated soil has a higher thermal diffusivity than a dry soil and will therefore, increase in temperature more rapidly than a dry soil (Andersland and Ladanyi 1994). The thermal diffusivity of ice is higher than water, meaning that a saturated frozen soil will increase in temperature more rapidly than an unfrozen soil (Andersland and Ladanyi 1994).

Ponded water on the surface traps more solar radiation and transmits it to the ground below (Hayashi et al. 2003). In this case, common to the Canadian Prairies, snow meltwater was prevented from infiltrating due to the presence of ice in the soil (van der Kamp et al. 2003, Hayashi et al. 2003). The meltwater was diverted as overland flow, collecting to topographic depressions. Temperature measurements under the depression showed a thawing front that progressed at 40 mm/day. Progression of the thawing front on the uplands, stubble fields outside of the depression and standing water, was slower than under the depression. Hayashi et al. (2003) attributed this to the differences in surface albedo between the two surfaces and the large heat content of the standing water. Stubble field has a surface albedo of ~12-30%, while standing water has a surface albedo of ~3-10% (Jury and Horton 2004). Thus, the stubble will reflect more solar radiation, while the standing water will absorb it.

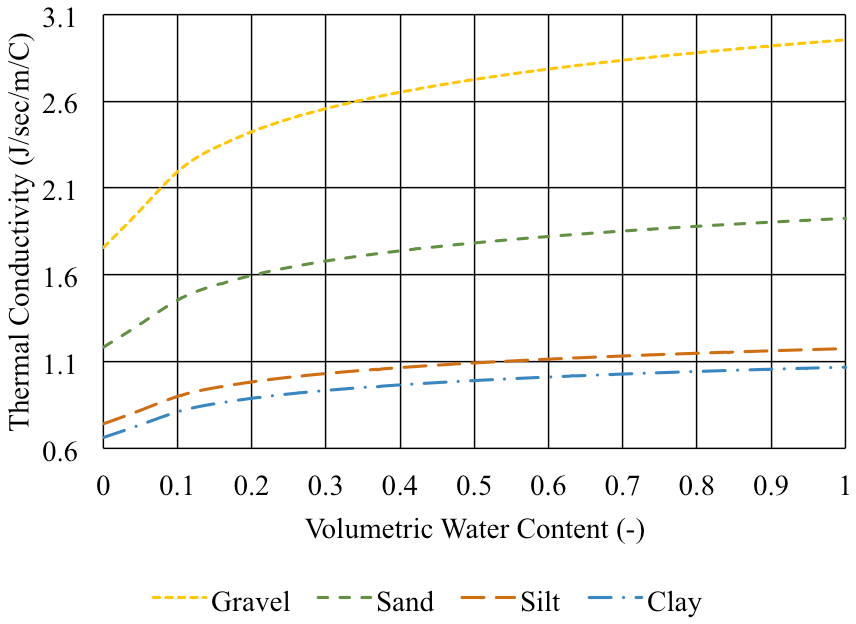

Figure 2.4 Thermal conductivity as a function of volumetric water content for four different textured soils (after Krahn 2004a).

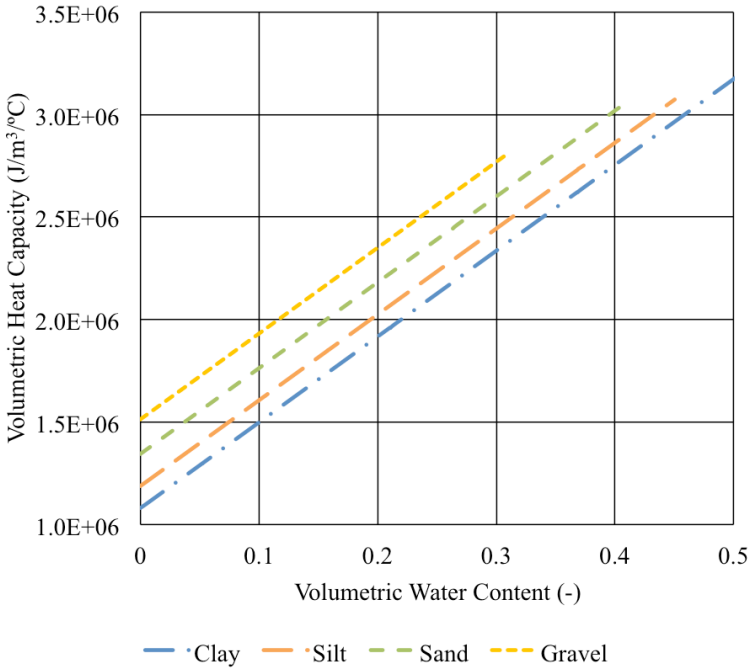

Figure 2.5 Volumetric heat capacity as a function of volumetric water content of four different textured soils (after Krahn 2004a).

2.3 Numerical Models

A number of numerical models have been developed to investigate the hydrologic processes occurring in cold regions. Several of the models are one-dimensional only, making their applicability limited within the current work. Hansson et al. (2004) modified the HYDRUS-1D model to simulate one-dimensional frozen column laboratory experiments. The SHAW (Flerchinger 2000) and COUP (Jansson and Karlberg 2004) models are also one-dimensional models of heat and mass transport and can take into account surface features, such as snow and vegetation, which can influence the surface energy flux. The COUP model can also account for the advection of heat by groundwater flow. The capabilities of the 1D models are summarized in Table 2-1. The current research was carried out primarily in two dimensions, limiting the use of one-dimensional models to comparison and benchmarking.

Table 2-1 Model capabilities of the one-dimensional coupled water and heat transfer models.

Capability Required	**HYDRUS-1D** (Hansson et al. 2004)	**SHAW** (Flerchinger 2000)	**COUP** (Jansson and Karlberg 2004)
1D/2D	1D	1D	1D
Unsaturated Flow	Unsaturated Only	Variable Saturation	Variable Saturation
Heat Transport	Conduction and Convection	Conduction and Convection	Conduction and Convection
Additional Features	-	Snow and Vegetation	Snow and Vegetation
Availability	Free Online	Free Online	Free Online

A variety of two and three-dimensional models that couple heat transport and water flow are available. The STOMP model (White and Oostrom 2000) was designed for multiphase flow in the subsurface and includes the freezing and thawing of porewater in three dimensions. McKenzie et al. (2007) developed the SUTRA-ICE model as a variation of the SUTRA model (Voss and Provost 2010) that includes freezing and thawing of the soil in three dimensions, but is limited to fully saturated freeze/thaw conditions and cannot account for unsaturated flow in the frozen condition. The numerical solution of Dall'Amico et al. (2011) to energy and mass transport, specifically freezing and thawing, in both saturated and unsaturated soils has been incorporated into the distributed 3D hydrological GEOtop model. The commercially available,

2D GeoStudio suite (Krahn 2004a, 2004b), which includes modules Temp/W and Seep/W, can also simulate the freezing and thawing of a soil. Temp/W and Seep/W can be used independently, but can also be coupled together to model thermal energy transfer and water flow. The GeoStudio suite can model both saturated and unsaturated soils. The WIT model, developed by Daanen et al. (2007), is similar to the HYDRUS-1D model developed by Hansson et al. (2004), but the WIT model is 3D, variably saturated and links the ice content to the temperature of the soil. The MarsFlo model (Painter 2011) was developed to model and study past and present hydrological conditions on Mars. It can model the interactions between three phases (liquid, ice and vapour) and includes vapour transport processes and phase changes between liquid and vapour for one gas species. Although it was designed for simulations of Mars, it can be used for Earth applications. The capabilities of the 2D and 3D models are highlighted in Table 2-2 and

The commercial finite element software, GeoStudio™ (GEO-SLOPE International Ltd 2014) was chosen as the numerical model to be used for this research based on a comparison of the various models described in the literature. The two key modules of the GeoStudio modelling package that were used in this work included the thermal model (Temp/W) and the water flow model (Seep/W). Both of these models can be run independently (e.g. thermal conduction, steady state or transient water flow) or they can be coupled to simulate forced convection as well as conduction. Temp/W also has the ability to simulate the surface energy balance associated with energy transfer between the atmosphere and the soil surface. The Land-Climate Interaction (LCI) condition in GeoStudio is able to solve the ground energy balance equation for the thermal heat flux and apply it to the simulation domain. This condition takes air temperature, wind speed, net or solar radiation and albedo as inputs. Vegetation height, evaporation and snow depth can also be taken into account, but are not required to solve the energy balance equation.

Table 2-3.

Table 2-2 Model capabilities of the three-dimensional coupled water and heat transfer models STOMP, SUTRA-ICE and GeoTOP.

Capability Required	**STOMP** (White and Oostrom 2000)	**SUTRA-ICE** (McKenzie et al. 2007)	**GeoTOP** (Dall'Amico et al. 2011)

1D/2D	3D	3D	3D
Unsaturated Flow	Variable Saturation	Saturated Only	Variable Saturation
Heat Transport	Conduction and Convection	Conduction and Convection	Conduction and Convection
Additional Features	Multiphase	-	Complex Topography
Availability	Research/ Commercial	Research/Not Available	Open Source

The commercial finite element software, GeoStudio™ (GEO-SLOPE International Ltd 2014) was chosen as the numerical model to be used for this research based on a comparison of the various models described in the literature. The two key modules of the GeoStudio modelling package that were used in this work included the thermal model (Temp/W) and the water flow model (Seep/W). Both of these models can be run independently (e.g. thermal conduction, steady state or transient water flow) or they can be coupled to simulate forced convection as well as conduction. Temp/W also has the ability to simulate the surface energy balance associated with energy transfer between the atmosphere and the soil surface. The Land-Climate Interaction (LCI) condition in GeoStudio is able to solve the ground energy balance equation for the thermal heat flux and apply it to the simulation domain. This condition takes air temperature, wind speed, net or solar radiation and albedo as inputs. Vegetation height, evaporation and snow depth can also be taken into account, but are not required to solve the energy balance equation.

Table 2-3 Model capabilities of the two and three dimensional coupled water and heat transfer models GeoStudio, WIT and MarsFlo.

Capability Required	**GeoStudio** (Krahn 2004a, 2004b)	**WIT** (Daanen et al. 2007)	**MarsFlo** (Painter 2011)
1D/2D	2D	3D	3D
Unsaturated Flow	Variable Saturation	Variable Saturation	Variable Saturation
Heat Transport	Conduction and Convection	Conduction and Convection	Conduction and Convection
Additional Features	Surface Energy Balance	Differential Surface Insulation	Vapour Phase
Availability	Commercial	Research/Not Available	Research/Not Available

Darcy's Law forms the basis of water flow in Seep/W under both saturated and unsaturated conditions and is defined as:

$$q_w = -k_w \frac{\partial h}{\partial x} \tag{2.2}$$

where q_w is the specific discharge (m/s), k_w is the hydraulic conductivity (m/s), h is the hydraulic head (m) and x is the distance (m). The hydraulic conductivity and the hydraulic head are based on constant fluid properties, including temperature-dependent viscosity and density, unless specified within the analysis in GeoStudio. In unsaturated conditions, the hydraulic conductivity becomes a function of the matric suction. This function is defined as part of the GeoStudio analysis, allowing Darcy's Law to be applied in unsaturated conditions. Two-dimensional seepage in Seep/W is governed by the partial differential equation (Krahn 2004b):

$$\frac{\partial \theta}{\partial t} = \frac{\partial}{\partial x}\left(k_{wx} \frac{\partial h}{\partial x}\right) + \frac{\partial}{\partial y}\left(k_{wy} \frac{\partial h}{\partial y}\right) + Q_w \tag{2.3}$$

where h is the total head (m), k_{wx} is the hydraulic conductivity in the x-direction (m/s), k_{wy} is the hydraulic conductivity in the y-direction (m/s), Q_w is the applied boundary flux (m^3/s), θ is the volumetric water content (m^3/m^3) and t is time (s).

Fourier's Law is the thermal analogue of Darcy's Law and is used to determine the conductive heat flux in Temp/W:

$$q_h = -\kappa \frac{\partial T}{\partial x} \tag{2.4}$$

where q_h is the heat flux (W/m^2), κ is the thermal conductivity (W m^{-1} K^{-1}), T is the temperature (K) and x is the distance (m). Conductive heat flow is governed by the partial differential equation (Krahn 2004a):

$$\lambda \frac{\partial T}{\partial t} = \frac{\partial}{\partial x}\left(\kappa_x \frac{\partial T}{\partial x}\right) + \frac{\partial}{\partial y}\left(\kappa_y \frac{\partial T}{\partial y}\right) + Q_h \tag{2.5}$$

where T is the temperature (K), κ_x is the thermal conductivity in the x-direction (W m^{-1} K^{-1}), κ_y is the thermal conductivity in the y-direction (W m^{-1} K^{-1}), Q_h is the applied boundary flux (J/s), λ is the capacity for heat storage (J m^{-3} K$^{-1)}$ and t is time (s). The heat capacity storage, λ, is a function of the material's volumetric heat capacity and the latent heat associated with a phase change. Defined mathematically, it is:

$$\lambda = c + L\frac{\partial w_u}{\partial T} \tag{2.6}$$

where c is the volumetric heat capacity of the material (J m^{-3} K^{-1}), L is the latent heat of water (J/m^3), w_u is the total unfrozen water content (m^3/m^3) and T is the temperature (K). The second term in Equation 2.6 represents the rate of change of latent heat.

The governing differential equations for Temp/W and Seep/W state that the difference between the flux into and out of the system is equal to change in storage of the system. Under steady state conditions, the flux into the system is equal to the flux out of the system and both equations can be simplified by setting the left side of the equation to zero. Equation 2.3 and Equation 2.5 become, respectively:

$$0 = \frac{\partial}{\partial x}\left(k_{wx} \frac{\partial h}{\partial x}\right) + \frac{\partial}{\partial y}\left(k_{wy} \frac{\partial h}{\partial y}\right) + Q_w \tag{2.7}$$

$$0 = \frac{\partial}{\partial x}\left(\kappa_x \frac{\partial T}{\partial x}\right) + \frac{\partial}{\partial y}\left(\kappa_y \frac{\partial T}{\partial y}\right) + Q_h \tag{2.8}$$

GeoStudio requires an unfrozen water content function be defined for each material. The total unfrozen water content can then be defined as:

$$w_u = W_u w \tag{2.9}$$

where w_u is the total unfrozen water content (m^3/m^3), W_u is the proportion of unfrozen water (between 0 and 1) and w is the volumetric water content of the material (m^3/m^3). Substituting Equations 2.6 and 2.9 into Equation 2.5 gives the complete governing partial differential equation for conductive heat transport (Krahn 2004a):

$$\left(c + Lw\frac{\partial W_u}{\partial T}\right)\frac{\partial T}{\partial t} = \frac{\partial}{\partial x}\left(\kappa_x \frac{\partial T}{\partial x}\right) + \frac{\partial}{\partial y}\left(\kappa_y \frac{\partial T}{\partial y}\right) + Q_h \tag{2.10}$$

Heat flow driven by forced convection couples heat transport to water flow and is governed in the coupled Temp/W and Seep/W by the differential equation (Krahn 2004a):

$$\left(\rho_s c_{ps} + L\theta_w \frac{\partial \theta_w}{\partial T}\right)\frac{\partial T}{\partial t} = \frac{\partial}{\partial y}\left[K_t \frac{\partial T}{\partial y}\right] + c_{pa}\frac{\partial\left(m_a T\right)}{\partial y} + \rho_w c_{pw}\frac{\partial\left(q_w T\right)}{\partial y} + Q \tag{2.11}$$

where $\rho_s c_{ps}$ is the volumetric heat capacity of the soil (J m^{-3} K^{-1}), $c_{pa/w}$ is the mass specific heat of air or water (J kg^{-1} K^{-1}), m_a is the mass flow rate of air (kg/s), $\partial\theta_w/\partial T$ is the slope of the unfrozen water content (K^{-1}), q_w is the specific discharge of water (m/s), Q is the thermal and hydraulic boundary flux (J/s and m^3/s, respectfully) and L is the latent heat of water (J/m^3). The term on the

left represents the changes in the sensible and latent heat contents. The first term on the right represents conductive heat transport, while the second and third represent convective heat transport.

The governing equations of many other coupled models are similar to those of GeoStudio. The one-dimensional models SHAW, modified HYDRUS-1D and COUP use slightly different expanded versions of Equation 2.11 that include the latent heat of vaporization (Flerchinger 2000, Hansson et al. 2004, Jansson and Karlberg 2004). Evaporation is not explicitly included in every GeoStudio analysis, but can be included through the application of soil-vegetation-atmosphere transfers coupled to a surface energy balance. All three one-dimensional models use a finite difference method to solve the governing equations. The modified HYDUS-1D model mixes the finite element method with finite difference however.

The governing equations of STOMP (White and Oostrom 2000) and MarsFlo (Painter 2011) are quite similar to each other and to Equation 2.11. The STOMP model, however, was designed for multi-phase flow and includes terms for non-aqueous phase liquids. Both models use the integral volume finite difference method to discretize the governing equations. The WIT model (Daanen et al. 2007) is similar to the modified HYDRUS-1D model, but uses the volumetric water content and links the ice content to the temperature of the soil. It uses a mid-point finite difference (or mixed finite element) approach to solve the system of equations.

The finite-element SUTRA-ICE model (McKenzie et al. 2007) requires full saturation in the soil, allowing only water or ice to fill the pores. The governing equations are written in expanded form and in terms of porosity, saturation of water and saturation of ice, instead of the volumetric and unfrozen water contents. The SUTRA-ICE equations also include terms relating to energy sources in the fluid and in the solid grains.

The governing equations of Temp/W and Seep/W are consistent with the other coupled models available. Benchmarks of the coupled and uncoupled Temp/W and Seep/W were carried out against analytical and semi-analytical solutions, along with other numerical models, to ensure that the GeoStudio modules were capable of accurately modelling the processes involved. The methodology and results of each benchmark test are contained in the Appendix.

3 CASE STUDIES

3.1 Introduction

The research undertaken in this study involved three phases of numerical modelling including; benchmark testing of the model capabilities, simulation of existing case histories taken from the literature and finally application of model to a virtual cover design scenario.

In the first phase, the capability of the GeoStudio models to replicate a range of flow and heat transport problems was assessed by comparing the performance of the numerical models to known analytical, semi-analytical or numerical cases from the literature. The results from this first phase of benchmark testing are presented in the Appendix. The second phase of the modelling program, presented in this chapter, investigated the relative influence of forced convection and conduction on rates of ground thaw based on a re-analyses of three different case histories from the literature. The final phase of the modelling study is presented in Chapter 4. In this final phase, the lessons learned from these case studies are applied in an illustrative series of models meant to replicate the conditions that might be present for a SFCDB constructed on mine waste.

The case studies simulated in this phase were chosen as analogues to the processes that will be occurring and could influence the performance of a SFCBD cover. Each case study highlights one thermal process that could result in failure of the cover system. The first is that of rapid infiltration into an unsaturated, frozen soil profile under controlled laboratory conditions (Watanabe et al. 2013). The second explored the mechanisms of runoff and ground thaw observed for a set of natural slopes at the Wolf Creek Watershed in the Yukon by Carey and Woo (1998, 2001a, 2001b). The final set of simulations were

used to evaluate the mechanism of preferential thaw proposed by Hayashi et al. (2003) in which the formation of ponded water during snowmelt leads to accelerated thawing and subsequently focused infiltration through previously frozen soils.

The laboratory column experiments focused on the potential of vertical convection to cause increased thaw and failure. The Wolf Creek simulations focused on the effect of lateral convection on thaw and the ability to generate lateral diverted water flow above a frozen layer. The ponded water simulations explored the potential of increased conduction leading to accelerated thaw and preferential infiltration. The case studies also provided another opportunity to compare the numerical model to laboratory and field data in cases involving multiple processes.

3.2 Failure Through Vertical Convection

3.2.1 Introduction

Failure of a SFCBD cover could potentially occur through premature thawing due to the vertical convection of energy into the cover. This mechanism was investigated by modelling the soil column experiments of Watanabe et al. (2013). One of the columns was modelled as a benchmark for GeoStudio and is summarized in the Appendix. The goal of the models presented in this section is to investigate the effect of vertical convection when thawing a frozen soil.

In the column experiments of Watanabe et al. (2013), three columns of volcanic ash soil at different initial water contents were subject to freezing conditions for a period of 48 hours. During this time, a frozen layer developed in the upper half of the columns, with its thickness dependent on the initial water content. After 48 hours, the freezing conditions were replaced by positive temperature conditions and 3.5 ºC water was added to the top of the columns.

In all columns, three phases of infiltration were observed (Watanabe et al. 2013). During the first phase, the infiltrating water froze at or near the surface of the column due to the sub-zero soil temperatures. The formation of an ice layer prevented further infiltration

and caused water to pond on the column surface. During the second phase, the soil temperature reached 0 ºC, allowing water and ice to coexist in the soil. Water from the surface slowly infiltrated through the frozen layer at a fraction of the unfrozen infiltration rate. After water penetrated the frozen layer, the third phase began and the frozen infiltration rate increased until it approached the rate for unfrozen soil. The columns with the higher initial water contents experienced longer first and second phases.

3.2.2 Model Setup

3.2.2.1 Domain

The model was setup to replicate the column used by Watanabe et al. (2013) in one dimension. The experimental column had a height of 35 cm and an inner diameter of 7.8 cm. The 1D model column domain is shown in Figure 3.1A. The model represented a one-dimensional version of the two-dimensional experimental column, shown in Figure 3.1B.

The timing of the model was set to match the timing used in the original experiments. A steady state condition was first used to set the initial temperature conditions and water contents. The freezing condition was then applied for 48 hours in a transient analysis. The surface temperature condition and infiltration occurred during the next 48 hour transient analysis.

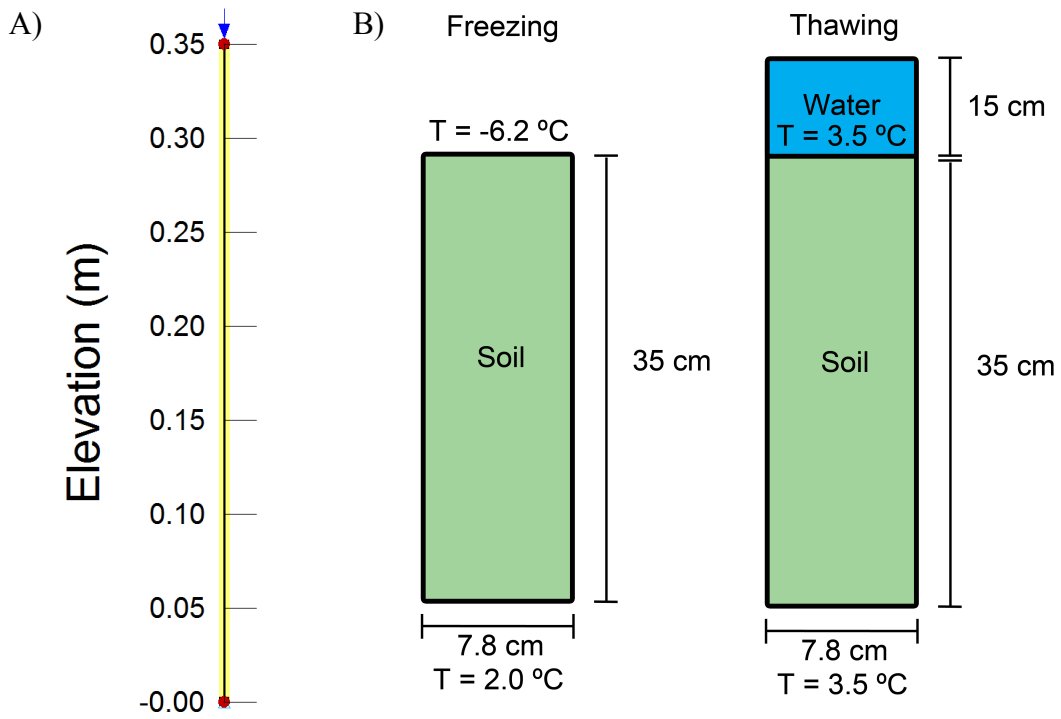

Figure 3.1 Model domain of the vertical convection simulations (A). The column is a one-dimensional representation of the column used by Watanabe et al. (2013), shown in (B).

3.2.2.2 Material Properties

The soil properties were similar to those described by Watanabe et al. (2013) and typical properties for a volcanic ash soil. Watanabe et al. (2013) used samples from the A horizon of the volcanic ash soil at a Japanese experimental field site, which had a bulk density of 1.18 g/cm^3. The hydraulic conductivity ranged from 5.8 x 10^{-7} m/s to 4.6 x 10^{-6} m/s and the texture of the soil was that of a silt loam (Iwata et al. 2008).

The water retention curve was specified in GeoStudio using the van Genutchen equation (van Genuchten 1980, Krahn 2004b) and the parameters from Watanabe et al. (2013):

$$\theta_w = \theta_r + \frac{\theta_s - \theta_r}{\left[1 + \left(\frac{\Psi}{a}\right)^n\right]^m} \tag{3.1}$$

where θ_w is the volumetric water content (m^3/m^3), θ_r is the residual water content (m^3/m^3), θ_s is the saturated water content (m^3/m^3), Ψ is the negative pore-water pressure in m (matric suction in kPa) and a, n, and m are curve fitting parameters. The equation was solved by GeoStudio using a value of 11.2 kPa for a, 1.25 for n, 0.2 for m, 1 x 10^{-5} kPa^{-1} for compressibility (m_v), 0.617 m^3 m^{-3} for saturated water content and 0.006 m^3 m^{-3} for residual water content (Watanabe et al. 2013). The water retention curve found by Equation 3.1 is shown in Figure 3.2.

The hydraulic conductivity function was estimated using GeoStudio's built-in Van Genuchten function (van Genuchten 1980, Krahn 2004b):

$$K_w = K_s \frac{\left[1 - \left(a\Psi^{(n-1)}\right)\left(1 + \left(a\Psi^n\right)^{-m}\right)\right]^2}{\left[\left((1 + a\Psi)^n\right)^{\frac{m}{2}}\right]} \tag{3.2}$$

where K_s is the saturated hydraulic conductivity (m/s). The GeoStudio function uses the water retention curve along with the saturated hydraulic conductivity and residual water content as inputs to calculate the hydraulic conductivity function. The Van Genuchten function was solved using a saturated hydraulic conductivity of 2.3 x 10^{-6} m/s, a residual water content of 0.006 m^3/m^3 and the water retention curve defined by Equation 3.1. The calculated hydraulic conductivity function for the volcanic ash soil is shown in Figure 3.2

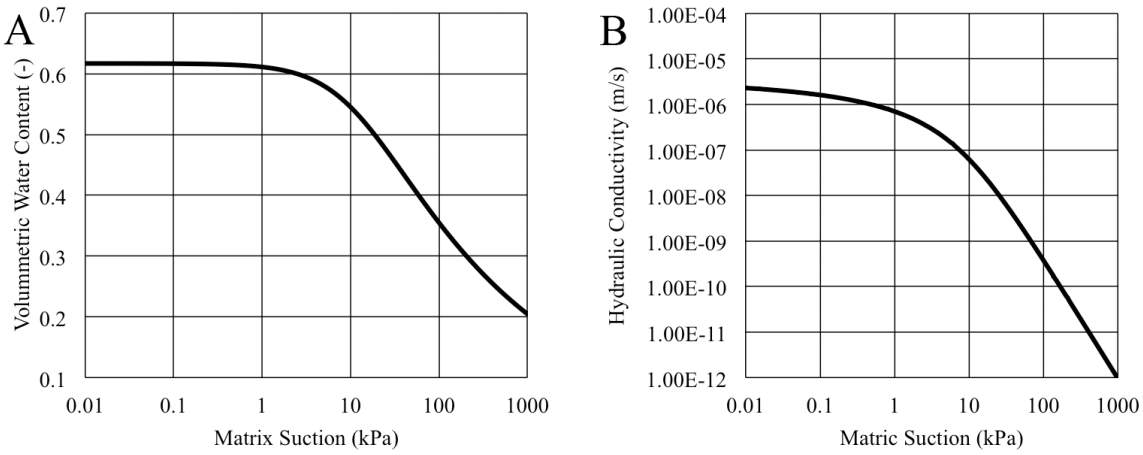

Figure 3.2 Water retention curve (A) and hydraulic conductivity function (B) for the A Horizon Volcanic Ash soil used in the simulations of the column experiments carried out by Watanabe et al. (2013).

The thermal properties were estimated from literature values and by the estimation routines provided within GeoStudio. Thermal conductivity was calculated following the equations and procedure of the Johansen method (Johansen 1977) outlined in Farouki (1981) and Carey and Woo (2005). A dry thermal conductivity, k_{dry}, of 0.14 J m^{-1} s^{-1} K^{-1} was used to find the thermal conductivity function and was calculated from the equations in Farouki (1981) and Carey and Woo (2005):

$$k_{dry} = \frac{\left(0.135\rho_b + 64.7\right)}{\left(2700 - 0.947\rho_b\right)} \tag{3.3}$$

where ρ_b is the soil bulk density (kg/m^3). The saturated thermal conductivity, k_{sat}, was calculated by (Farouki 1981, Carey and Woo 2005):

$$k_{sat} = \prod_{n=1}^{5} k\left(j\right)^{f(j)} \tag{3.4}$$

where $k(j)$ and $f(j)$ are the thermal conductivity (J s^{-1} m^{-1} K^{-1}) and volumetric fraction of the j^{th} type of substance making up the soil, including minerals, organics, water, air and

ice. The frozen thermal conductivity (J s^{-1} m^{-1} K^{-1}), k_f, was found by (Farouki 1981, Carey and Woo 2005):

$$k_f = \left(k_{sat} - k_{dry}\right)\left(\theta / \phi\right) + k_{dry} \tag{3.5}$$

where θ is the volumetric water content (m^3/m^3) and Φ is the soil porosity (-). The thermal conductivity function calculated through the Johansen method is shown in Figure 3.3.

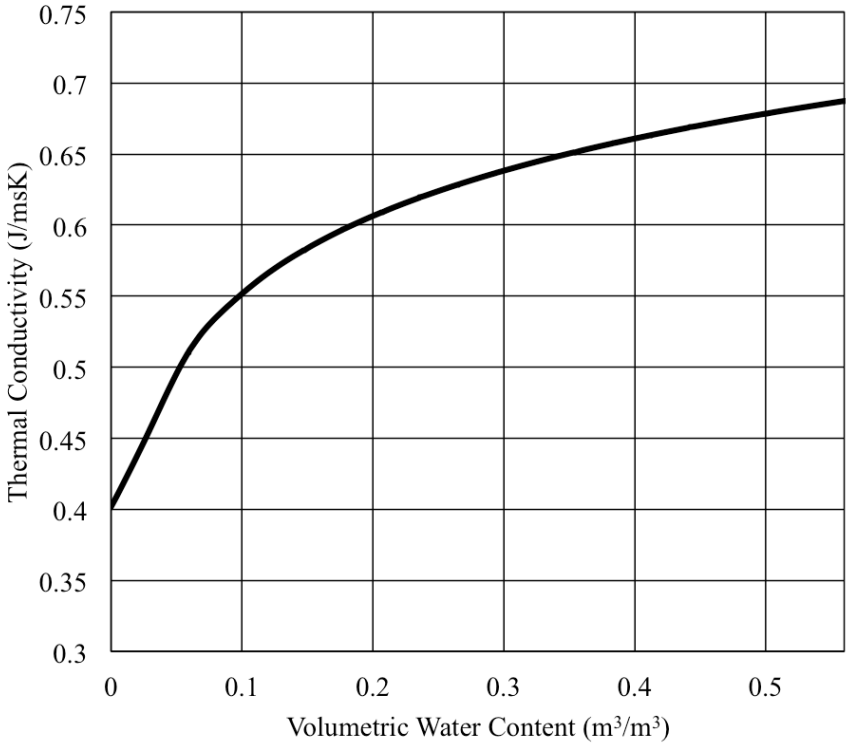

Figure 3.3 The thermal conductivity function determined through the Johansen method (Equation 3.4) for the unfrozen volcanic ash soil.

The volumetric heat capacity of the soil was estimated within GeoStudio by (Johnston et al. 1981):

$$C = c\gamma = \gamma_d \left[c_s + c_w w_u + c_i w_f\right] \tag{3.6}$$

where C is the volumetric heat capacity of the soil (J m^{-3} K^{-1}), c is the specific heat of the soil (J kg^{-1} K^{-1}), γ is the bulk density of the soil (kg/m^3), γ_d is the dry density of the soil (kg/m^3), c_s is the specific heat capacity of the soil particle (J kg^{-1} K^{-1}), c_w is the specific heat of water (J kg^{-1} K^{-1}), c_i is the specific heat of ice (J kg^{-1} K^{-1}), w_u is the unfrozen water content expressed as a percent of the dry weight of the soil and w_f is the frozen water content expressed as a percent of the dry weight of the soil. The calculated volumetric heat capacity function is shown in Figure 3.4. The unfrozen water content function was estimated based on soil texture, as shown in Figure 3.5.

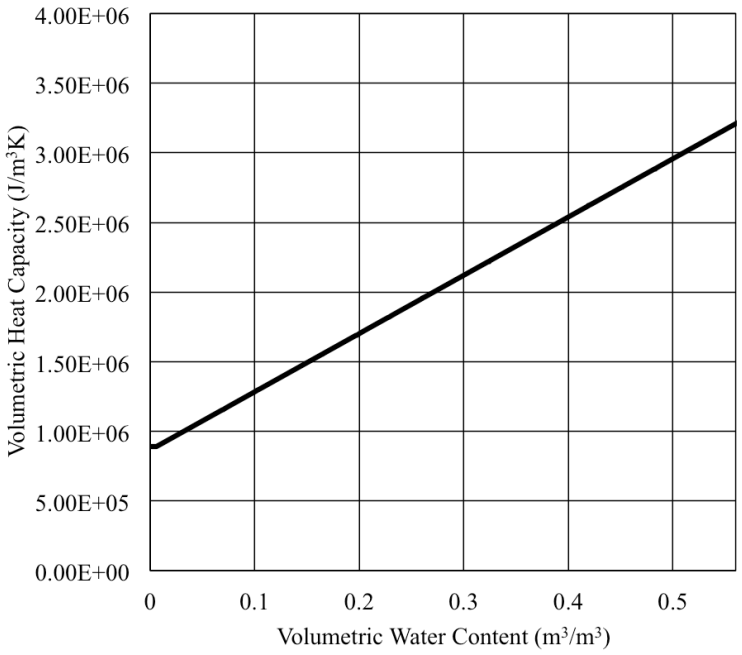

Figure 3.4 The volumetric heat capacity as a function of the volumetric water content for the unfrozen volcanic ash soil.

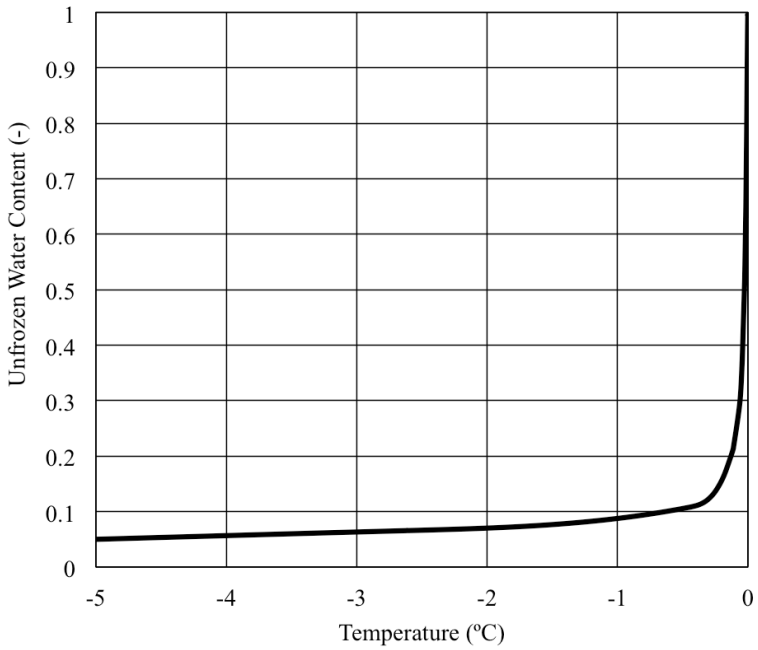

Figure 3.5 The unfrozen water content of the volcanic ash soil estimated from the soil texture.

3.2.2.3 Boundary Conditions

The three soil columns were modelled with the same thermal and hydraulic boundary conditions described by Watanabe et al. (2013).

Thermal Boundary Conditions

The column simulations were modelled using fixed temperature boundary conditions with the intention of matching the conditions present in the actual experiments. The simulation began with the initial temperature within the column set to 3.5 ºC. Freezing conditions were then applied for 48 hours, with a bottom temperature boundary of 2.0 ºC and a top boundary of -6.2 ºC. After 48 hours, the temperatures at the top and bottom of the column were returned to 3.5 ºC for the remainder of the simulation.

Hydraulic Boundary Conditions

The three initial water contents were obtained by setting the initial pressure head to a value that corresponded with the desired water content on the water retention curve. During the freezing stage, the external boundaries were set to zero flux conditions to

prevent water flow into or out of the column. After freezing, a free drainage boundary condition was applied to the bottom of the model and a water flux was applied at the surface. Three different water fluxes were simulated: a low flux, middle flux and a high flux. The low flux was based on the water added during the experiment, while the middle flux was approximately 20 times higher and the high flux was a further 2.5 times higher than the middle value. The low water flux across the upper boundary was 4.00×10^{-8} m/s, the middle water flux was 8.00×10^{-7} m/s and the high water flux was 2.00×10^{-6} m/s. These fluxes were applied to the surface, but due to free surface review and runoff, the actual flux into the model was lower. These conditions remained for the duration of the model.

3.2.3 Results

The simulations of the soil column models were able to successfully reproduce the results observed by Watanabe et al. (2013). The three initial water contents were simulated and as expected, the higher initial water contents experienced longer first and second phases. The different surface water fluxes showed different thaw rates and depths, revealing the influence of convection on thaw.

3.2.3.1 Frozen Layer Thickness

The thickness of the frozen layer within each column did not vary with the initial water content, consistent with the findings of Watanabe et al. (2013). Experimental temperature profiles are shown in Figure 3.6. The three columns were frozen to a depth of 0.15 m after 48 hours of freezing conditions. The ice content of the frozen layer varied, with the higher water contents having greater ice contents. The lowest initial water content (31%) column had an ice content of 28%, while the highest initial water content (46%) column had an ice content of 41%. The column with the middle value initial water content (38%) had an ice content of 34%. The higher ice contents experienced longer thaw times.

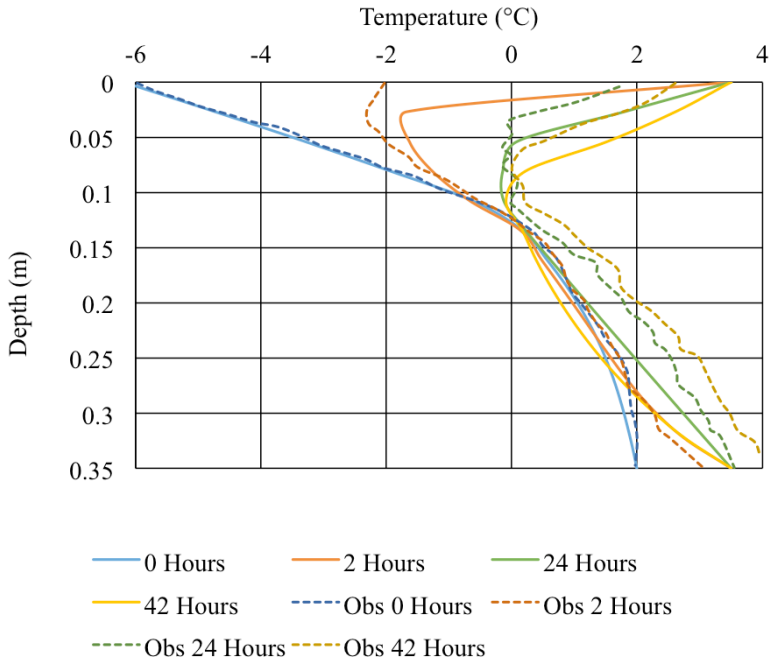

Figure 3.6 The temperature profiles of the benchmark simulation and experimental column. The solid lines represent the simulation results while the dashed lines represent the results of Watanabe et al. (2013).

Thaw of the frozen layer was influenced by the initial water content, but was mainly affected by the water flux. Contrary to what might be expected, a higher flux rate did not lead to additional thawing. In fact, progression of the thawing front was slowed with the higher surface flux rates. Figure 3.7 shows the thickness of the frozen layer within the column through time in the middle water content column. When a low water flux of 4.00×10^{-8} m/s is applied to the surface of the column, the thickness of the frozen layer decreases at a rate of 1.6 mm/hour and is only 30 mm thick at the end of the simulation. Increasing the surface flux rate to 8.00×10^{-7} m/s lowered the rate at which the thickness of the frozen layer decreased to 1.4 mm/hour. The frozen layer was 40 mm thick at the end of the simulation. At the highest flow rate (2.00×10^{-6} m/s) the frozen layer decreased in thickness at a rate of 1.2 mm/hour and was 40 mm thick at the end of the simulation. The other columns with different initial water contents showed similar

results, as seen in Table 3-1. The highest rate of decrease was observed in the low water content column with the lowest infiltration flux.

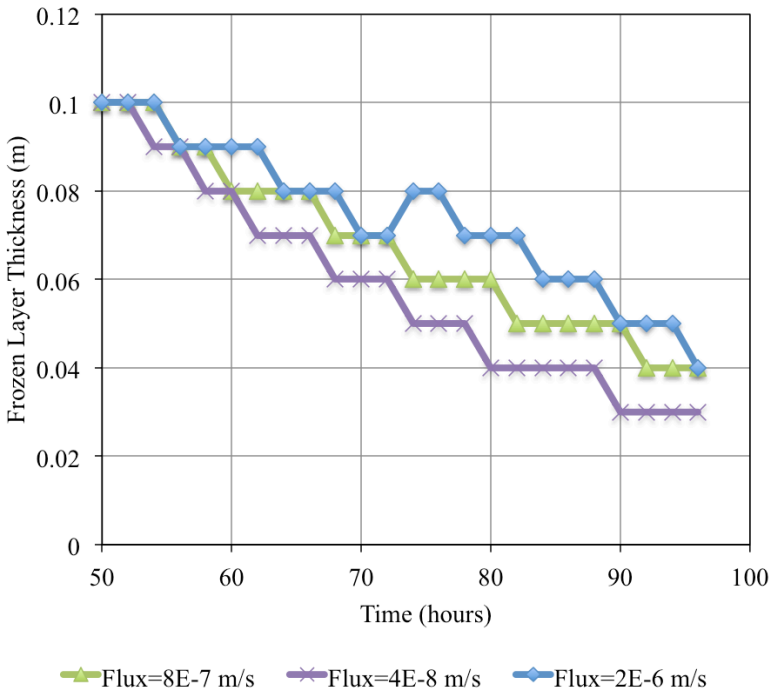

Figure 3.7 The frozen layer thickness as a function of time in the middle water content column under the three surface fluxes simulated. The "steps" in the plots are due to the development of zero-curtain conditions within the columns.

A zero-curtain effect was observed in the simulation, as shown by the "steps" in Figure 3.7. The temperature at the top of the frozen layer would hover around 0 °C for several hours, resulting in a constant frozen thickness for the duration of each zero-curtain. The latent heat absorption reduces the warming rate and keeps the soil isothermal near 0 °C.

The bottom of the ice layer either remained at the same level or thawed upwards for the low and medium water fluxes. The high water flux resulted in the bottom of the ice layer progressing downwards, increasing the thickness of the ice layer, as shown by the increase in thickness of the high water flux rate in Figure 3.7. Additional heat from the constant temperature bottom boundary was added through conduction. The higher water

flux rates reduced the upward conductive heat flux compared to the lower water flux (Figure 3.8), limiting the impact on thaw.

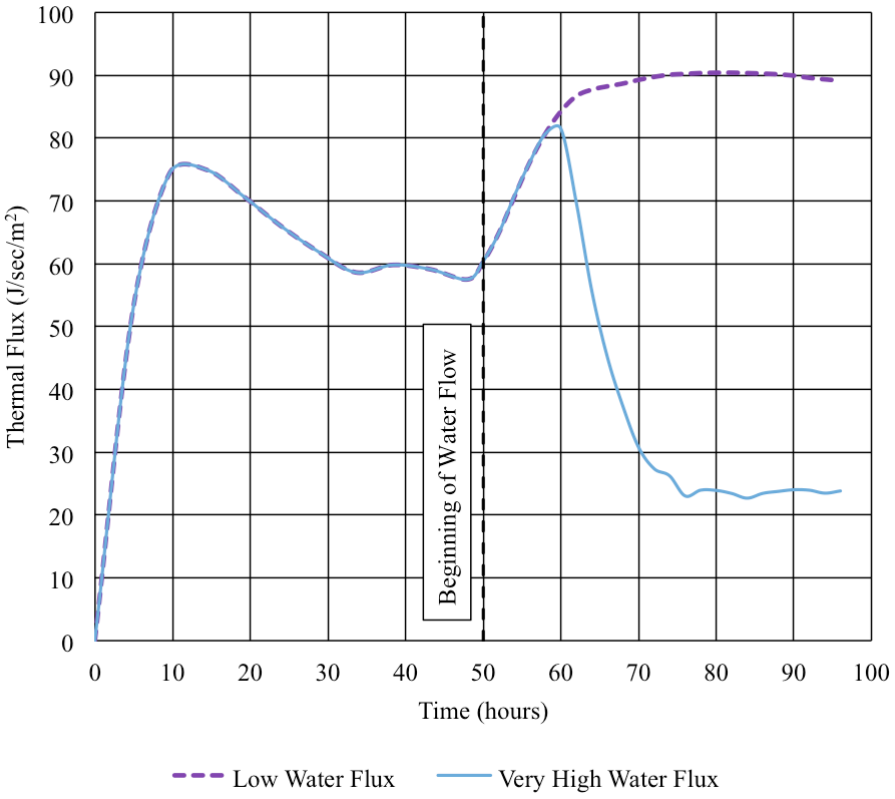

Figure 3.8 Upward vertical conductive thermal flux underneath the frozen section.

These results suggest an increased water flow through the column does not increase the thaw rate, but instead increases the refreezing and decreases the overall thaw rate.

Table 3-1 The rate of decrease in the thickness of the frozen layer in the column for the three column simulations.

Flux Rate (m/s)	Rate of Decrease in Frozen Layer Thickness (mm/hour)		
	Low Initial Water Content (31%)	Middle Initial Water Content (38%)	High Initial Water Content (46%)
4×10^{-8}	2.1	1.6	1.5
8×10^{-7}	1.3	1.4	1.3
2×10^{-6}	1.2	1.2	1.2

The top of the frozen layer thaws at a quicker rate than the bottom of the frozen layer. The depth of the bottom of the layer moved only a centimetre or two during the course of the simulation. Figure 3.9 compares the positions of the frozen layer for the low water content column and the low water flux. The top of the ice layer thaws at a rate of 1.8 mm/hour, while the bottom thaws at only 0.8 mm/hour.

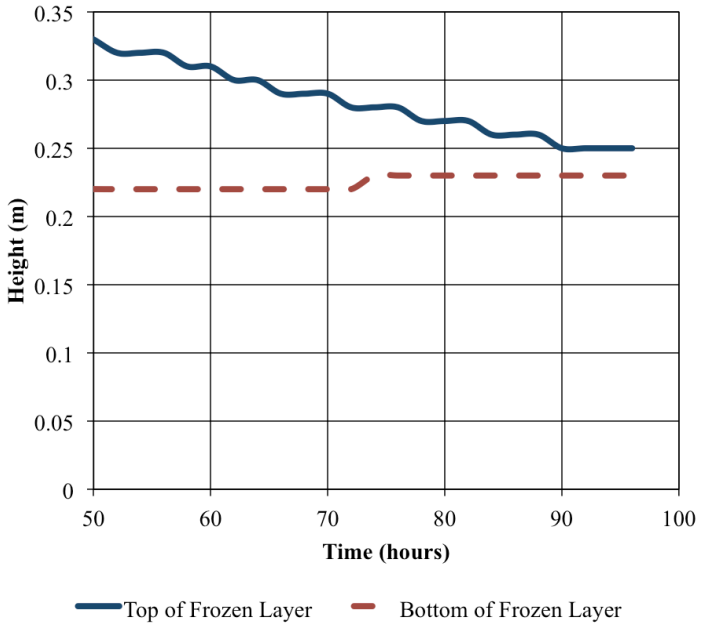

Figure 3.9 The position of the top and bottom boundary of the frozen layer for the case of low water flow through the low water content column following the start of infiltration and thaw (t=50 hours).

3.2.3.2 Infiltration and Percolation

Infiltration into and percolation through the columns were also influenced by the presence of the frozen layer. Infiltration was slowed due to the presence of the frozen layer in all columns. At the beginning of the infiltration and percolation phase, flow at the top of the column ranged from approximately 3.5 x 10^{-7} m/s under the high flux to approximately 5 x 10^{-11} m/s under the low surface flux. The measured flow rate within the frozen layer for all columns was less than 10^{-20} m/s, essentially no flow.

As the column thawed, more water was able to flow. Two flux sections in the columns monitored the water flow rate during the simulations. The top flux section was near the top of the column at a height of 33 cm. The location of the other flux section, at a height of 25 cm, was chosen so that it remained within the frozen layer for most of the simulations and is referred to as the bottom flux section. Measurements from these flux sections follow the same phases as Watanabe et al. (2013). Water flow is initially restricted due to presence of ice, but as the frozen layer becomes saturated, the flow rate increases. Once the water has reached the bottom of the ice layer, the flow rate in the frozen section is almost equivalent to the flow rate in the thawed section. Experimental water content profiles are shown in Figure A.8.

The time required for water to reach the bottom of the ice layer and cause an increase in the flow rate at the bottom flux section decreased as the flow rate increased. In the middle water content column, the flow rate at the two sections became roughly equal after 75 hours under the low surface flux conditions, whereas it only required 60 hours under the medium surface flux and 55 hours under the high water flux conditions.

The initial water content also influenced the time required for water to initially flow through the frozen layer. Under the low water flux conditions, the same pattern described by Watanabe et al. (2013) was seen in the simulations, with the low water content column entering the third phase earliest, 70 hours after application of the surface flux, followed by the middle water content column at 76 hours and the high water content column at 80 hours (Figure 3.10). The medium water flux conditions, however, showed the opposite, with the highest water content column reaching the third phase after 58 hours, while the middle water content column took 60 hours and the low water content column took 62 hours. Under the high water flux conditions, all three columns entered the third phase at the same time, after 58 hours.

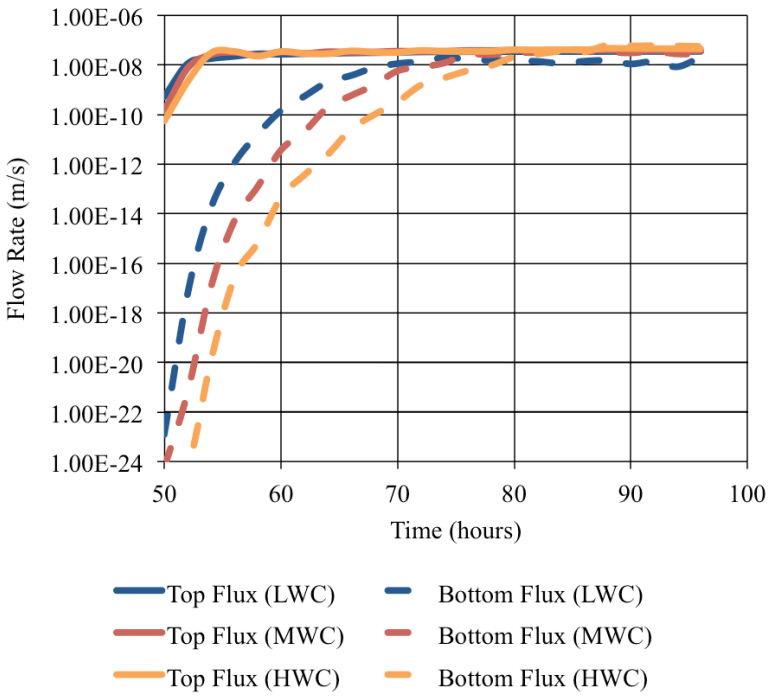

Figure 3.10 The flow rates at the top flux section (solid lines) and the bottom flux section (dashed lines) under the low surface flux conditions for the low, middle and high water content column.

3.2.3.3 Peclet Number

The thermal Peclet number for each simulation was determined through Equation 3.7. This equation differs from the definition of the Peclet number expressed earlier (Equation 2.1) since convection occurs in the same direction and over the same length scale as conduction, eliminating the need for the length scale ratio. The definition found in Bredehoeft and Papadopulos (1965), van der Kamp and Bachu (1989), and Ferguson (2014) was used to calculate the Peclet number for each flux rate at each water content:

$$P_e = \frac{\rho_w c_w q L}{\kappa_e} \tag{3.7}$$

where P_e is the Peclet number, ρ_w is the density of water (kg/m^3), c_w is the specific heat of water (J kg^{-1} K^{-1}), q is the specific discharge (m/s), L is the characteristic length (m) and κ_e is the thermal conductivity of the material (J s^{-1} m^{-1} K^{-1}). For the column simulations,

the characteristic length was chosen as the height of the column due to the length over which convection is occurring.

At the low water flux rate, the Peclet number was 0.050 for the low water content column, 0.051 for the middle water content column and 0.056 for the high water content column. The middle flux produced Peclet numbers of 1.06 for the low water content column and 1.05 for the medium and high water content columns. At the highest water flux, the Peclet number was 2.64 for both the low and medium water content columns and 2.62 for the high water content column. The maximum Peclet number was calculated using the saturated hydraulic conductivity of the volcanic ash soil at a gradient of 1, i.e. under fully saturated gravity drainage with no ponding. The soil was the same in each column simulation, and therefore, the maximum Peclet number was the same for all columns at a value of 3.12. The Peclet numbers for all simulations are shown in Table 3-2.

The larger Peclet numbers correspond to the slower thaw rates in these simulations. Since a large portion of conduction is actually upwards from the bottom in the column, the Peclet number is, counterintuitively, an accurate representation of the convection occurring, despite the small thaw rates. The larger water flows, and thus larger Peclet numbers, diminish the impact of upward conduction and slow thaw.

Table 3-2 Peclet numbers determined using the specific discharges and Equation 3.7 for each column in the simulations.

Flux Rate (m/s)	Peclet Number		
	Low Initial Water Content (31%)	Middle Initial Water Content (38%)	High Initial Water Content (46%)
4×10^{-8}	0.050	0.051	0.056
8×10^{-7}	1.06	1.05	1.05
2×10^{-6}	2.64	2.64	2.62
Maximum	3.12	3.12	3.12

3.3 Failure Through Lateral Convection

3.3.1 Introduction

Potential failure of a SFCBD cover system may be the result of lateral convection causing premature thaw of the frozen layer. Convective heat transfer has the potential to play a large role in the thawing of a frozen slope. A case study of the Wolf Creek basin, Yukon was undertaken to determine the role of convection in thawing the slope and the extent to which it might act as a failure mode for a SFCBD cover.

3.3.2 Study Site – Wolf Creek Basin, Yukon

The Wolf Creek basin is located 15 km south of Whitehorse, Yukon (Figure 3.11). Extensive research was carried out on four slopes within the basin to determine the hydrology of the basin (Carey and Woo 1998, 1999, 2001a, 2001b, 2005, Quinton et al. 2009, Shirazi et al. 2009). Of particular interest to this study were the north-facing and west-facing slopes and their behaviour during the spring freshet.

The west and north slopes were composed of an organic-rich layer overlying a mineral soil. The mineral soil of the west slope was made up of a sandy material, while the mineral soil of the north slope was mainly clay. The sandy west slope provides a natural analogue for a SFCBD constructed with coarse textured soils, albeit without the engineered high saturation layer. The clay rich north slope provides an analogue to a frozen low hydraulic conductivity frozen zone overlain by a high hydraulic conductivity upper layer.

A more detailed description of each slope is contained within Carey and Woo (2001b). The north and west slopes both showed lateral water flow over the frozen layer (Carey and Woo 2001b). A perched saturated zone above the organic-mineral interface was observed on both slopes during the spring freshet. Upwards of 80% of snowmelt was diverted downslope on the north slope, while 25% was diverted on the west slope.

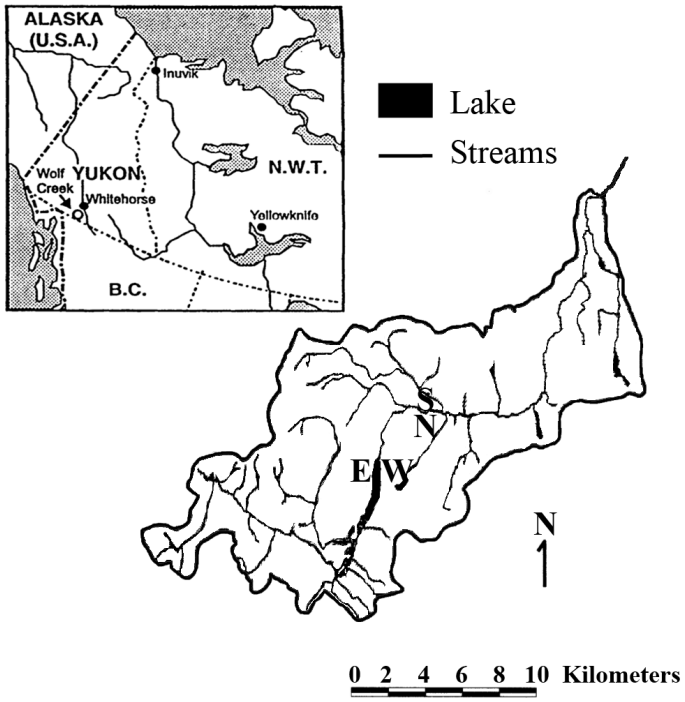

Figure 3.11 Map of the Wolf Creek basin showing the location within the basin of the four slopes, including the north and west-facing slopes that were simulated, and the location of the basin in the world (adapted from Carey and Woo (2005)).

Ground temperature measurements were taken at several locations along the north slope during the 1997 spring freshet (Carey and Woo 1998), while frost table depths were measured on the west slope. Ground temperature measurements on the north slope showed above zero ground temperatures at the top of the slope a few days prior to the toe of the slope (Figure 3.12).

The difference in thaw pattern is postulated in the current research to be occurring as a result of convection. A delay in heat transfer associated with the time of water transfer from top to toe could explain the difference in timing. Theoretically, the advective front of heat transfer within a soil is retarded due to the equilibrium of the heat within the pore-fluid with the solid phase. For example, the thermal retardation factor for sand was calculated to be approximately 1.8 by Oldenburg and Pruess (1998) using the following equation:

$$R^h = 1 + \frac{1-\phi}{\phi}\frac{\rho_R C_R}{\rho C} \tag{3.8}$$

where R_h is the effective retardation factor, ϕ is the porosity, ρ_R and C_R are the density (kg/m^3) and specific heat (J kg^{-1} K^{-1}) of the entire soil-fluid matrix, respectively, and ρ and C are the density (kg/m^3) and specific heat (J kg^{-1} K^{-1}) of the fluid. The heat carried with the infiltrating snowmelt, along with latent heat released during refreezing, would therefore be delayed in reaching the toe of the slope by almost double the time it would take water to travel the length of the slope, even in the absence of any freeze/thaw effects. The infiltrating snowmelt is likely to be around 0 ºC, the temperature at which snow melts, which could remove heat that would otherwise be conducted from the atmosphere to the soil, slowing the thaw at the toe.

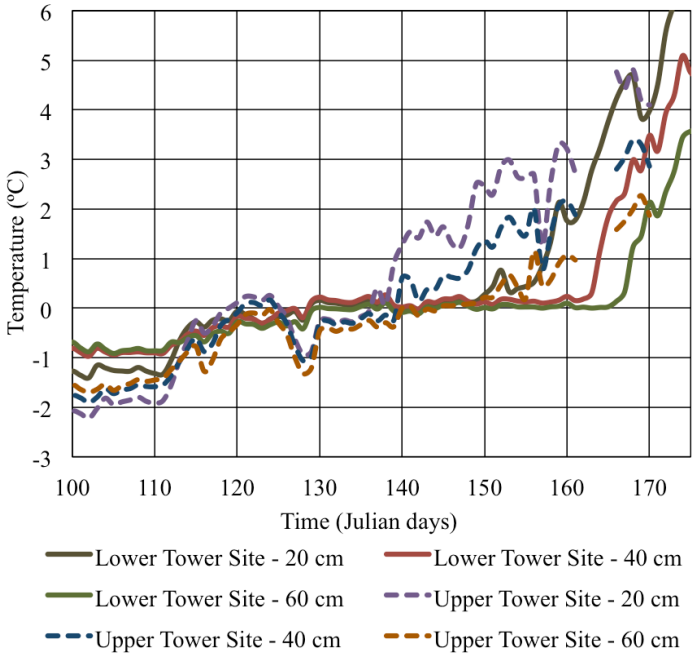

Figure 3.12 Ground temperatures of the north slope at various soil depths at the top of the slope (Upper Tower Sites) and toe of the slope (Lower Tower Sites). The ground temperature at the top of the slope reaches positive temperature values a few days before the toe of the slope.

Although the potential for lateral heat convection is enhanced by larger water fluxes; it is not always possible to generate these high flux values. The largest hydrological event of the year for most northern regions is the spring snowmelt (Marsh 1990). The simulations will determine if the snowmelt flux is large enough to generate the convective transfer necessary to influence thaw.

3.3.3 Model Setup

3.3.3.1 Domain

The west slope was modelled as a 40 m long slope with a gradient of 0.18. Benches at the top and the toe of the slope extended approximately 10 m outward from the slope. Several control points were used at each end of the slope to ensure a gradual, more natural transition to the benches. The organic-rich layer was 0.5 m thick, while the mineral soil was 4 m thick (Figure 3.13). Dimensions were chosen to represent the actual slope. The thick mineral soil reduced the influence of any thermal effects the bottom boundary could have on the rest of the profile.

The dimensions of the north slope were quite similar to the west slope. The north slope was made up of a fairly thin (less than 0.5 m thick) organic-rich layer overlying a mineral soil varying in thickness from one to two metres (Figure 3.13). The gradient of the slope was also 0.18. Therefore, the same model domains used for the west slope were also used for the north slope. The model domain of the north slope is shown in Figure 3.14. Ten vertical elements formed the discretization of the ground surface layer in both slopes. Quad and triangle elements, approximately 0.2 m in size, created the finite element mesh in the rest of the domain.

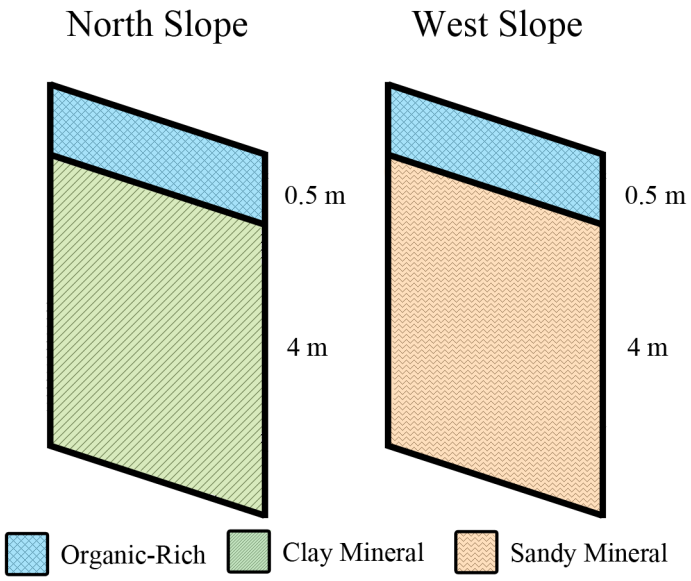

Figure 3.13 Modelled geology of the north slope and the west slope.

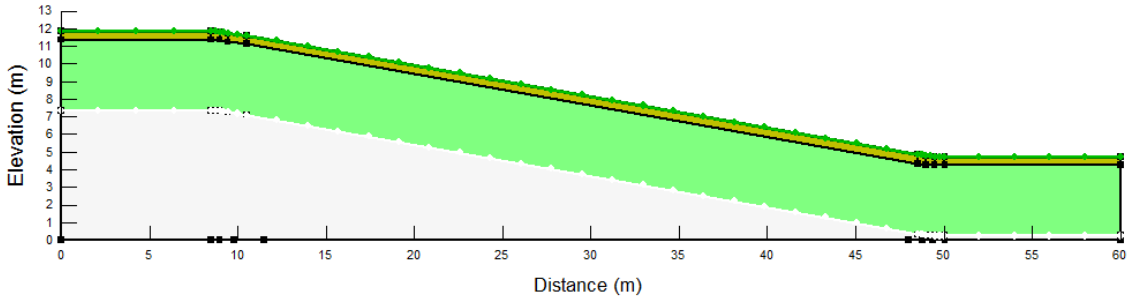

Figure 3.14 The model domain for the north slope is composed of a thin organic-rich layer overlying a thick clay mineral soil.

3.3.3.2 Material Properties

Both the west slope and north slope were modelled as simple two-layer slopes with gradual transitions to benches at the top and toe of the slope. The upper layer of organic-rich material was similar for both slopes. The lower layer was different for each slope; sandy mineral soil on the west slope and a clay mineral soil on the north slope.

The organic-rich soil for both slopes was modelled using the same properties. It was composed mainly of peat, lichens, and mosses with some sedges and grasses (Carey and Woo 2001b), which resulted in a low bulk density of 0.075 g/cm^3 and high porosity of 85%. The sandy mineral soil of the west slope was a sandy soil with large stone inclusions. The soil was modelled as a sand with a bulk density of 1.57 g/cm^3 and a porosity of 47%, but without the stone inclusions (Carey and Woo 2001b). The clay mineral soil also had stone inclusions that were not modelled, but had a lower bulk density of 1.34 g/cm^3 and a higher porosity of 52%.

The water retention curves were determined using the texture-based sample functions within GeoStudio (Krahn 2004b) and the saturated volumetric water content. The saturated water contents are contained in Table 3-3 and the generated water retention curves are shown in Figure 3.15. The hydraulic conductivity functions were determined through the van Genuchten method (van Genuchten 1980). The water retention curve, saturated hydraulic conductivity and residual water content of each soil were input to determine the hydraulic conductivity function of each soil, as shown in Figure 3.16. Input parameters are shown in Table 3-3. The saturated hydraulic conductivity of the sandy mineral soil was increased by approximately two orders of magnitude to provide more variability between the two mineral soils.

Table 3-3 Hydraulic properties of the three Wolf Creek soils used to determine the water retention curves and the hydraulic conductivity functions (from Carey and Woo 2001b).

Property	Organic-Rich	Clay Mineral	Sandy Mineral
Saturated hydraulic conductivity (m/s)	0.007	5.00×10^{-9}	1.00×10^{-5}
Saturated volumetric water content (-)	0.85	0.52	0.47
Residual volumetric water content (-)	0.46	0.31	0.1

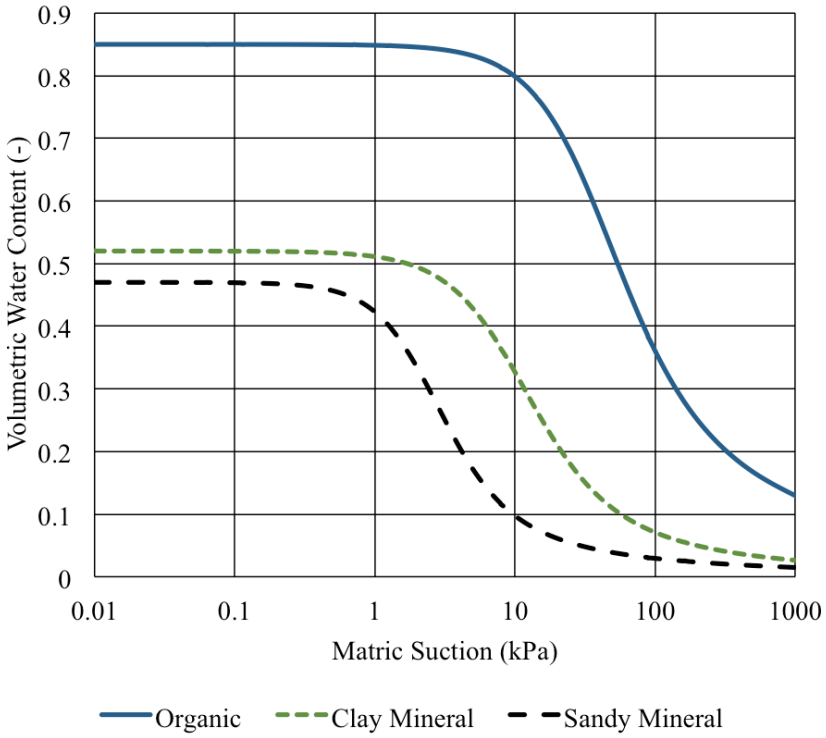

Figure 3.15 Water retention curves for the organic-rich, clay mineral and sandy mineral soils used in the Wolf Creek simulations.

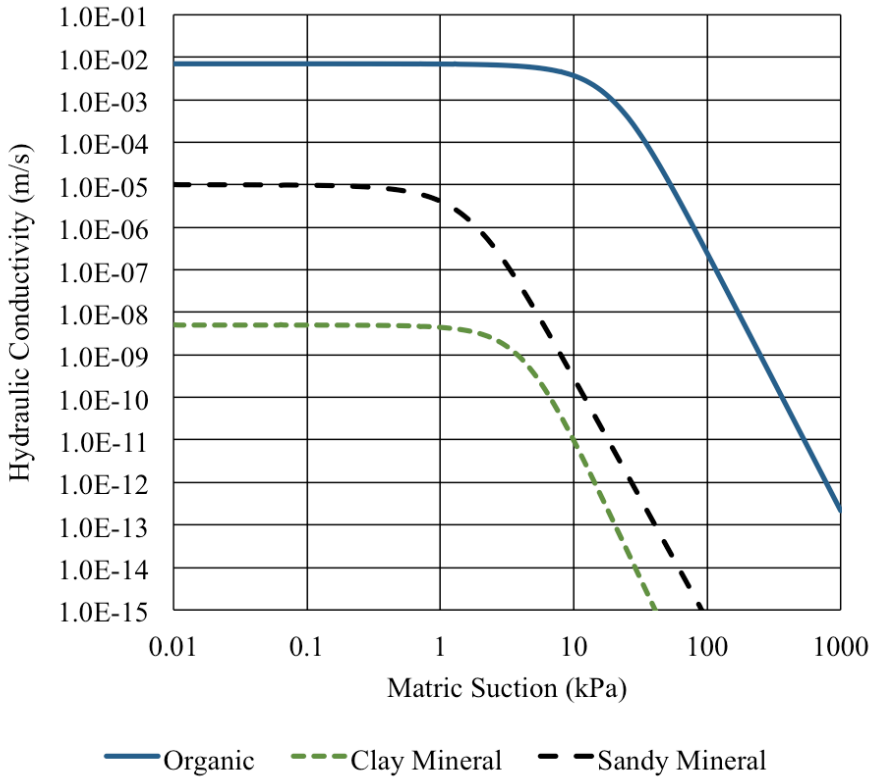

Figure 3.16 The hydraulic conductivity functions for the organic-rich, clay mineral and sandy mineral soils used in the Wolf Creek simulations.

The thermal properties of the soils were calculated using field data (Carey and Woo 2001a, 2001b) and the Johansen method and other equations outlined in the previous section. The thermal conductivity function was determined using 0.028 J m^{-1} s^{-1} K^{-1} as the mineral material thermal conductivity input for the organic-rich, 0.23 J m^{-1} s^{-1} K^{-1} for the sandy mineral soil and 0.17 J m^{-1} s^{-1} K^{-1} for the clay mineral soil. The estimated functions are shown in Figure 3.17.

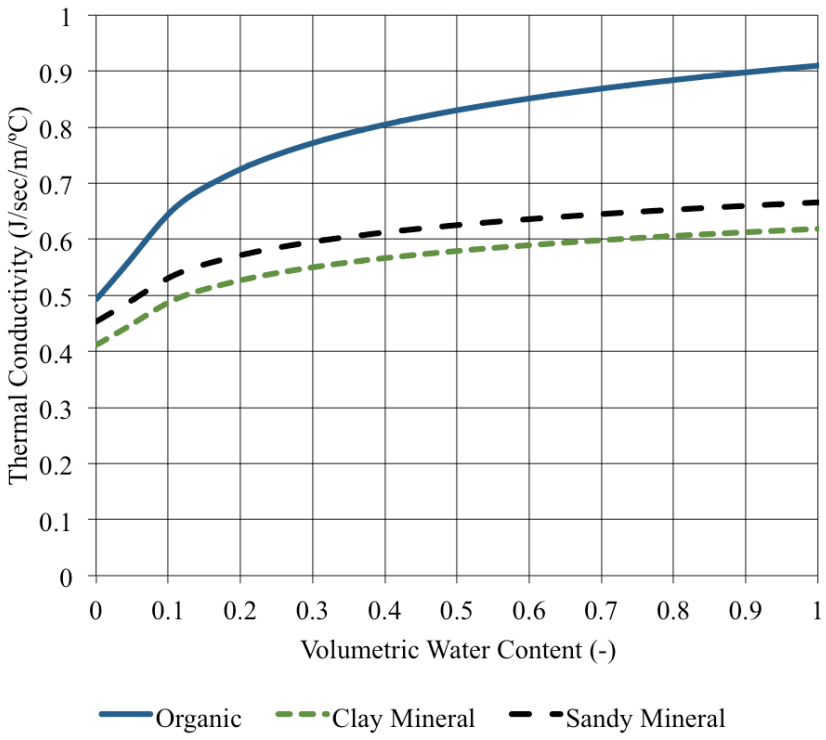

Figure 3.17 The thermal conductivity functions for the three soils used in the Wolf Creek simulations as determined through the Johansen method.

The volumetric heat capacity functions for the three soils were determined in GeoStudio using Equation 3.6, as shown in Figure 3.18. The unfrozen water contents were estimated by GeoStudio based on soil texture and are shown in Figure 3.19.

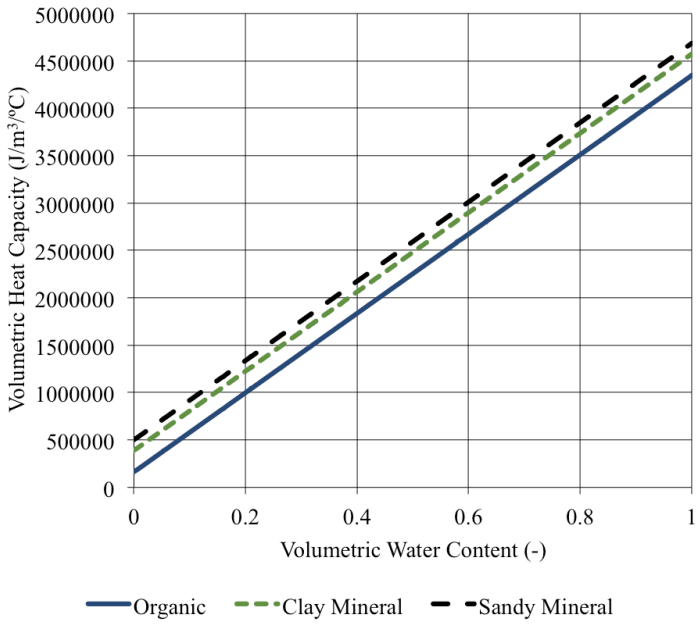

Figure 3.18 Volumetric heat capacity functions for the three soils used in the Wolf Creek simulations.

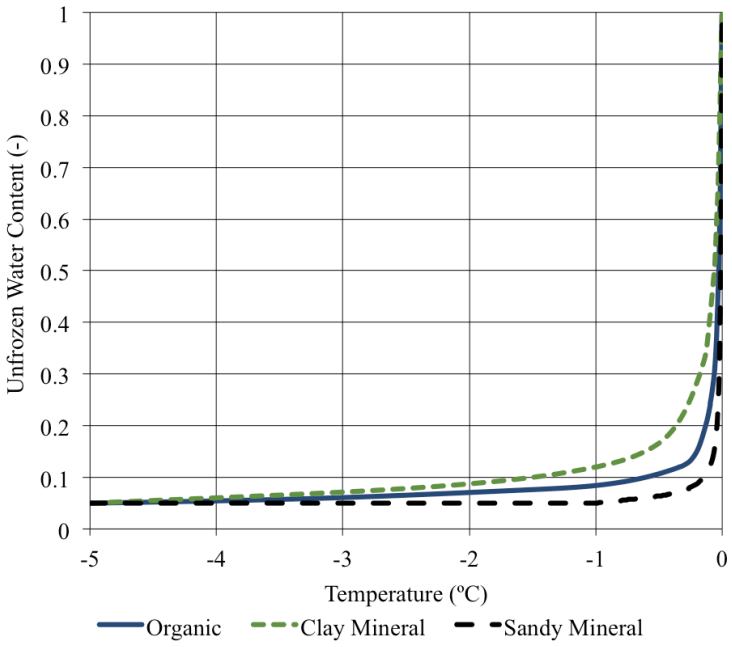

Figure 3.19 Unfrozen water content functions for the three soils used in the Wolf Creek simulations.

3.3.3.3 Initial and Boundary Conditions

The west and north slopes were modelled using the same boundary conditions. Realistic surface boundary conditions, that included a surface energy balance, were applied to both slopes. Soil temperature and water content field measurements, along with actual precipitation and evapotranspiration, were incorporated, allowing for an in-depth analysis and comparison to field observations.

Thermal Initial and Boundary Conditions

The modelling required some spin up to determine the initial and boundary conditions of the models. Due to limitations of the numerical model, a rigorous surface energy balance could not be applied directly. Instead, a one-dimensional profile of the slope was used along with a surface energy balance boundary to determine the ground surface temperature, which was then applied to the 2D model as the surface boundary condition. The 2D slopes were simulated for 5 years, with the first 4 years acting as the spin up. During the first four years of the simulations, the models achieved consistent temperature profiles from year to year, allowing the 5^{th} year model to be an accurate representation of the initial thermal conditions within the slopes. Initial soil temperatures were applied prior to spin up using a spatial function and the 1998 soil temperature measurements provided by Sean Carey (personal communication, 2013).

An LCI boundary condition was applied to the 1D model to solve the surface energy balance. Climate data, provided by Sean Carey (personal communication, 2013), from 1998 was used for the air temperature and wind speed inputs (Figure 3.20 and Figure 3.21). Solar radiation was estimated using the latitude and albedo was based on literature values. The bottom boundary of the 1D model simulated permafrost and was set to a constant temperature of 0 ºC.

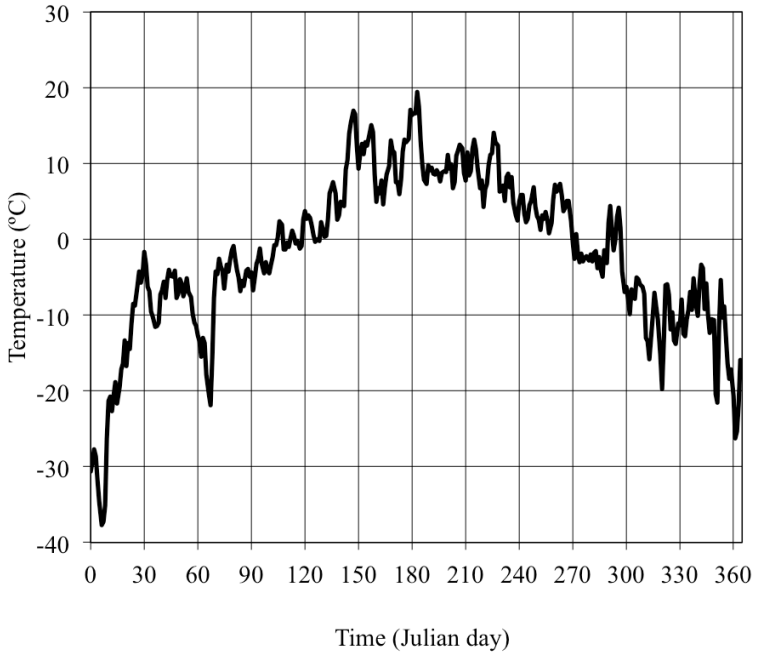

Figure 3.20 Air temperature in the Wolf Creek basin for 1998. Data provided by Sean Carey (personal communication, 2013).

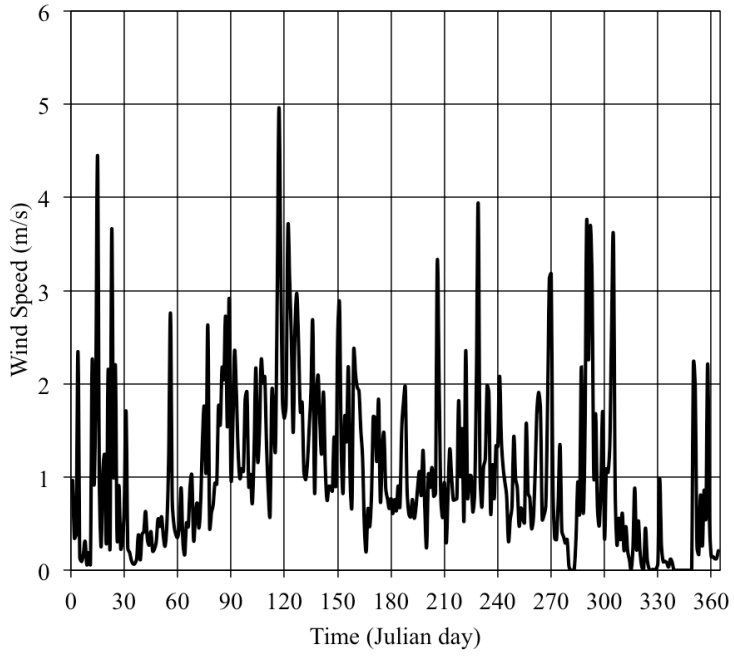

Figure 3.21 Wind speed measurements taken in the Wolf Creek basin during 1998. Data provided by Sean Carey (personal communication, 2013).

The 1D simulation produced a ground surface temperature profile that was applied as the surface boundary condition of the 2D simulation. This profile is shown in Figure 3.22 and was applied to both slopes.

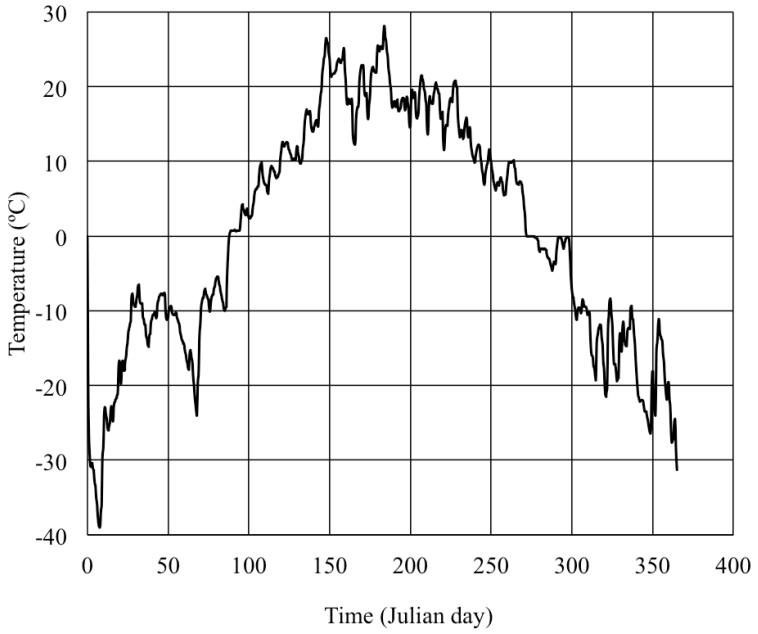

Figure 3.22 Surface temperatures for the Wolf Creek basin based on a 1D model using an LCI condition and Wolf Creek climate data.

Hydraulic Initial and Boundary Conditions

The hydraulic initial conditions were set during the initial spin up of the model. The initial water content of the slopes were set through the use of pressure head boundary conditions. The volumetric water content function of each material was used to determine the appropriate pressure head condition required within the material to achieve the desired initial water content.

The initial water contents were set to the 1998 soil moisture measurements provided by Sean Carey (personal communication, 2013). The water content reached a consistent profile from year to year during the first four years of the simulations. The results of the fifth year were used in this investigation.

Snowmelt and the ensuing infiltration on both slopes occurred over a period of a few weeks in the spring each year (Carey and Woo 2001b). To simulate the snowmelt infiltration in the model, a water flux boundary condition was applied at the upper surface. Precipitation data, along with total snowpack and snowmelt duration, were used to determine an average flow rate across the surface for the duration of snowmelt.

The upper water boundary flux was generated using a function that allowed the flux to slowly increase from zero to the average flow rate over the period of a few days. This was done to alleviate stability issues in the model that occurred when the flux rose to the maximum value almost instantly. The total volume of snowmelt and any precipitation received during the melt period was divided evenly by the number of days in the melt period. Precipitation and snowpack data from 1998 was used, along with an average melt duration of 3 weeks. This resulted in a flux of 5.58×10^{-8} m/s, or 4.82 mm/day, as the applied surface flux.

Summer precipitation and evapotranspiration were also simulated, permitting the slopes to be modelled year round and creating the year-to-year stability required. Precipitation data was provided by Sean Carey (personal communication, 2013). Evapotranspiration was modelled as 220 mm over 120 days on the west slope and 315 mm over the same time period on the north slope (Carey and Woo 2001b).

Water was able to exit the domain at the toe of the slope through a potential seepage face boundary condition. The bottom and top lateral boundary were set to zero flux conditions to ensure no water exited the model through these boundaries.

3.3.4 Results

The results of the Wolf Creek simulations were compared to measured discharge fluxes and ground temperatures, as well as thaw patterns and depths as reported by Carey and Woo (2001b). The implications of the simulations were assessed through the thermal Peclet number, determining the role of convection

3.3.4.1 Organic-Rich Layer

The simulation results for the organic-rich layer of the north and west slopes showed that there is the potential for lateral convection to influence thaw if large flow velocities can be achieved in the organic-rich layer.

Thaw depth was relatively uniform through the organic-rich layer on both slopes. Water began to flow within the thawed zone almost immediately after melting began. Flow at the toe of the slope tended to be greater than flow at the top of the slope and grew larger with time. On the west slope, the total volumetric water content (liquid and ice) increased and decreased at the same rate at the same times at the top and toe of the slope (Figure 3.23). The increased interflow at the toe of the slope during the snowmelt runoff period can therefore be attributed to lateral diversion of additional water due to melt.

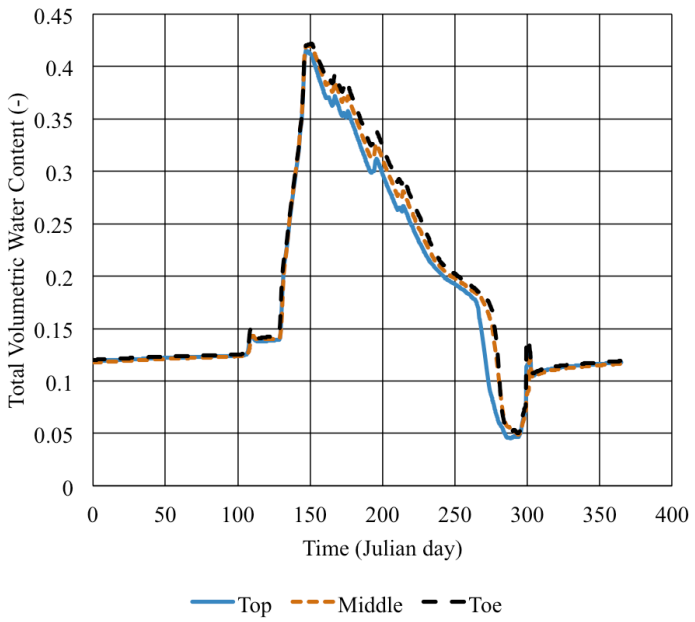

Figure 3.23 The total volumetric water content at the top, middle and toe of the west slope organic-rich layer.

The water content of the north slope also experienced increases and decreases at the same times at the top and toe, but the water content increased with lateral distance down the slope (Figure 3.24). The initial total water content (liquid and ice) at the toe of the north slope was higher than the top, but the difference in peak values during the snowmelt was greater than the difference at the beginning of the year. The increased interflow at the toe can therefore be partially attributed to lateral flow of additional water due to melt, but also to loss of storage at the top of the slope.

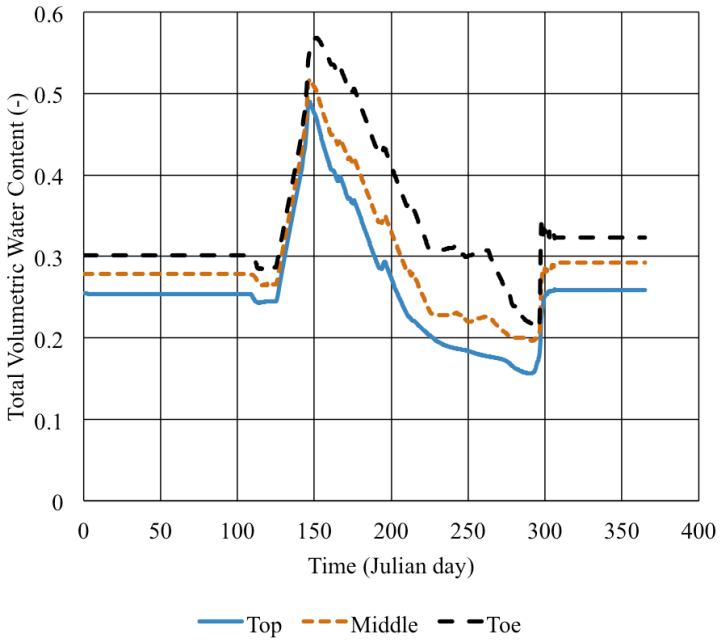

Figure 3.24 The total volumetric water content at the top, middle and toe of the north slope organic-rich layer.

The lateral flow through the slope influenced the progression of the thaw front. The effect was more pronounced on the north slope, where the top of the slope began to thaw faster than at the toe (Figure 3.25), consistent with the soil temperature data collected on the north slope (Carey and Woo 1998), suggesting convection may have delayed thaw downslope. The top of the slope reached zero-curtain approximately two days prior to the toe of the north slope. Thaw on the west slope occurred only a few hours apart. However,

the west slope organic-rich layer thawed a few days prior to the thaw of the north slope. Unexpectedly, the middle of the slope was the slowest region of the slope to thaw. Overall, the temperature at depth was relatively consistent at the different regions throughout the year (Figure 3.26).

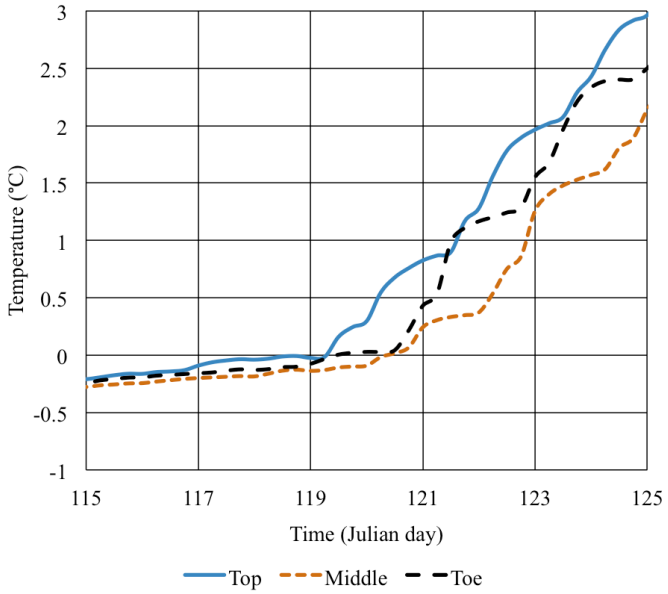

Figure 3.25 The temperature at the top, middle and toe of the north slope at approximately 0.4 m depth.

This pattern of increased thaw at the top of the slope relative to the toe of the slope continued with depth into the slope (Figure 3.27). The difference in thaw at the different regions is likely the result of a mixture of convection and conduction. The influence of each can be determined through the Peclet number.

The theoretical maximum Peclet number for a soil is found from the maximum discharge of the saturated soil draining under gravity. This discharge is given by the saturated hydraulic conductivity multiplied by the gradient of the slope. The organic-rich layer had a high maximum Peclet number, orders of magnitudes larger than 1, as seen in Table 3-4. The high hydraulic conductivity of the organic-rich layer increases the potential for convection. If enough water flow occurred through the organic-rich layer, convection

would dominate. However, under climatic snowmelt infiltration conditions, the specific discharge does not approach the saturated specific discharge under gravity drainage.

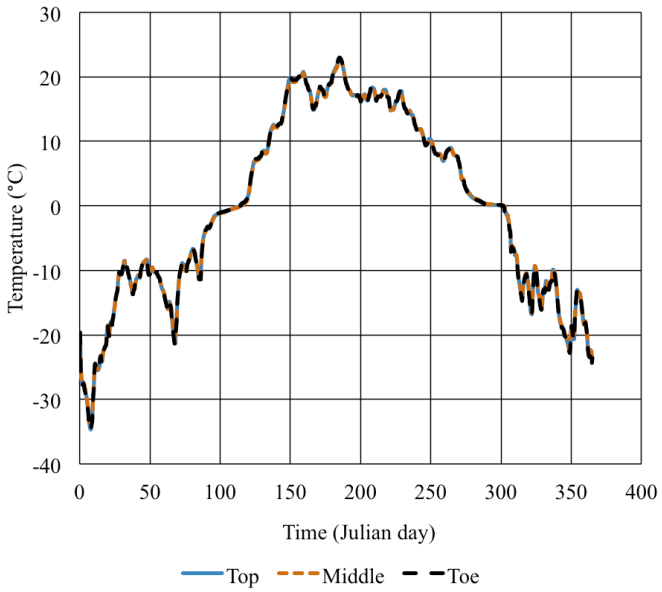

Figure 3.26 The temperature at the top, middle and toe of the west slope organic-rich layer at approximately 0.4 m depth.

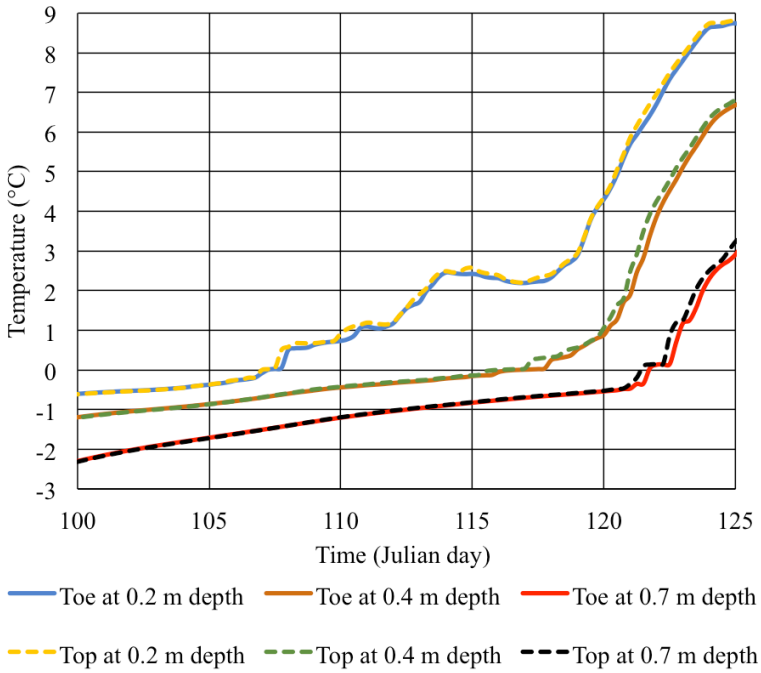

Figure 3.27 Ground temperatures of the west slope model at various soil depths. Dashed lines represent the top of the slope, while solid lines represent the toe of the slope.

The Peclet number was also found from the average snowmelt infiltration rate, 5.58×10^{-8} m/s. The infiltrating water was mostly laterally diverted and resulted in a specific discharge of 8.00×10^{-8} m/s in the west slope simulation and 1.27×10^{-7} m/s in the north slope simulation. The Peclet number was less than 1 in both cases, indicating conduction was the dominant heat transfer process (Table 3-4). Both values, however, still suggest an important role for convection.

Table 3-4 Peclet numbers for the organic-rich layer of the west and north slopes.

Scenario	West Slope	North Slope
Theoretical Maximum	753	753
Snowmelt Infiltration	0.33	0.53

There is a large potential for convection to occur within the organic-rich layer and contribute to thaw. For large fluxes, convection can dominate. The thaw pattern observed, however, is not likely due to convection, as the Peclet number for climatic snowmelt infiltration suggests conduction dominates. The observed pattern is more likely the result of the difference in ice content from top to toe. The toe of the north slope had an initial ice content of 29.2%, higher than the top's 24.2%, requiring more energy, and thus more time, to thaw. The ice content of the west slope was relatively equal from top to toe, 10.8% and 10.9% respectfully, resulting in little difference in thaw timing. These observations suggest that although convection may have contributed to different rates of ground thaw with slope position, it is not the dominant heat transfer mechanism within the organic-rich layer.

3.3.4.2 Mineral Soil

The mineral soils of the north and west slopes differed in their thermal and hydraulic properties. The clay-rich mineral soil of the north slope had lower thermal and hydraulic

conductivities than the west slope. Despite the differences in properties, the two mineral soils showed similar results.

Thaw in the mineral soil showed a similar pattern to that observed in the organic-rich layer. The top of the slope thawed faster than the toe, as shown by the 0.7 m depth temperature profile of Figure 3.27. This pattern was more pronounced on the north slope, with the top thawing two days prior to the toe (Figure 3.28). The continuation of the thaw pattern observed in the organic-rich layer is postulated to be a result of conduction and not convection.

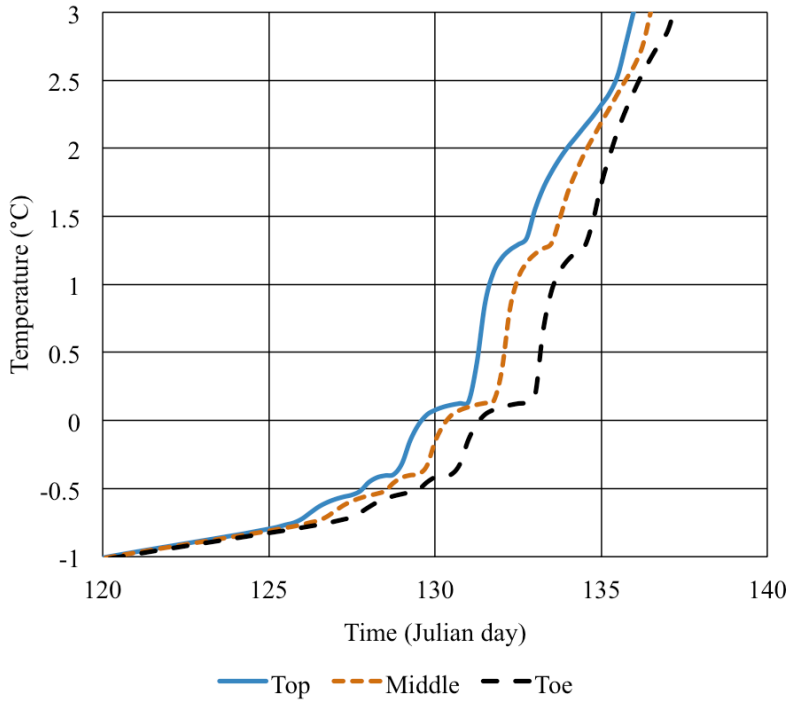

Figure 3.28 Ground temperatures taken 0.4 m into the mineral soil at the top, middle and toe of the north slope during the thaw period.

The mineral soil of the west slope thawed faster than the north slope. The thawing front reached the 0.4 m depth of the mineral layer by the 123rd day on the west slope, but not until the 129th day on the north slope. This is consistent with the thaw through the organic-rich layer. Both slopes had a zero-curtain window that lasted for approximately

two days before thaw progressed. Temperatures throughout the rest of the year remained consistent between the top, middle and toe of the slope, as shown in Figure 3.29.

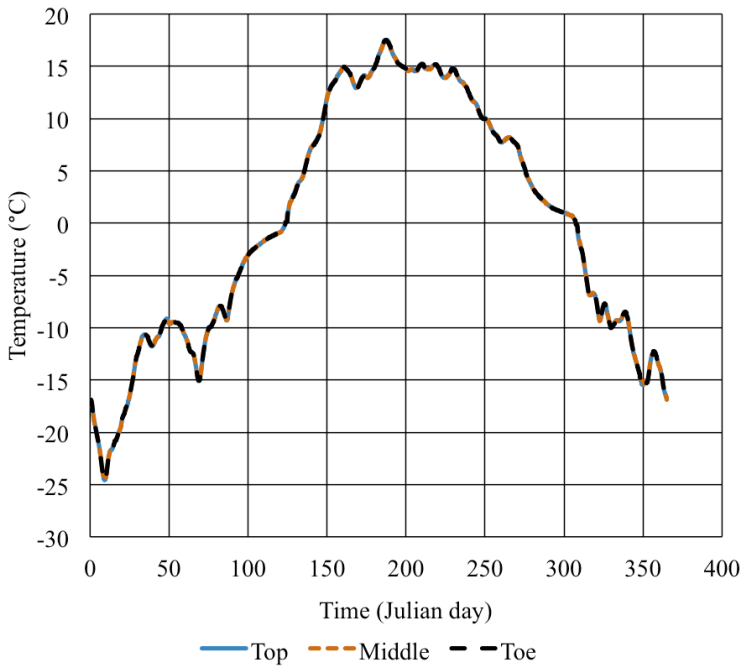

Figure 3.29 Ground temperatures taken 0.4 m into the mineral soil at the top, middle and toe of the west slope.

The textural difference between the overlying organic-rich layer and the mineral soil, and their resulting hydraulic properties, limits the amount of flow to the mineral soil. The majority of infiltrating water is either laterally diverted or released to the surface as a result of the formation of a seepage face and does not percolate beyond the organic-rich layer into the mineral soil. Therefore, the vertical flux reaching the mineral soil will be lower than the initial surface influx, reducing the water available for lateral flow.

The theoretical gravitational maximum Peclet number was determined from the maximum specific discharge that could be achieved under gravity flow. For the west slope mineral soil, the maximum specific discharge was 1.80×10^{-8} m/s. The north slope had a lower saturated hydraulic conductivity, resulting in a lower maximum specific

discharge of 9.00 x 10^{-10} m/s. The maximum Peclet number for the west slope was 0.19 and 0.075 for the north slope (Table 3-5). Both of these numbers suggest that convection cannot play a large role in heat transfer within the mineral soil of both slopes.

The west slope had larger thermal and hydraulic conductivities than the north slope, allowing more heat to be transferred through conduction and convection. The larger hydraulic conductivity of the west slope resulted in a lateral specific discharge under climatic snowmelt conditions of 4.00 x 10^{-10} m/s. Lateral flow through the north slope mineral soil achieved a specific discharge of 1.5 x 10^{-11} m/s.

Table 3-5 Peclet numbers for the mineral soil of the west and north slopes.

Scenario	West Slope	North Slope
Theoretical Maximum	0.19	0.075
Snowmelt Infiltration	0.004	0.001

The calculated Peclet number for the west slope was 0.004 and 0.001 for the north slope (Table 3-5). These small values indicate convection plays virtually no role in the transfer of heat within the mineral soil. Most of the infiltration water is laterally diverted within the organic-rich layer, limiting the amount of water percolating into the mineral soil.

Thaw through the mineral soil mirrored the pattern observed in the organic-rich layer, with the top thawing slightly faster than the toe. The Peclet numbers reveal that convection does not have a large influence on thaw in the mineral soil. The observed pattern is therefore the result of conduction continuing the pattern set in the organic-rich layer.

3.4 Failure Through Increased Conduction and Ponding

3.4.1 Introduction

Increased rates of heat conduction as a result of elevated water contents is another potential failure mode for a SFCBD cover system. Conduction is often assumed to be the

dominant mechanism of heat transfer in a soil (Smerdon et al. 2003, 2004). This section will investigate conduction and the effect of surface ponding on thaw through a simulation of a depression.

The phenomenon of increased thaw due to ponding water has been observed in the Canadian Prairies. Hayashi et al. (2003) observed that during spring snowmelt, the ground remained frozen, preventing infiltration and creating surface runoff, which collected in local depressions. The ponded water increased radiation trapping and conductive energy transfer to the ground beneath the depression, resulting in increased rates of thaw and infiltration below the depression.

Air has a thermal diffusivity of approximately 0.21 x 10^{-7} m^2/s (Andersland and Ladanyi 1994), while water has a thermal diffusivity of 1.4 x 10^{-7} m^2/s (Andersland and Ladanyi 1994). Both the thermal conductivity and volumetric heat capacity increase as air is replaced with water in the soil (Figure 2.4 and Figure 2.5), resulting in a rapid increase, at first, in thermal diffusivity with increasing water content, followed by a slower decrease in thermal diffusivity at higher water contents. This occurs as a result of the more rapid increase in thermal conductivity at lower water contents, while the increase in volumetric heat capacity is linear. The higher thermal diffusivity means that the average temperature of a higher water content soil will increase more rapidly than the same soil at lower water contents.

3.4.2 Model Setup

3.4.2.1 Domain

Modelling of this potential failure mode differed from the previous two models in that these models were not based on an actual field site; rather, the phenomenon was examined at a hypothetical site based on prairie hydrostratigraphy and Wolf Creek climate. A synthetic model was built to provide optimal conditions for ponding and increased conduction to occur. A representative prairie soil profile of three materials was used. The uppermost material, an organic-rich clay, was 0.4 m thick. The underlying clay was 1 m thick. The base of the profile was a thick layer of unoxidized till.

The model was setup as a two-dimensional model with two slopes leading into a depression, as shown in Figure 3.30. The main portion of each slope had a slope gradient of 0.1. Shallower slopes provided a more natural transition between the steep slopes and the horizontal areas of the model. The simulation was run for 365 days in two-hour time steps.

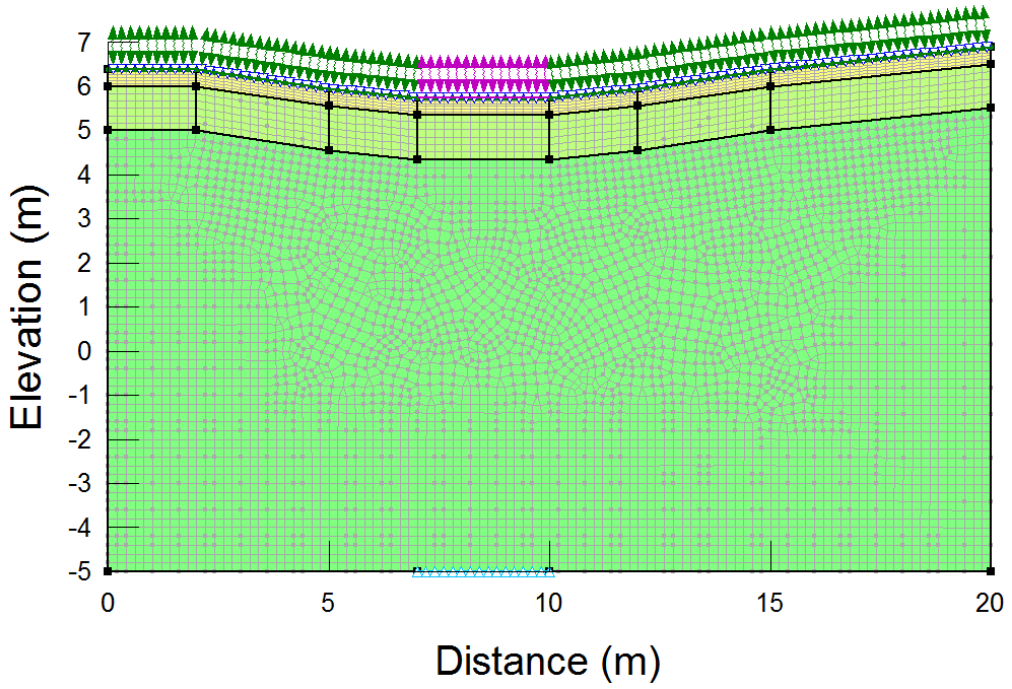

Figure 3.30 Model domain for the increased conduction simulations. The model was setup to allow water to pond in the depression.

A ground surface layer allowed for fine discretization of the near surface zone and surface ponding. Six vertical elements formed the discretization of the ground surface layer. Quad and triangle elements, approximately 0.2 m in size, created the finite element mesh in the rest of the domain.

3.4.2.2 Material Properties

The study site of Hayashi et al. (2003) was underlain by tills with high clay contents. The thermal conductivity of clay does not vary as much with water content as for other materials, as seen in Figure 2.4. A soil profile similar to the one presented in van der

Kamp and Hayashi (1998) was used in the simulation, consisting of an upper organic-rich clay mixture underlain by a clay and followed by an unoxidized till.

Typical properties of each of the materials defined the material functions needed for analysis. The water retention curves were determined through the van Genuchten equation (Equation 3.4) and the texture-based estimator in GeoStudio, which requires the saturated volumetric water content. This value was 0.81 for the organic-rich clay and 0.71 for the clay and unoxidized till (Fredlund and Rahardjo 1993). The water retention curves are shown in Figure 3.31. The hydraulic conductivity functions were determined with the van Genuchten method (van Genuchten 1980) within GeoStudio. The saturated hydraulic conductivity of the organic-rich clay was 3.00×10^{-6} m/s, 3.00×10^{-7} m/s for the clay and the 3.00×10^{-8} m/s for the unoxidized till (van der Kamp and Hayashi 1998). The estimated functions are shown in Figure 3.32.

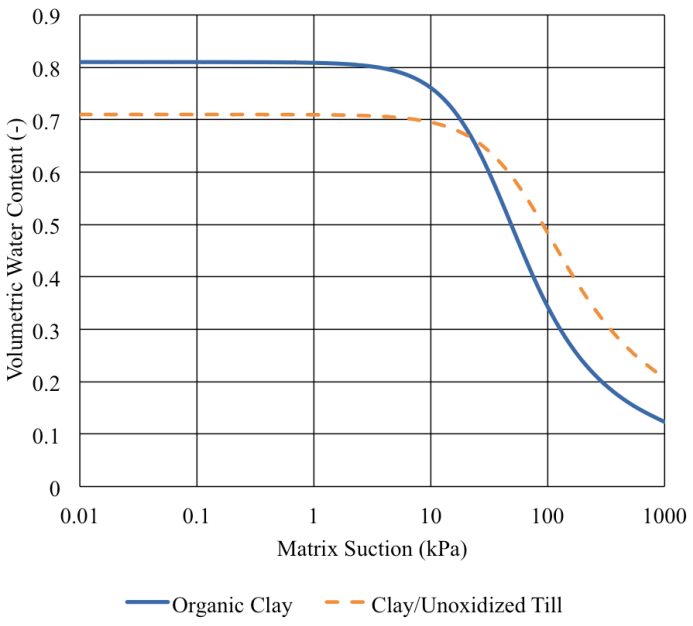

Figure 3.31 The water retention curve for the materials used in the ponding and increased conduction simulation.

The thermal properties of the clay and unoxidized till were assumed to be similar enough that they could be modelled using the same properties. The thermal conductivity function for each material was estimated in GeoStudio using the Johansen Method. The material mineral thermal conductivity used in this method was 0.1 J s^{-1} m^{-1} K^{-1} for the organic-rich clay and 1 J s^{-1} m^{-1} K^{-1} for the clay and unoxidized till. The resulting functions of thermal conductivity against volumetric water content are shown in Figure 3.33.

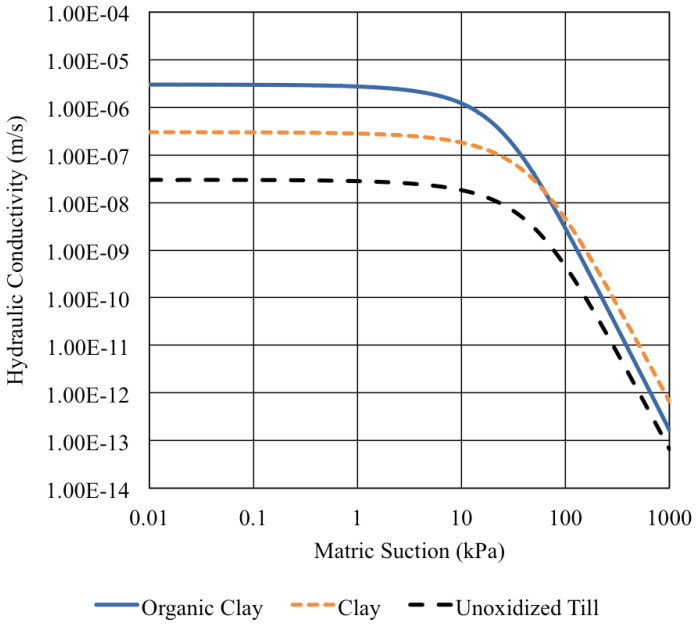

Figure 3.32 The hydraulic conductivity function of the materials used in the increased conduction and ponding simulation.

The volumetric heat capacity function was estimated with the de Vries Method in GeoStudio. A mass specific heat capacity of 0.92 J kg^{-1} K^{-1} was used for both materials to generate the volumetric heat capacity function, as shown in Figure 3.34. The unfrozen water content function was calculated based on texture and is shown in Figure 3.35.

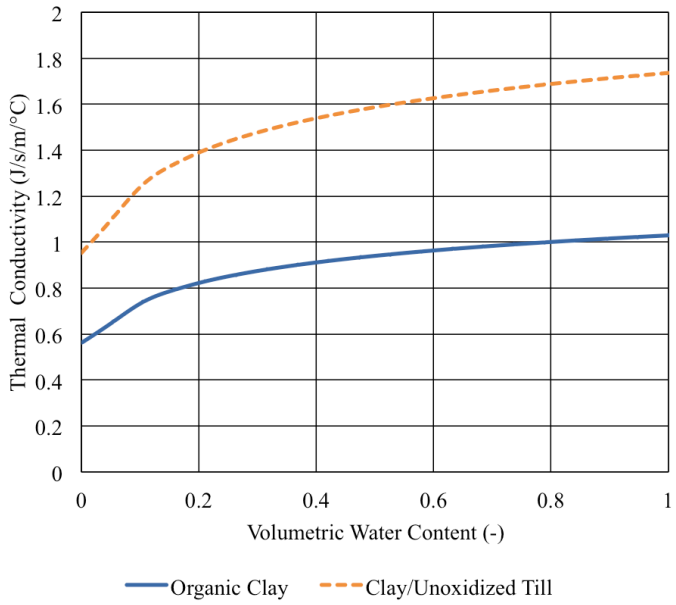

Figure 3.33 The thermal conductivity function of the materials used in the ponding and increased conduction simulation.

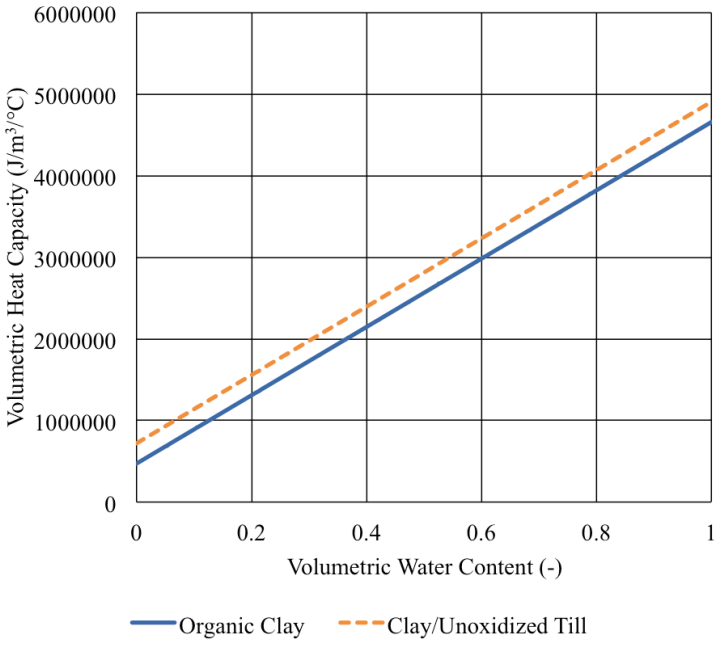

Figure 3.34 Volumetric heat capacity function for the materials used in the ponding and increased conduction simulations.

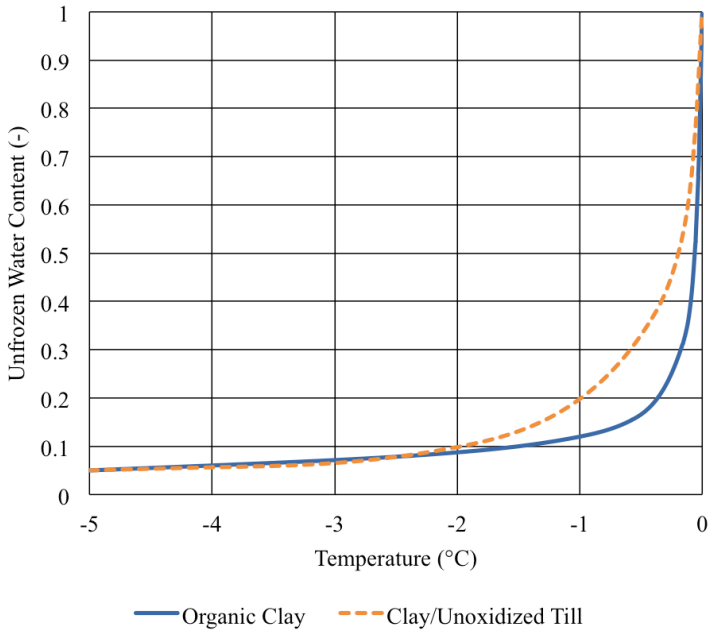

Figure 3.35 The unfrozen water content function for the materials used in the ponding and increased conduction simulations.

3.4.2.3 Boundary Conditions

A full surface energy balance was required to take into account the increased capture of energy and subsequent conduction by the ponding surface water. GeoStudio's Land Climate Interface (LCI) boundary condition calculated the surface energy balance. The LCI boundary was implemented using the Wolf Creek climate data set outlined in the previous section, which was chosen for consistency between models and its availability. Figure 3.20 and Figure 3.21 show the air temperature and wind speed used as inputs for the LCI condition. The latitude of the Wolf Creek basin was used to estimate the solar radiation and albedo was based on literature values. The albedo of the surface in the depression was changed to represent surface ponding for a few weeks following snowmelt.

As in previous analyses, a surface flux function was used to simulate snowmelt and infiltration. A step function building up to maximum surface flux of 1.00×10^{-7} m/s was created and applied over 30 days. The initial water content of the materials was set at high levels of saturation, around 90%, to encourage rapid ponding.

3.4.3 Results

The results of the simulations were assessed mainly through changes in water content, ground thaw depths and patterns, changes in thermal conductivity and ground temperatures. As this simulation was not a replication of a field site, there are no direct observations for comparison. Instead, patterns and phenomena can be compared to similar field studies.

3.4.3.1 Thaw Patterns

Thaw of the depression was accelerated relative to the uplands due to the surface ponding that occurred during the simulation. The volumetric water content in the depression of the organic-rich clay increases to saturation by the 119th day of the year and remained saturated for the several days before declining slowly. The uplands do not reach saturation but experience a slight increase in water content around the time of melt (Figure 3.36). The water content in the depression remains at elevated saturation relative to the uplands for the remainder of the simulation.

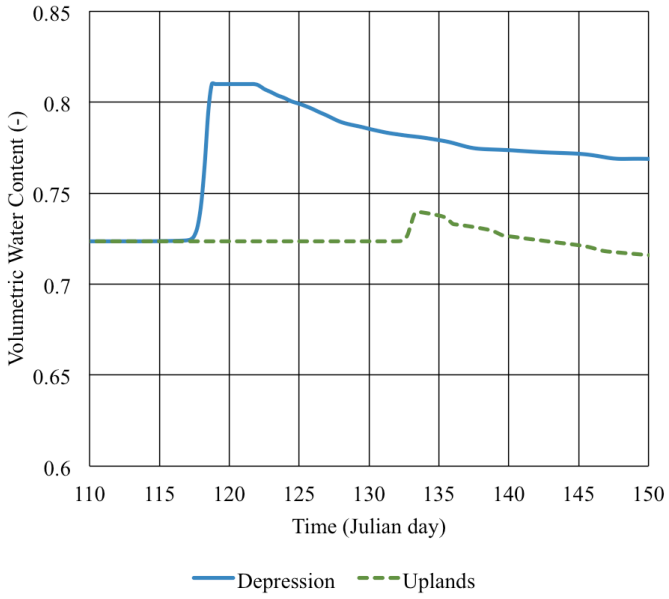

Figure 3.36 Volumetric water content under the uplands and the depression.

Thaw beneath the depression reached the base of the organic-rich clay by the 121st day. A zero-curtain developed that lasted for two days (Figure 3.37). Thaw on the uplands was slower, reaching the base of the organic-rich clay 14 days after the depression on the 135th day. This pattern of greater thaw under the depression continued until the thawing front at the uplands reached a zone of saturation. At 135 days, thaw had reached a depth of 1 m in some places beneath the pond, but only 0.7 m on the uplands.

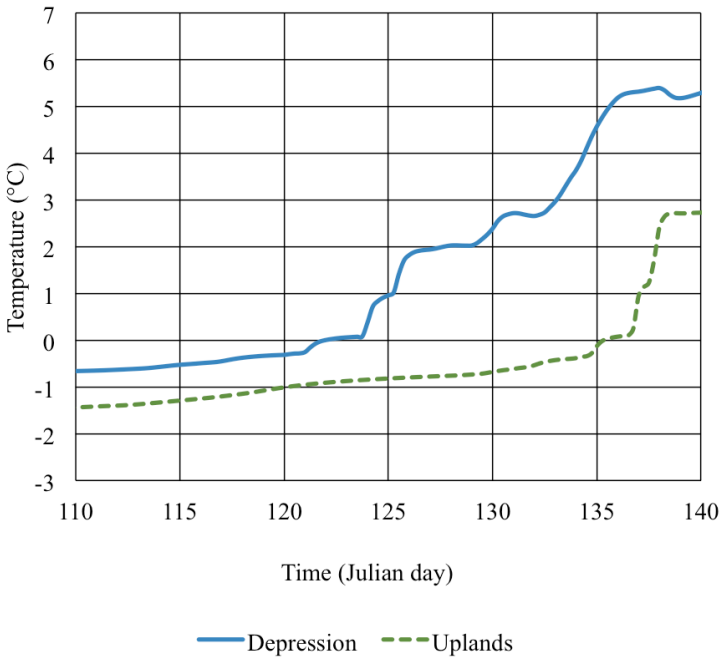

Figure 3.37 Temperatures simulated at the base of the organic-rich clay beneath the depression and the uplands.

Thaw beneath the pond progressed as described in and shown by the conceptual model of Figure 10a in Hayashi et al. (2003). Thaw was not uniform, but occurred in localized areas under the depression. The thaw front propagated downward behind the wetting front at all locations in the model after reaching the zone of saturation on the uplands.

3.4.3.2 Heat Transfer

The degree of saturation influences the thermal conductivity and diffusivity of an unfrozen soil due to differences in thermal conductivity and diffusivity between air and water. A frozen soil has a higher thermal conductivity and diffusivity than if it was

unfrozen due to the larger thermal conductivity and diffusivity of ice compared to water or air.

At the beginning of the simulation, the uplands and the depression shared the same value of thermal conductivity (2.50 J s^{-1} m^{-1} K^{-1}) due to the ice content being the same at both locations. Once thaw began, the thermal conductivity dropped as the ice was replaced with unfrozen water. However, at the same time as thaw in the depression, the thermal conductivity increased for a few days during the zero-curtain, at which time ice and water could coexist in the soil. The thermal conductivity below the depression dropped and stabilized at a value of 1.00 J s^{-1} m^{-1} K^{-1} after thaw, while the uplands remained at the higher thermal conductivity due to the still frozen soil (Figure 3.38).

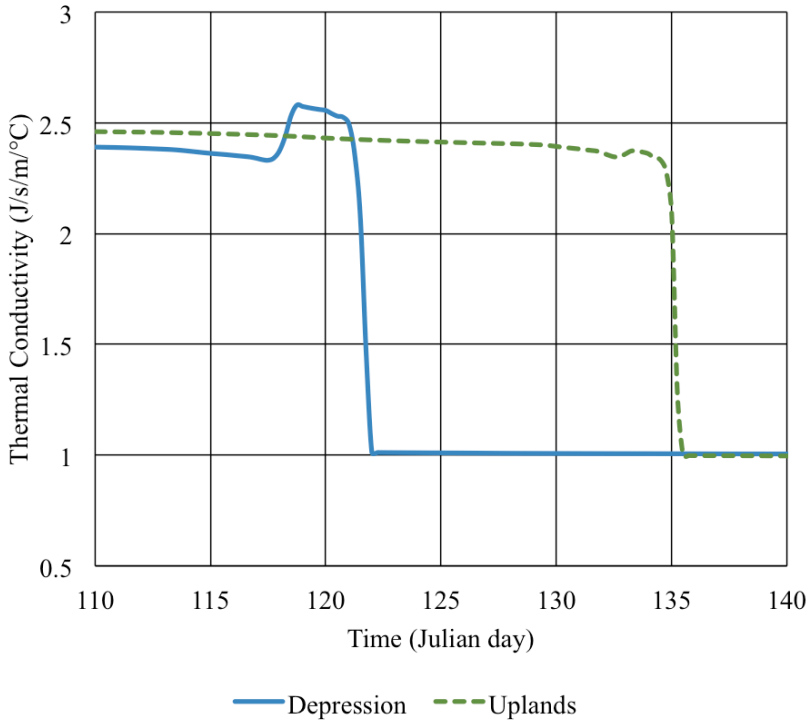

Figure 3.38 Thermal conductivity values of the soil beneath the depression and the uplands.

The thermal diffusivity during the same time period was initially higher beneath the uplands than under the depression, but during thaw of the depression, the thermal

diffusivity of the depression increased and remained higher than the uplands until thaw occurred in that region (Figure 3.39). The larger thermal conductivity and diffusivity during thaw under the pond and the decreased albedo on the surface encouraged more heat flow to occur during the thaw period than at the uplands. The heat flux through the surface increased in the depression following the end of snowmelt at around the 85th day. The uplands did not experience a major increase until the 120th day. During this period, more energy was transferred through the surface at the depression than at the uplands, contributing to the increased thaw.

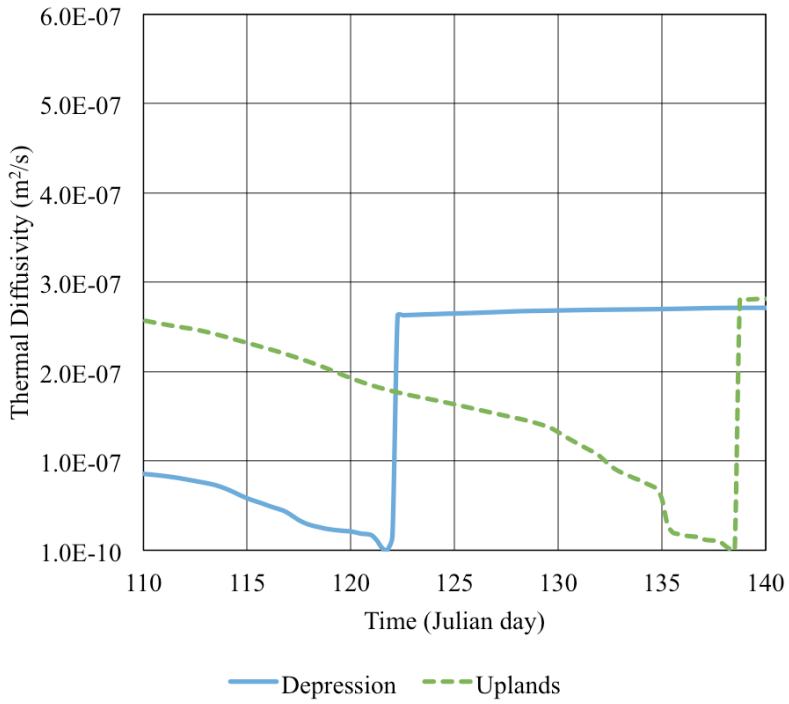

Figure 3.39 Thermal diffusivity values of the soil beneath the depression and the uplands.

The depression began to experience an increase in the heat flux at the base of the organic-rich clay relative to the uplands starting around the 90th day (Figure 3.40). The depression remained at an increased heat flux relative to the uplands until the 140th day, increasing the thaw under the depression. The increased thermal conductivity and diffusivity of the soil under the depression during the thaw period and the lower surface albedo allowed

more heat to be transferred to the soil below, thereby increasing the thaw under the depression.

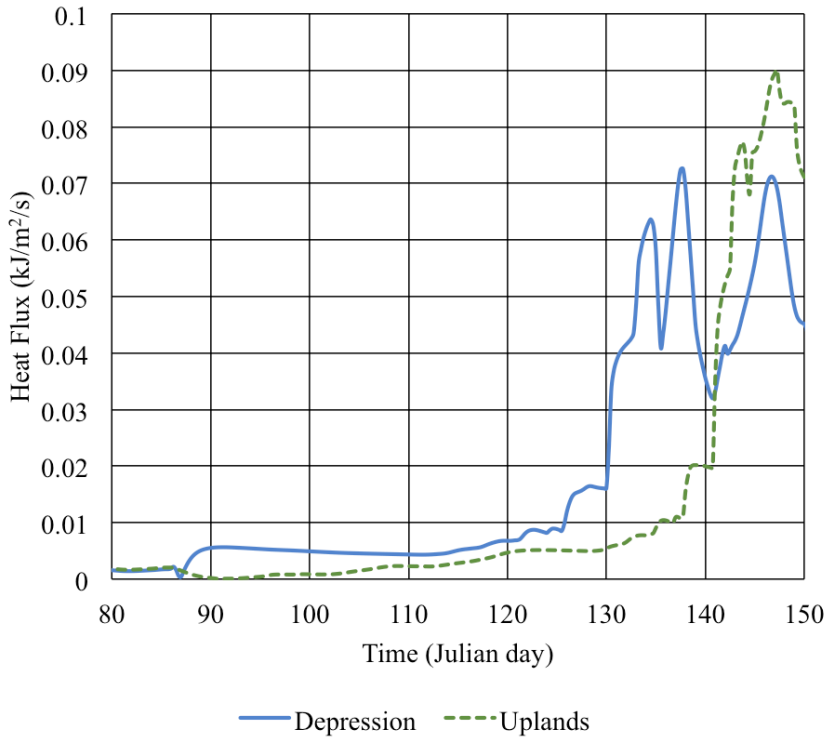

Figure 3.40 Heat flux under the depression and the uplands.

Water flow through the base of the organic-rich layer was greater under the depression than at the uplands during thaw. Figure 3.41 shows the temperature of the organic-rich layer along with the water flow vectors, represented by the blue arrows. The water flow under the depression on the 140th day was 3.4 x 10^{-8} m/s, compared to 1.1 x 10^{-13} m/s under the uplands.

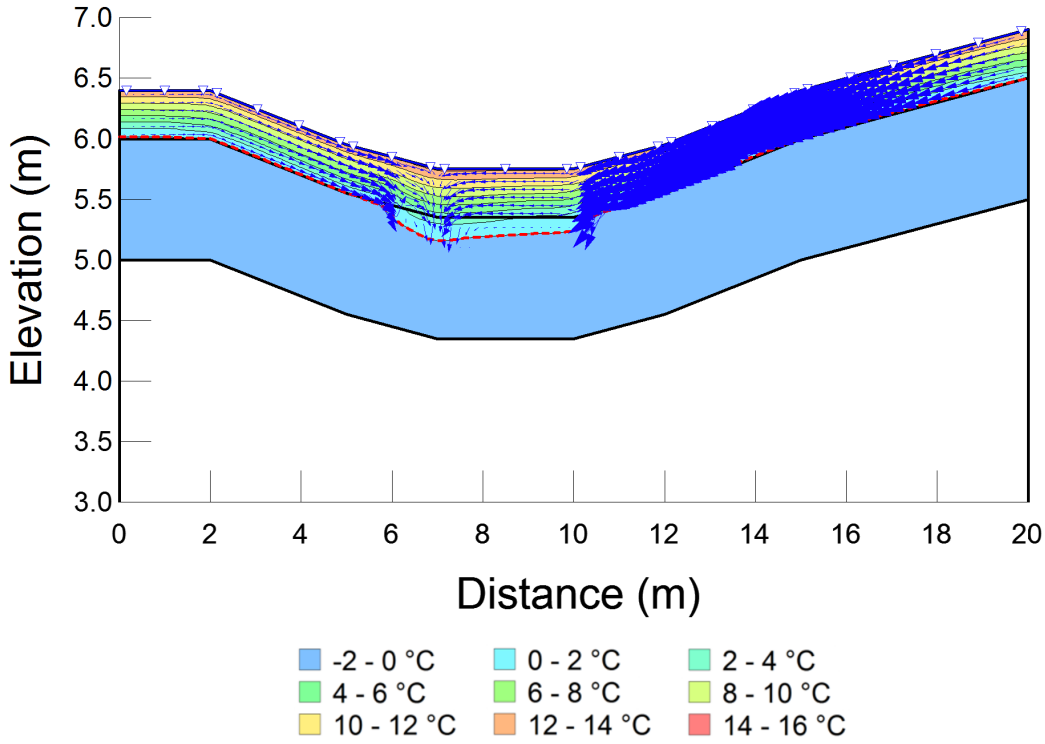

Figure 3.41 Temperature and water flow (blue arrows) through the organic-rich layer on day 140. The red dashed line represents the zero-degree isotherm, or the thawing front. Note the vertical exaggeration.

3.5 Discussion

3.5.1 Vertical Convection

The temperature results and the calculated Peclet numbers of the Watanabe column simulations tend to suggest different impacts of convection on thaw. The calculated Peclet numbers increased with increases in specific discharge, while the thaw rate decreased. The higher Peclet numbers indicate an increased role for convection. In the cases of the middle and high fluxes, the Peclet number was above one, suggesting that convection should be the dominant heat transfer process. However, the thaw rates show that thaw actually decreases when more water is added to the system. If, as the Peclet numbers suggest, convection was the dominant heat transfer process occurring, it would be expected for the increase in water flow through the column to increase the heat being

convected with the water and thus increasing the thaw occurring. However, another alternative would be that convection is countering conduction from the base of the column, slowing thaw.

The quickest thaw occurred in the low water content column with the low flux, where the Peclet number is only 0.05. This would indicate that the heat transfer within the column is heavily dominated by conduction. This simulation also experienced the least increase in volumetric water content due to the surface flux.

The difference in thaw rates between the simulations can be attributed to different initial water contents, refreezing and the conductive heat transfer from the column bottom. The thaw rate varied between the columns of different initial water contents even with the surface flux held constant. This is likely the result of the increase in ice content that results from higher initial water contents. Higher ice contents require more energy to thaw and therefore, more time.

The surface fluxes added additional water to the columns, increasing the water content. Some of the percolating water froze upon reaching the sub-zero temperatures of the frozen layer. The larger amounts of water added to the system would result in more refreezing at the frozen zone, increasing the time required for thaw and decreasing the overall thaw rate. Freezing of water releases latent heat, which can be conducted downwards, upwards or carried away by flowing water. The larger water flows are able to carry more of this heat away, decreasing the energy available for thaw. The smaller flows transport less heat away, leaving more energy to warm up the surrounding soil.

During the simulations, additional heat was added through conductive heat transfer from the constant temperature bottom boundary condition. More heat from the bottom reached the frozen layer and contributed to thaw during the low flow scenarios compared to higher flows (Figure 3.8). The larger water flows counteracted the upward conduction, limiting the amount of heat that arrived at the frozen layer from the bottom of the column. Underneath the frozen layer, the water flow was in the opposite direction of thaw. Lunardini (1998) found that water flow in the direction opposite of thaw reduces the amount of melt that occurs.

The larger Peclet numbers support this conclusion, as they indicate a larger role for convection relative to conduction. In these simulations, with the dominant conduction being from the bottom, the role of convection is not to increase thaw, but to diminish it by diminishing conduction.

Convection, despite the large Peclet numbers for several of the simulations, does not appear to play a large role in increasing the thaw of a frozen soil. The larger water flows, with higher Peclet numbers, instead strip heat from the frozen soil and delay thaw. In the simulations where conduction dominates, thaw is the quickest.

3.5.2 Lateral Convection

The modelled slopes showed similar patterns of thaw depth and water flow within the organic-rich and mineral layers. The calculated Peclet numbers reveal the limited influence of convection on thaw in most cases. The assumption that conduction dominates in soil heat transfer holds for the spring freshet in the Wolf Creek basin.

For large fluxes of water, the large Peclet numbers of the organic-rich soil for both slopes indicates the potential for convection to dominate. Under climatic conditions of snowmelt infiltration however, the influence of convection drops and conduction dominates.

The Peclet numbers for the north slope mineral soil make it clear that convection plays little to no role in thawing the layer. The low hydraulic conductivity restricts water flow, which reduces convection's influence.

The calculated Peclet numbers for the organic-rich layer can be compared to the Peclet numbers found by Kane et al. (2001) for an organic mat in the Imnavait Creek watershed. The maximum specific discharge of the model gave Peclet numbers several orders of magnitude larger than the approximately 0.04 found by Kane et al. (2001). However, these values are the maximum theoretical values and are based on the saturated hydraulic conductivity. The specific discharges obtained under the climatic snowmelt infiltration conditions are a more realistic comparison. The Imnavait Creek had a surface flux of 2.8×10^{-7} m/s (Kane et al. 2001), while the simulations used an influx of 5.58×10^{-8} m/s.

The simulations produced Peclet numbers that were approximately one order of magnitude larger than the Imnavait Creek Peclet number.

The theoretical values of the mineral soils were also larger than the Imnavait Creek value of ~0.001 (Kane et al. 2001), but did not differ as greatly as the organic layer. Under the climatic snowmelt conditions, the mineral soil of both slopes had a Peclet number of the same order of magnitude as Imnavait Creek.

The slightly increased thaw at the top of the slope relative to the toe of the slope, as observed by Carey and Woo (1998) on the north slope (Figure 3.12), is likely not a result of convective energy transfers. Instead, it is likely that the differential thaw occurs as a result of differences in ice content along with variability in local snow depth and melt. Although snow cover was not included in the 2D simulations, variability in depth and melt timing is likely a large contributor to the observed differential thaw (Quinton et al. 2009). Within the simulations, the toe of the north slope had a higher ice content, requiring more energy and time to thaw than the top. On the west slope, the difference in ice content was much smaller than on the north slope, resulting in a small difference in thaw times.

The low Peclet numbers for the mineral soil of both slopes confirms that the observed thaw pattern is not a result of convection, but a continuation of the thaw pattern of the organic-rich layer through conduction.

In a soil with a large hydraulic conductivity, like the organic-rich layers of both slopes, there is the potential for convection dominated heat transfer. However, it is unlikely that snowmelt infiltration itself would be able to produce a large enough lateral flux for this to occur. Larger fluxes than snowmelt infiltration could be generated through the addition of water from run-on. Ponded water or surface run-off moving onto the slope from above could create the flow necessary for convection to dominate.

The use of a temperature boundary condition simplifies the problem greatly. However, as water moves downslope, the water content at the toe increases and there may be a greater potential for energy flux at the toe due to the wetter conditions, potentially increasing

radiation and conduction. In addition, the current modelling cannot account for water flow across the surface of the ground. If there is surface runoff, this may also have an influence on thawing as this flow accumulates towards the base of the slope. Therefore, a true surface energy balance approach should be taken to fully understand the Wolf Creek basin.

The materials selected for use in a SFCBD cover system could include high hydraulic conductivity sands and gravels. It is important to note that the thermal conductivity of sands and gravels are typically an order of magnitude larger than for organic soils (Andersland and Ladanyi 1994). The increase in thermal conductivity would allow more heat to be transferred by conduction, lowering the influence of convection and the Peclet number. Larger hydraulic conductivity could generate larger discharges, but recharge tends to be limited by the availability of water, rather than the hydraulic conductivity for coarser-grained material.

The likelihood of convection causing premature thaw and failure of the frozen barrier layer during the spring freshet is quite small. As the thaw will be dominated by conduction, convection will be minor and not be the cause if such a failure were to occur.

3.5.3 Increased Conduction

The results of the increased conduction simulation are consistent with the phenomenon observed by Hayashi et al. (2003). During the simulation, water from the uplands collected and ponded in the surface depression, thereby increasing the energy transfer to soil below the depression. Increased energy transfer caused more thaw below the depression than on the uplands. During the zero-curtain under the depression, the thermal conductivity and diffusivity increased, which would increase the energy transfer and promote further thaw.

Increased radiation capture due the surface ponding was represented in the simulation by the lowered surface albedo of the depression during the ponding period. The lowered albedo increased the energy transfer through the surface, increasing thaw. This process

was observed by Hayashi et al. (2003) and was postulated to have a major influence on the thaw beneath the depression.

This simulation was not a replication of field conditions, but a synthetic domain that provided optimal conditions for ponding. The slopes into the depression are likely to be at a steeper grade than would be expected in a natural Prairie environment, such as Hayashi et al. (2003), but also lesser than the possible slope of a mine waste cover system like the SFCBD cover.

Steeper slopes were used to ensure that the model focused on only one process. Shallower slopes would allow greater amounts of vertical percolation, limiting the amount of water in the surface pond and influencing the final outcome.

Of the three possible failure modes explored, the increased conduction failure mode seems to provide the most likely scenario that could cause a SFCBD cover system to fail. While a surface depression that could develop on a SFCBD cover would likely not be as large as the depression used in the simulation, even a small depression, like an erosion feature or animal burrow, could cause ponding and increased water contents in the soil around the feature. Mine waste is likely to have depressions, as there will always be some differential settlement due to consolidation, weathering or thaw of previously frozen zones. The ponding and increased water contents associated with depressions would lead to increased energy transfer and accelerated thaw. Once the frozen layer has thawed completely under the depression, it would become the path of least resistance for water flow, causing infiltration and percolation into the soil below the frozen layer.

The three failure modes and their application to cover design are explored in more detail in simulations of a SFCBD cover system in the next chapter.

4 SFCBD MODEL AND DESIGN

4.1 Introduction

The final phase of the research was to illustrate how the performance of a potential SFCBD cover design could be simulated for a number of different design alternatives. The geometry of each simulation was varied to create the conditions that would allow one of the potential failure modes to dominate. The cover was designed using the climatic conditions and materials available at the Giant Mine site in Northwest Territories, Canada.

4.2 Site Background

The Giant Mine is former gold mine located approximately 5 km north of the city centre of Yellowknife, NWT. It operated from 1948 until closure in 2004. Gold was mined from a deposit containing arsenopyrite, which created arsenic-rich gases. From 1951 until 1999, the arsenic gas was captured as arsenic trioxide dust and stored in sealed underground storage areas. The captured dust is about 60% arsenic in a form that is soluble in water (SRK Consulting 2007). During the life of the mine, 16 million tonnes of tailings were also produced and stored on site, which are also contaminated with arsenic (SRK Consulting 2010).

Ownership of the mine changed several times during operation of the mine. In 1999, the then owner of the mine, Royal Oak Mines Inc., went into receivership and the mine was transferred to the Department of Indian Affairs and Northern Development, now Aboriginal Affairs and Northern Development Canada (AANDC). Miramar Giant Mine Ltd. purchased the mine from AANDC but was indemnified for existing environmental liabilities, which remained with AANDC. Mining at a reduced scale continued until July

2004. In 2005, Miramar Giant Mine Ltd terminated its obligations under the Reclamation Security Agreement and Giant Mine became orphaned and abandoned (SRK Consulting 2007). The mine is now part of the Northern Contaminated Sites Program and is in the process of being remediated by AANDC and its contractors (INAC 2010).

4.3 Model Setup

4.3.1 Domain

Modelling was performed using the Preview release of GeoStudio 2014. Due to convergence issues with the Preview release, the maximum slope length that could be simulated was 30 m. With the length limited, the simulation represents only a part of a larger cover system. The slope length remained the same for all simulations and the primary difference between simulations was in slope geometry.

The three models shared the same soil profile, varying only in the overall geometry of the slope. The slopes were modelled as a cover system overlying mine waste/tailings. The cover was composed of a sand layer placed between two gravel layers. The surface gravel layer was 0.5 m thick in all models and was discretized by ten vertical elements. The bottom gravel layer was 2 m thick and the middle sand layer was 0.5 m thick, each discretized by quad and triangle elements approximately 0.2 m in size. In an actual SFCBD cover system, it is likely the uppermost gravel would be overlain by an organic soil that would promote vegetation growth. This was not simulated in order to simplify the model and focus on the fundamental mechanisms of the cover itself.

The mine waste/tailings were represented in all of the models as a 6 metre thick, low hydraulic conductivity, saturated silt. This ensured the bottom of the cover would not be heavily influenced by boundary conditions applied at the base of the model.

4.3.1.1 Model 1: Steep Slope

The first simulation used conditions which were more likely to create lateral convection by using a steep slope of 0.2 (vertical/horizontal distance) as shown in Figure 4.1. The high gradient should promote lateral water flow within the sand and gravel layers, which can carry heat down the slope through advection.

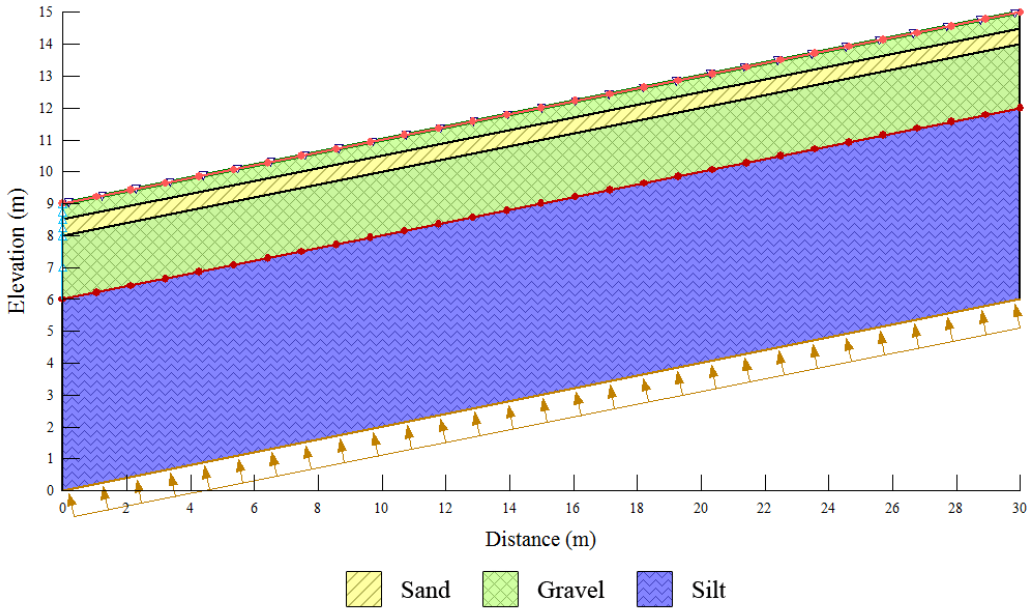

Figure 4.1 Model domain for a steep sloped SFCBD cover system. The steep slope should encourage lateral flow within the upper gravel and increase the role of lateral convection.

4.3.1.2 Model 2: Shallow Slope

The second simulation was selected to enhance vertical convection. The slope gradient was reduced to 0.1 to reduce lateral flow and encourage vertical flow (Figure 4.2). With increased vertical flow, there is a greater likelihood of heat being convected vertically rather than laterally. This situation would not be ideal for an actual SFCBD, as the main function of the cover is to limit net percolation by shedding the melt water downslope. However, it remains a possible failure mode, especially for shallow slopes.

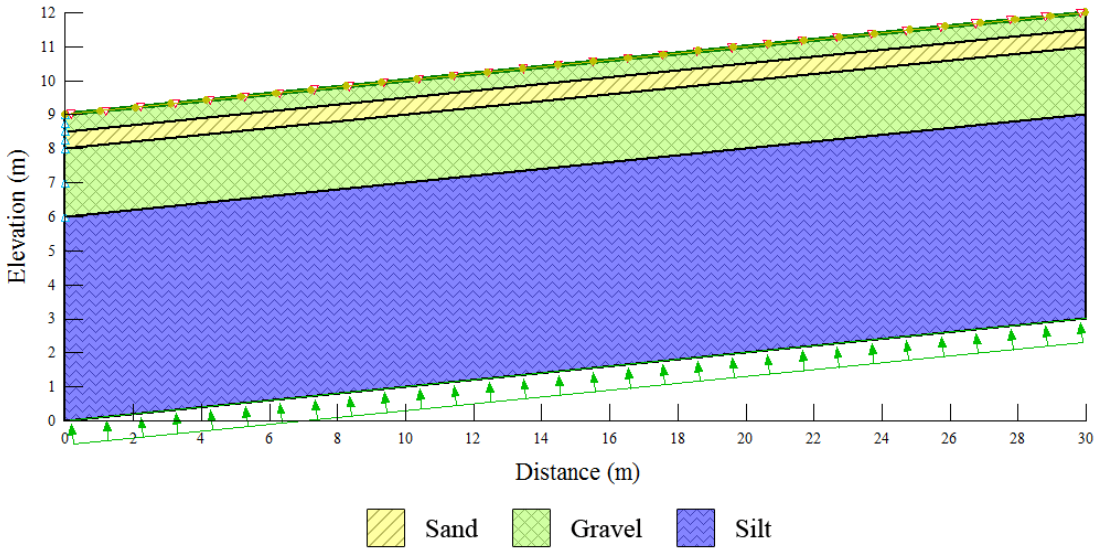

Figure 4.2 Model domain for a shallow sloped SFCBD cover. The shallow slope should encourage vertical flow and vertical convection.

4.3.1.3 Model 3: Slope with Depression

The third simulation evaluated the potential impact of a mid-slope depression which might create conditions for depression-focused recharge and increased conduction. The model domain was more complicated than the previous SFCBD models, as a bench/depression needed to be introduced to allow water to pond. A 1 m bench was added in the middle of the 0.1 gradient slope (Figure 4.3). A depression that could represent an erosional or subsidence feature was added to the bench of the uppermost gravel layer. The depression was a surface feature, but also had a subsurface expression at the bottom of the gravel layer, allowing interflow to collect within the gravel layer and increase the thermal conductivity.

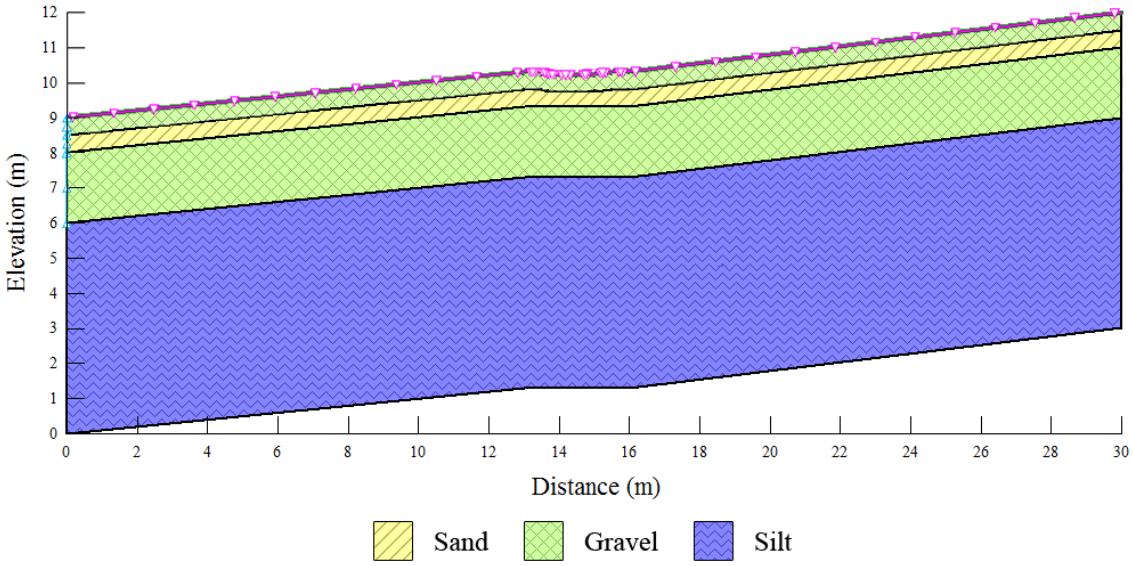

Figure 4.3 The model domain for a SFCBD cover system with a bench and depression to allow water to pond and create the conditions for increased conduction.

4.3.2 Material Properties

The cover materials selected for the simulations reflect materials that are available at the Giant Mine site. Borrow material reports focused mainly on fine-grained materials, but also mention nearby sands and gravels obtainable offsite (Golder Associates Ltd. 2004). One of the key features of the SFCBD cover system is its ability to incorporate coarse-grained materials, as many northern locations lack fine-grained materials. Therefore, despite the presence of fine material at the Giant Mine site, sand and gravel were used in the simulations.

The properties of the fine-grained material at the site had been undertaken; however no test data was available for the coarse-grained materials. For these simulations, typical idealized properties of sand and gravel were used. GeoStudio includes built-in functions to estimate properties of different materials. These functions, along with data from other sources, were used to estimate the properties of the materials. The mine waste/tailings were simulated through the use of a low hydraulic conductivity silt material.

The sand had a bulk density of 1.6 g/cm^3 and a porosity of 0.4, while the gravel had a bulk density of 1.9 g/cm^3 and a porosity of 0.25 (Fredlund and Rahardjo 1993). The silt had a bulk density of 1.5 g/cm^3 and a porosity of 0.45 (Fredlund and Rahardjo 1993). The water retention curves (WRC) for all three materials were estimated in GeoStudio using the built in sample functions and the saturated water content, which was given by the porosity for the materials used. The water retention curves for the materials are shown in Figure 4.4.

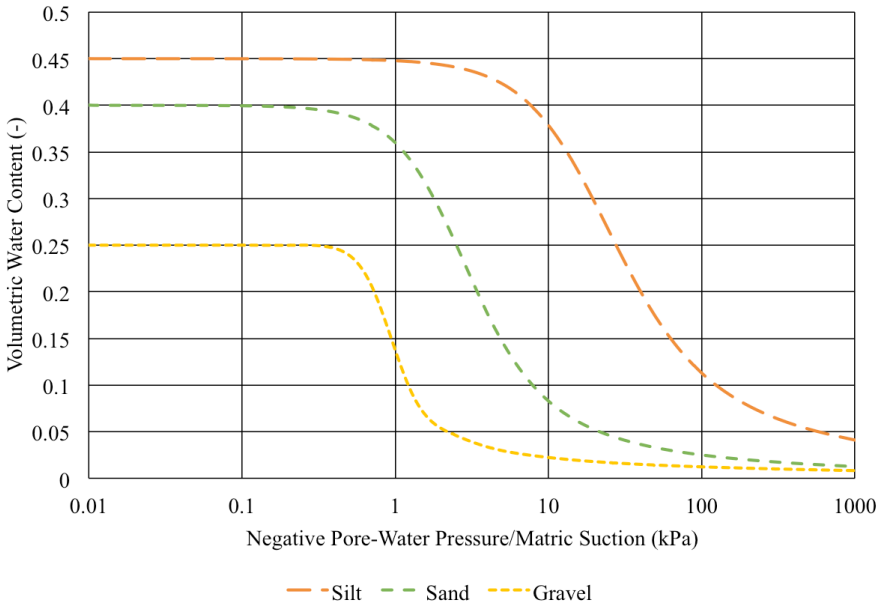

Figure 4.4 The water retention curve (WRC) for the sand, gravel and silt materials used in the SFCBD cover simulations.

The hydraulic conductivity functions for the materials were estimated in GeoStudio with the van Genuchten method (van Genuchten 1980) using the saturated hydraulic conductivity, the residual water content and the water retention curve. A saturated hydraulic conductivity of 1.00 x 10^{-4} m/s was used for gravel, 1.00 x 10^{-7} m/s for sand and 1.00 x 10^{-8} m/s for the silt (Freeze and Cherry 1979). The sand had a residual water content of 0.01, while the silt was 0.04 and the gravel was 0.01. The hydraulic conductivity functions for the materials are shown in Figure 4.5. Anisotropy was arbitrarily introduced into Model 1 to further encourage lateral flow, but it would be

reasonable to expect anisotropy in the layers due to construction of the layers in lifts. The vertical hydraulic conductivity of the upper gravel and the sand was reduced to 75% of the saturated horizontal conductivity.

At low values of matric suction, the hydraulic conductivity of the gravel is higher than the sand, promoting flow within the gravel layer instead of the sand layer. At these low matric suctions, the gravel remains at sufficient levels of saturation to ensure a higher hydraulic conductivity and allowing water to flow through the larger pores. As the matric suction increases, the larger pores begin to drain, lowering the hydraulic conductivity of the gravel, while the sand remains at a higher saturation. At a matric suction of approximately 5.7 kPa, the hydraulic conductivity of the sand starts to be higher than that of the gravel. Therefore, flow at higher matric suctions will preferentially occur in the sand layer.

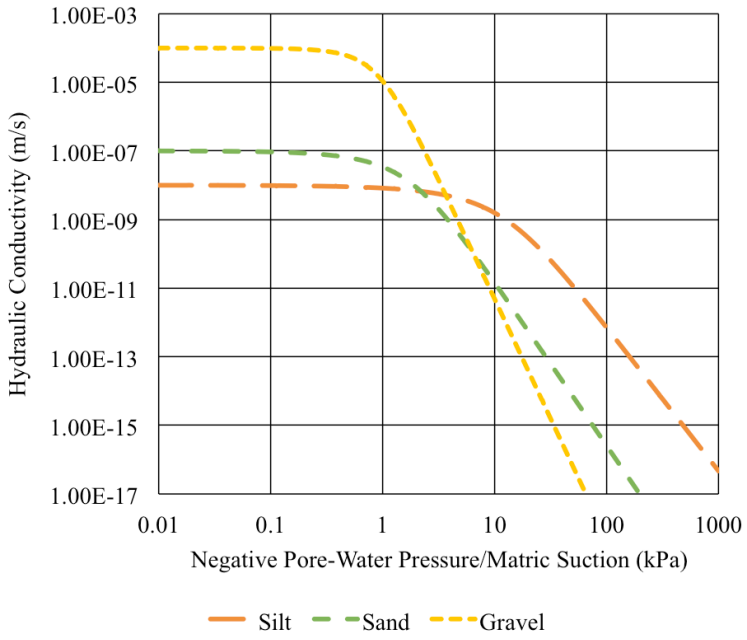

Figure 4.5 The hydraulic conductivity functions for the materials used in the SFCBD cover simulations.

Thermal properties for all three materials, like hydraulic properties, were determined using the estimation tools within GeoStudio. The thermal conductivity functions of the materials were estimated using the Johansen Method in the software. Material mineral thermal conductivities of 1 J s^{-1} m^{-1} K^{-1} for sand, 1.8 J s^{-1} m^{-1} K^{-1} for gravel and 0.5 J s^{-1} m^{-1} K^{-1} for silt were used as inputs. The thermal conductivity functions are shown in Figure 4.6.

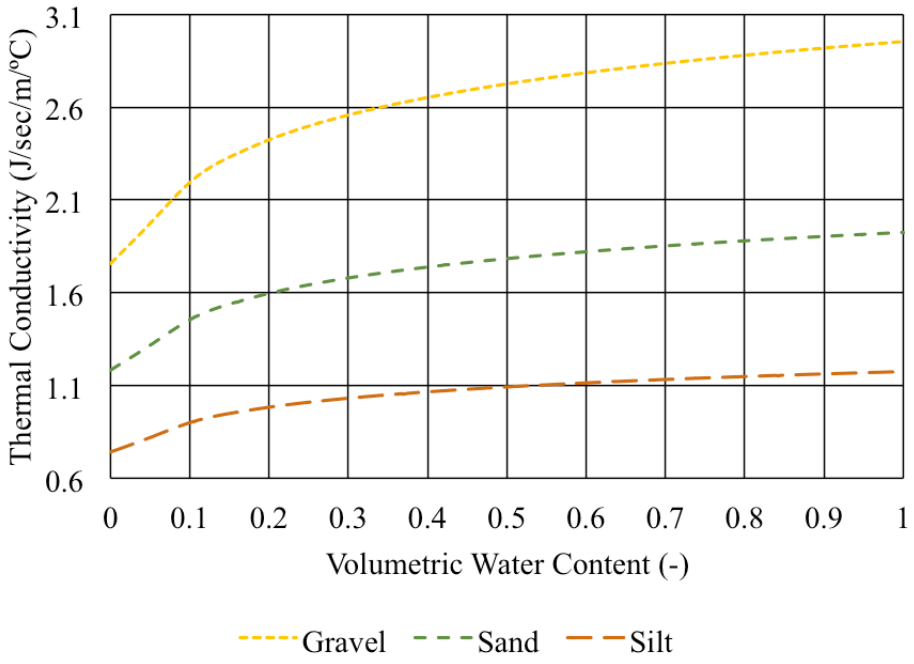

Figure 4.6 The thermal conductivity functions for the sand, gravel and silt used in the SFCBD cover simulations.

The volumetric heat capacity functions were estimated using the de Vries Method in GeoStudio. The saturated unfrozen volumetric heat capacity was determined as 3.10 x 10^6 J m^{-3} K^{-1} for the silt, 2.90 x 10^6 J m^{-3} K^{-1} for the gravel and 3.00 x 10^6 J m^{-3} K^{-1} for the sand. The volumetric heat capacity functions are shown in Figure 4.7. The unfrozen water content functions were determined based on texture and are shown in Figure 4.8.

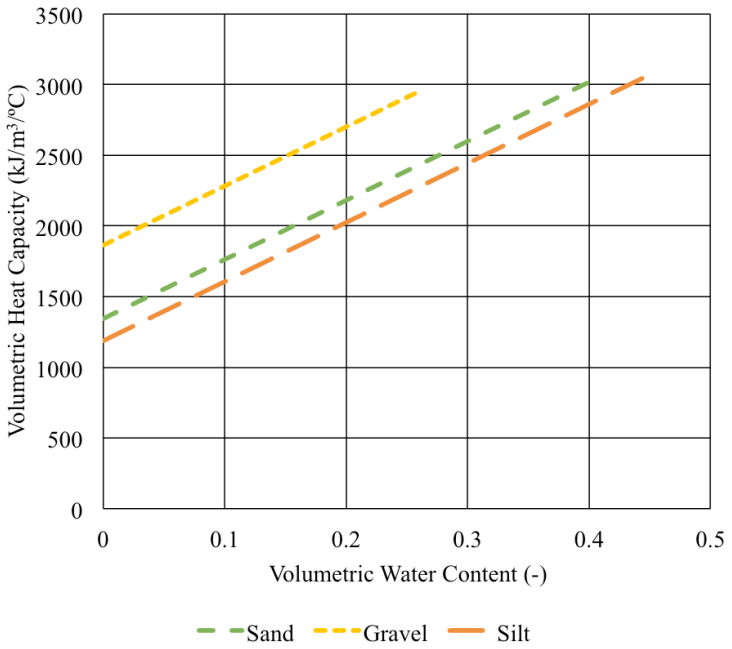

Figure 4.7 Volumetric heat capacity functions for the three materials used in the SFCBD simulations.

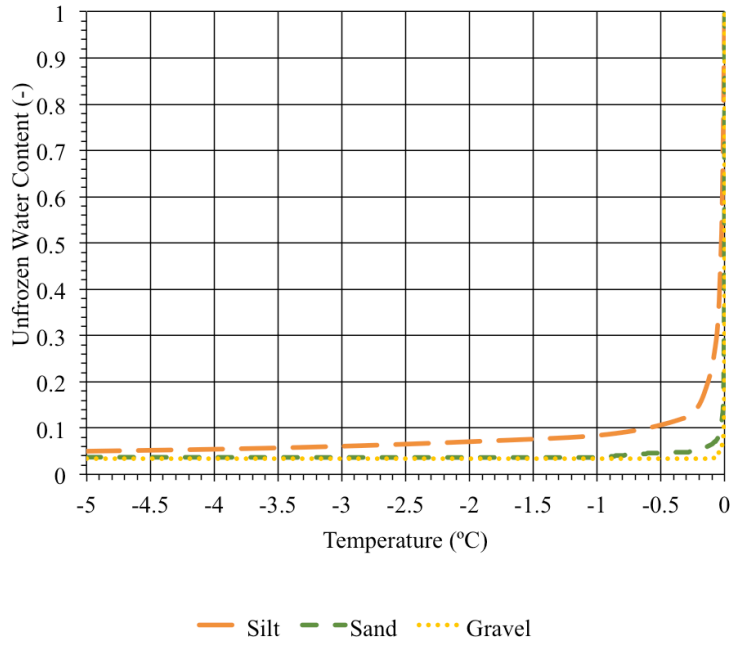

Figure 4.8 Unfrozen water contents for the three materials used in the SFCBD simulations.

4.3.3 Boundary Conditions

The boundary conditions for the simulated SFCBD cover were set to replicate the cold climatic conditions of Yellowknife. To simplify the simulations and reduce solution times, an n-factor air temperature boundary condition was applied in place of a full surface energy balance. The n-factor method uses an empirical coefficient (the n-factor) to link the air temperature to the ground surface temperature, simplifying the boundary condition (Klene et al. 2001). The appropriate n-factor was determined through one-dimensional modelling of the full Land Climate Interface (LCI) boundary condition to capture the surface energy balance at the site. Climate data from the Environment and Climate Change Canada weather station at the Yellowknife airport (Station ID: 2204100) was used as the input functions for the LCI condition. The one-dimensional LCI model also acted as a spin-up model and provided the initial temperature and water content conditions applied to the 2D slope models. The 1D model was run for 15 years, allowing the annual climate cycle to stabilize. The simulated ground temperature for the 15^{th} year was compared to the air temperature using the root mean square error (RMSE) to determine the n-factor.

The daily air temperatures were divided into three sections based on the season and the surface condition, i.e. snow cover and above or below 0 °C, and a separate n-factor was determined for each section by minimizing the RMSE between the air temperature and the simulated LCI ground temperature. The n-factor for the winter/spring season was calculated to be 0.17. The n-factor for the spring/summer season was 1.27. During the fall/winter season, the n-factor declined to 0.13. The n-factors varied between the seasons due to the different soil and surface conditions. The freezing n-factor of the fall/winter/spring is influenced by the frozen ground and insulating snowpack, resulting in ground temperatures warmer than air temperatures. During the warmer, snow-free months, ground heating results in slightly higher surface temperatures than air temperatures. Applying these n-factors to the measured air temperature produced the ground surface temperature that was used in the 2D models (Figure 4.9). The bottom boundary condition of the 2D models was set to a heat flux of 5.00×10^{-5} kJ s^{-1} m^{-2} to simulate the annual average continental geothermal flux in Northern Canada (Pollack et

al. 1993). The estimated annual flux in Yellowknife is slightly higher at 8.00×10^{-5} kJ s^{-1} m^{-2} (Grasby et al. 2013), but the lower flux was chosen to be more representative of the entire northern region. A lateral potential seepage face boundary condition at the toe of the slope for the three cover layers allowed water and heat to exit the model. The lateral boundary conditions of the silt and the top of the slope were set to no flow boundaries.

Yellowknife is located on the Great Slave Lake, about 400 km south of the Arctic Circle at a latitude of 62º N. It has a subarctic climate that results in cold winters and mild summers (Environment Canada 2010). Average annual precipitation is approximately 300 mm, of which about half falls as snow (Environment Canada 2010). Yellowknife receives approximately 160 cm of snow annually, with the highest average monthly snowfall occurring in November.

Climate data from 2012 was used for the 1D LCI boundary conditions. Temperature varied from a minimum of -36.6 ºC in the winter to a maximum of 25.2 ºC in the summer (Environment Canada 2012). Yellowknife experiences seasonal freezing and is frost-free during the summer due to the approximately 150 days of above-freezing air temperatures. The air temperatures recorded at the Yellowknife Airport are shown in Figure 4.9 in blue, while the ground temperature as predicted by the 1D simulation is shown in red and the air temperature adjusted by the n-factor to match the LCI ground temperature is shown in green.

Snowmelt infiltration, along with summer precipitation and evaporation were also simulated in the 1D model using climate data from Environment and Climate Change Canada. The initial water content profile of the slopes was therefore also obtained from this simulation.

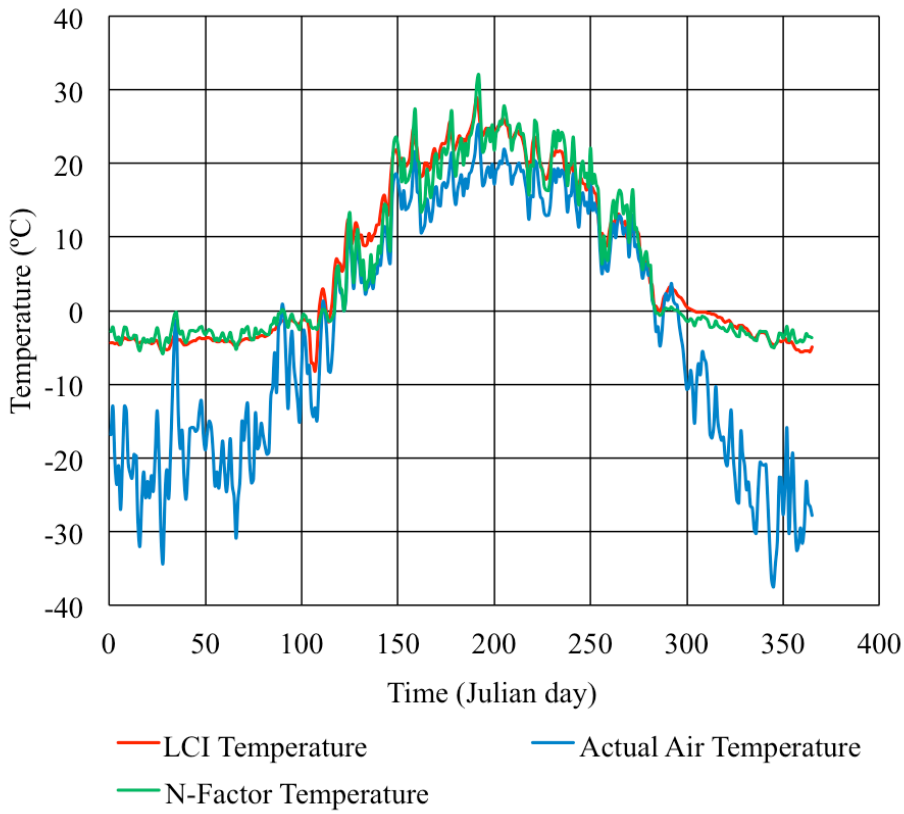

Figure 4.9 Average daily temperatures for 2012 at the Yellowknife Airport (Environment Canada 2012), along with the ground temperatures from the 1D LCI simulation and the air temperature adjusted by the n-factor.

Daily average wind speed at the Yellowknife Airport for 2012 was also used in the LCI boundary condition. The data provided by Environment and Climate Change Canada was the daily maximum gust and was only recorded if it was greater than 31 km/h. On days that the maximum gust was less than that, the value is simply recorded as less than 31 km/h. In order to be used as an input for the LCI condition, a proper numerical value needed to be assigned to each of the days where this occurred. For simplicity, it was assumed that each of these days had an average daily wind speed of 31 km/h, overestimating the wind. The resulting wind speed profile is shown in Figure 4.10.

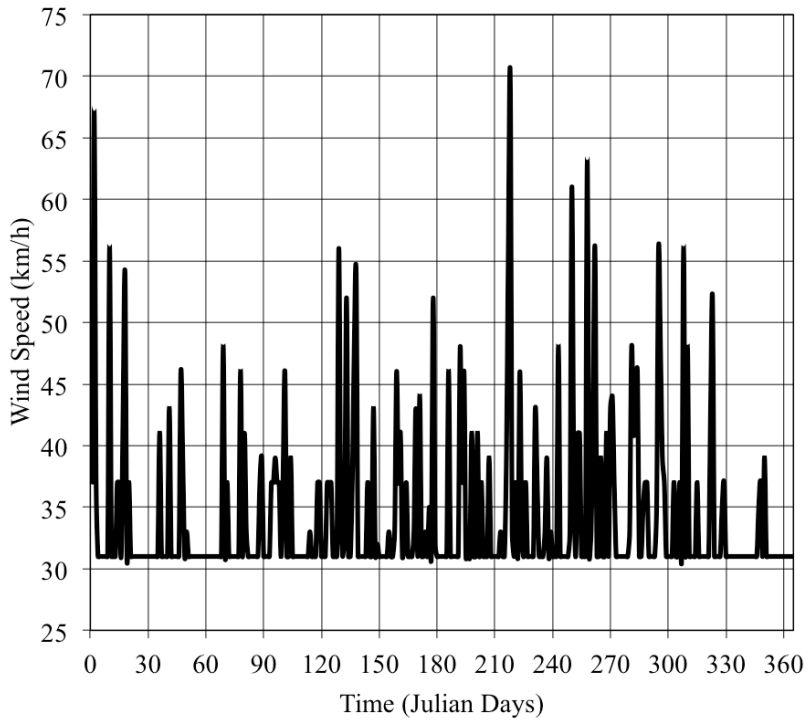

Figure 4.10 The daily maximum wind gusts at the Yellowknife Airport for 2012. Wind speed values less than 31 km/h were not recorded, but were assumed to be 31 km/h (data from Environment Canada (2012)).

To ensure the n-factor condition was equivalent to the LCI condition, a 1D simulation compared the two boundary conditions. The temperature profile simulated using the n-factor matched quite well with that of the LCI simulation. The 1D temperature profile was then applied to the slope models as the initial temperature conditions using a spatial function. The initial temperature conditions of the shallow slope model are shown in Figure 4.11. Initial water content conditions were set using the activation matric suction for all models.

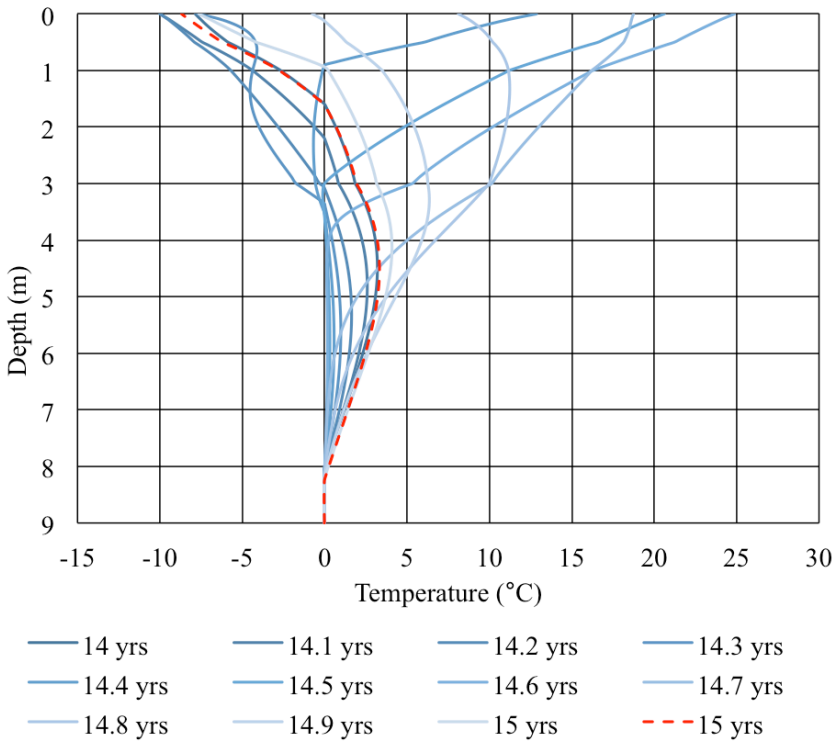

Figure 4.11 The temperature results from the 14th year of the 1D model. The profile at the beginning of the 15th year, shown in red, was applied to the 2D models as the initial conditions using a spatial function.

Snowmelt infiltration fluxes were based on the Wolf Creek fluxes and the Yellowknife climate data to determine the melt period. Like the Wolf Creek simulations, an incremental step function was created that allowed the influx to slowly increase over time to prevent numerical convergence problems. Snowmelt was able to infiltrate into the cover for a period of 30 days at a maximum rate of 1.00×10^{-7} m/s. Summer precipitation and evaporation were based on Environment and Climate Change Canada climate data for Yellowknife (Station ID: 2204100).

The 2D simulations were run for several years, with results being taken from the fifth year of the simulation. As with the Wolf Creek simulations, the previous years acted as a spin up period for the model, reducing the impact of the initial conditions on the simulation.

4.4 Results

4.4.1 Model 1: Steep Slope

The steep slope model was designed to create larger downslope water movement that could carry heat. The results of the simulation were assessed through ground temperatures, discharge rates and thaw patterns. The Peclet number (Equation 2.1) was used to determine the influence of lateral convection on thaw within the cover system.

In the months leading up to snowmelt, the slope froze to a depth of 3 metres, reaching the bottom of the lower gravel layer. The volumetric water content in the upper gravel was less than 0.1, while the sand layer remained at higher levels of saturation with a water content of 0.26.

Infiltrating snowmelt was successfully diverted laterally downslope within the upper gravel and sand layers. Large water flows were observed at the base of the upper gravel, after thaw of the gravel had occurred. Water flow in the sand layer was limited by the frozen hydraulic conductivity, limiting percolation into the sand until thaw occurred.

Thaw through the upper gravel layer was relatively uniform, but the top thawed slightly slower than rest of the slope. Thaw progressed at a rate of approximately 6.0 mm/hour at the top and 7.5 mm/hour at the middle and toe of the gravel layer. The temperature at a depth of 0.42 m in the upper gravel around the time of melt is shown in Figure 4.12. The thaw front reached the bottom of the upper gravel layer at around the 119th day. The temperature at the base declined to around 0 °C on the 122nd day before increasing rapidly over the next few days.

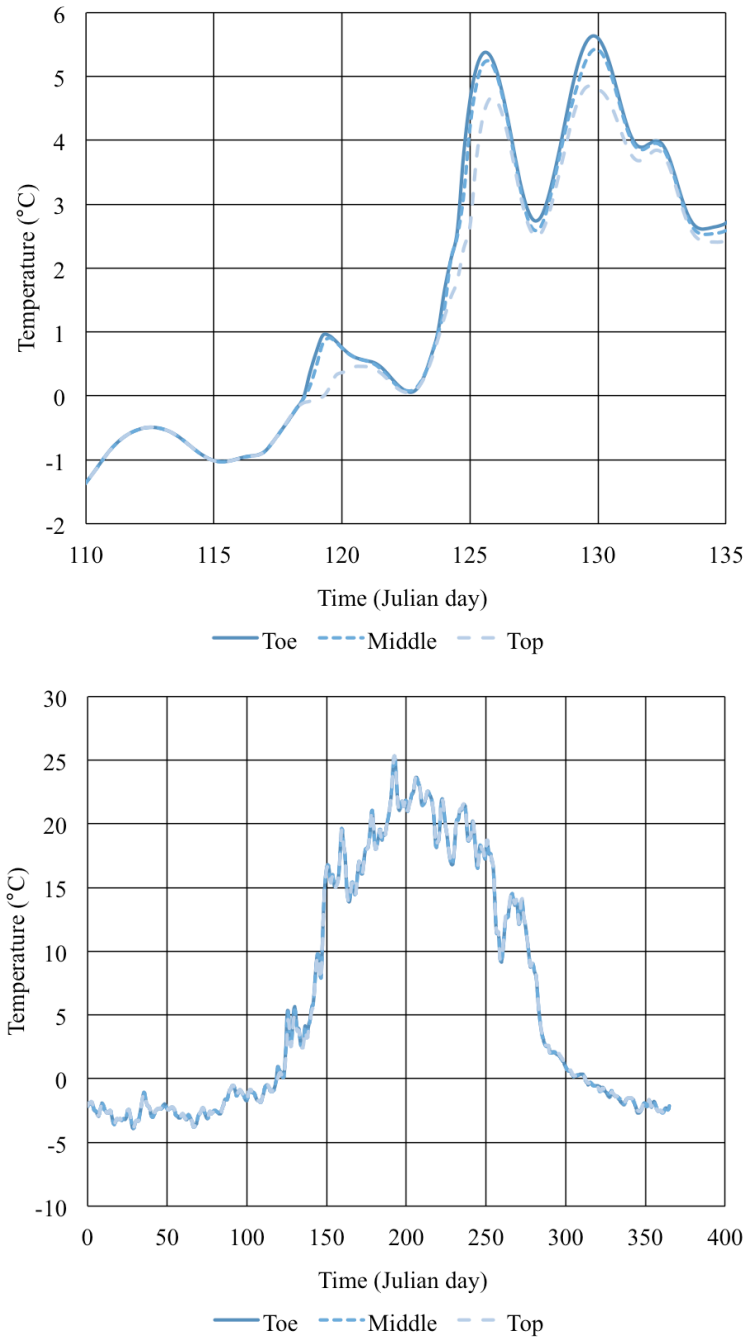

Figure 4.12 The temperature profile at 0.42 m depth in the upper gravel layer at the top, middle and toe of the Model 1 slope during the thaw period (top) and the whole year (bottom).

Thaw through the sand layer was slower than through the upper gravel and the rate of thaw increased from top to toe. The top thawed at an average rate of 1.6 mm/hour, while

the toe thawed at an average of 2.2 mm/hour. The sand had thawed completely by the 138th day. The temperature profile through the sand at the top and toe of the slope is shown in Figure 4.13. A zero-curtain developed in the sand layer that did not occur in the upper gravel. The length of the zero-curtain increased with depth in the sand layer. Near the upper gravel-sand interface, the zero-curtain lasted approximately 5 days at the middle of the slope. At the base of the sand, it lasted for about 7 days. As seen in Figure 4.13, the zero-curtain lasts longer at the toe than at the top. Thus, despite the higher thaw rate at the toe, the top of the slope thaws first. The zero-curtain is the result of latent heat absorption, which reduces the warming rate and keeps the soil isothermal at around 0 °C. This phenomenon likely developed in the sand, and not in the gravel, due to the lower thermal conductivity of the sand, which would increase the time required for heat exchange between the soil particles and the water and ice.

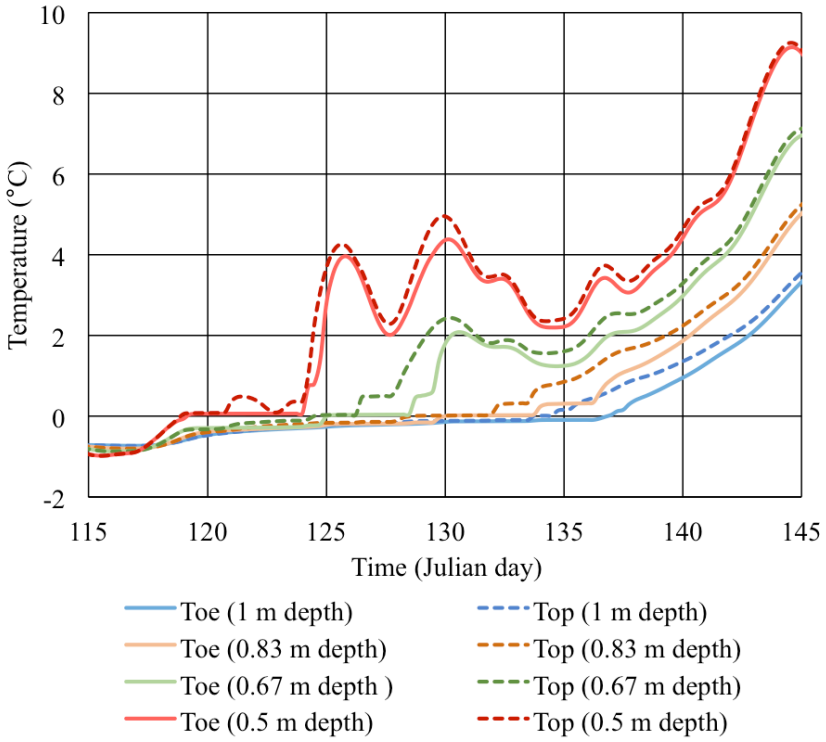

Figure 4.13 The temperature profile through the sand layer around the time of thaw at the top and toe of the Model 1 slope.

The sand was completely thawed by the 138th day, 12 days prior to the end of snowmelt infiltration at the surface. Soil frost penetrated the lower gravel layer, but did not reach the bottom until the 74th day. The minimum soil temperature reached at the base of the lower gravel layer was 0.01 °C, only slightly above the freezing mark. Thaw rates increased in the lower gravel, but due to its thickness, it did not completely thaw until the 158th day. Thaw through the layer was relatively uniform, but occurred at an accelerated rate toward the top of the slope. The toe and middle thawed at an average rate of approximately 3.7 and 4.0 mm/hour, respectfully, while the top thawed at an average rate of 4.3 mm/hour. Thaw through the lower gravel was faster than through the sand, but not as quick as through the upper sand.

The upper half of the silt layer did not freeze during the model year, while the lower half of the silt froze due to the initial conditions and remained frozen for the entire year. The temperature at the base of the silt remained relatively unchanged during the simulation, only varying within 0.01 °C.

The upper gravel remained at elevated saturation during snowmelt infiltration, declining following the end of snowmelt, as shown in Figure 4.14. The initial influx of snowmelt at the top of the slope at around the 120th day quickly percolates through the frozen upper gravel and into the sand. During the snowmelt period, the middle and toe of the slope reached and remained at higher levels of saturation than the top of the slope, due to downslope flow from the top of the slope. After the initial influx of snowmelt, the water content in the upper gravel dropped to nearly the residual water content, except during summer precipitation events.

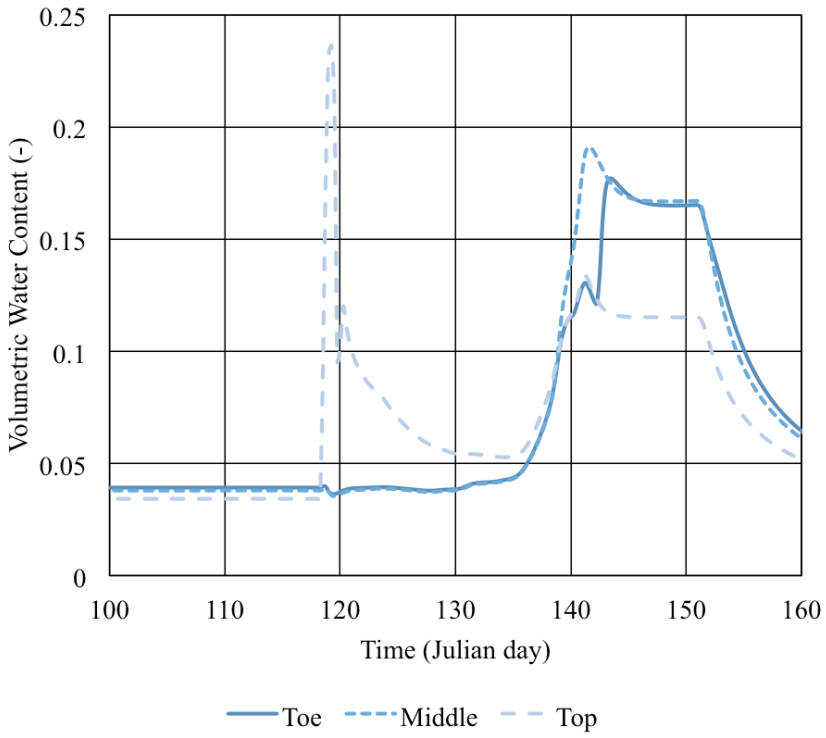

Figure 4.14 Volumetric water content at the top, middle and toe of the upper gravel layer of the Model 1 slope during the thaw period.

The sand remained at high levels of saturation for the duration of the simulation. The snowmelt infiltration resulted in an increase in the water content in the sand layer to saturation or near saturation for a period of approximately 10 days. After the snowmelt period, the water content slowly decreased to pre-melt saturation levels. The water content increased to near saturation for brief periods during the summer and experienced variability due to rainfall and evaporation, but declined in the fall as the soil temperature dropped and the ground began to freeze.

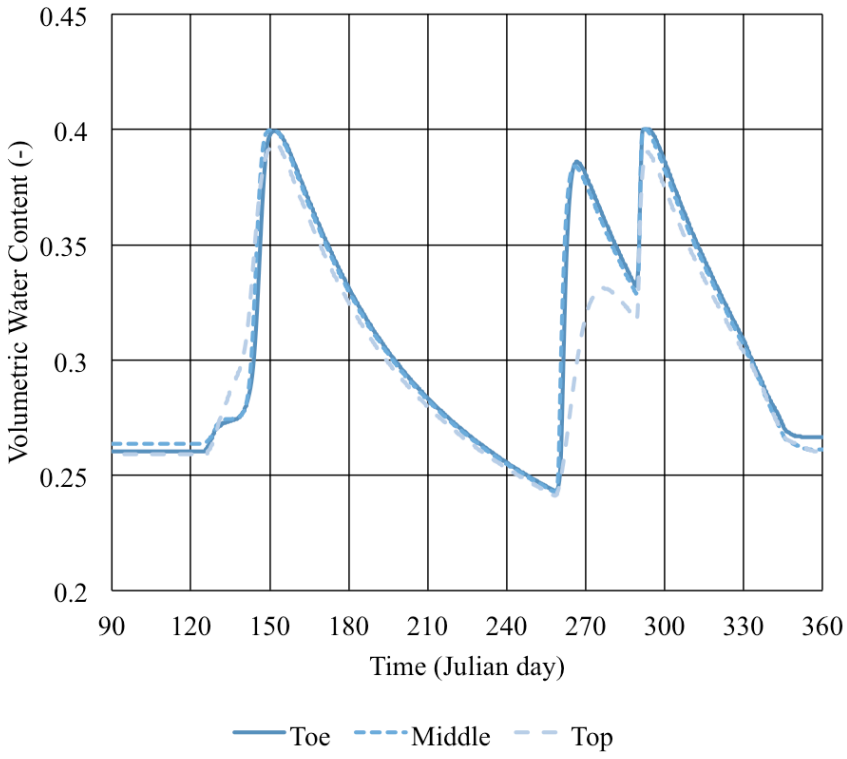

Figure 4.15 Volumetric water content at the top, middle and toe of the sand layer of the Model 1 slope.

The water content of the lower gravel increased slightly at the base of the lower gravel, resulting in lateral downslope flow above the silt layer.

Throughout the spring freshet, a large portion of the water, approximately 81%, was successfully diverted laterally downslope due to the presence of the frozen sand layer and the textural difference. During the snowmelt period, more water exited the model through the toe of the sand and upper gravel layers than infiltrated to the lower gravel layer. By about the 200th day, more cumulative water had exited through the base into the lower gravel than had exited through the toe (Figure 4.16). Overall, there was a slight decrease in the storage of the upper gravel and sand layer over the year.

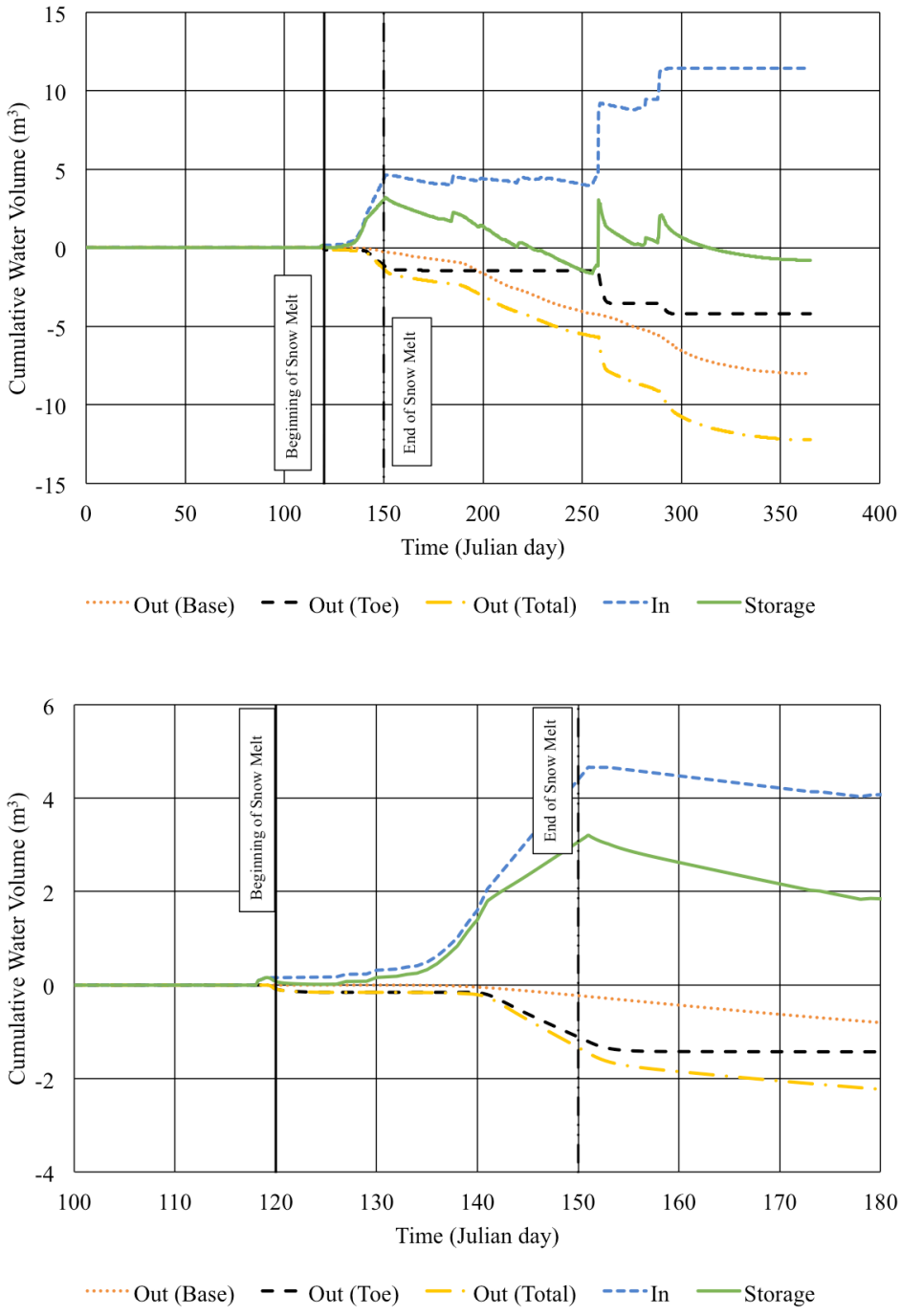

Figure 4.16 The cumulative water volumes entering and exiting the upper gravel and sand layers, along with the change in storage (top). An expanded view during the spring freshet is shown in the bottom graph.

When the entire SFCBD profile is considered, very little water flows out of the base of the cover into the silt (Figure 4.17). The water that exits the base of the sand into the lower gravel is therefore diverted out of the toe of the lower gravel due to the low hydraulic conductivity silt layer. The percolation of water beyond the sand layer into the lower gravel results in the failure of the cover system. By the end of the year, approximately 70% of the infiltrating precipitation percolated into the lower gravel.

After thaw, despite no longer being frozen, a large portion of lateral water flow occurred at the interface of the sand and upper gravel. This is due to the textural difference between the two layers and the larger saturated hydraulic conductivity of the gravel layer. Water began to flow within the lower gravel once the sand layer had thawed. This water, however, was diverted laterally downslope above the frozen soil interface.

The influence of diverted infiltrating water on thaw was determined through the Peclet number. The gravel layers had the greatest potential for lateral convection due to the high saturated hydraulic conductivity. The maximum achievable specific discharge due to gravity in the gravel layers was 2.00×10^{-5} m/s. The theoretical gravitational maximum Peclet number for the upper gravel was determined to be 5.58. The lower gravel had a higher maximum Peclet number due to the increased thickness, which increases the length-scale ratio. This ratio is directly proportional to the Peclet number and therefore an increase in the ratio results in an increase in the Peclet number. The gravitational maximum Peclet number for the lower gravel was an order of magnitude higher than the upper gravel at 22.3. The sand, due to its lower hydraulic conductivity, had a much lower maximum gravitational specific discharge, only 2.00×10^{-8} m/s. The maximum Peclet number that could be achieved due to gravity is therefore 8.20×10^{-3}.

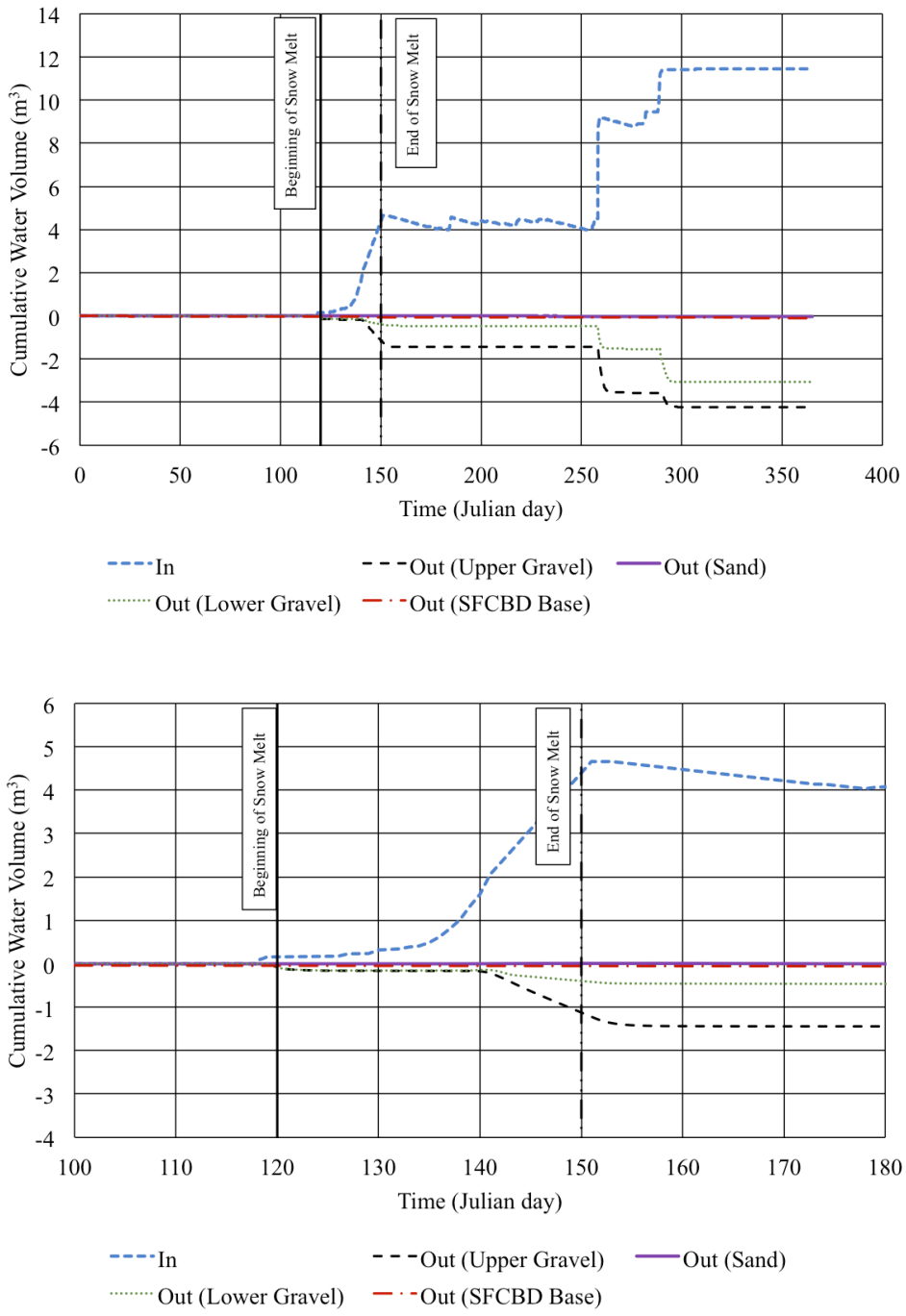

Figure 4.17 The cumulative water volumes entering and exiting the SFCBD cover system through the toe, with the exception of the SFCBD Base line, which is exiting through the base of the cover system into the silt (top). A close up during the spring freshet is shown in the bottom graph.

The lateral specific discharge measured in the upper gravel was equal to the maximum discharge under gravity at 2.00×10^{-5} m/s. The calculated Peclet number was therefore 5.58, above the value at which convection should dominate. Flow through the lower gravel layer peaked at a value of 1.00×10^{-6} m/s, resulting in a Peclet number of 1.12. The high discharge achieved lasted only a few days over a small spatial scale and therefore convection likely played only a small role in the thaw of the lower gravel layer, despite the Peclet number of 1.12.

The sand layer, due to the elevated levels of saturation, achieved a specific discharge that approached the gravitational maximum. The lateral specific discharge was measured as 1.85×10^{-8} m/s, leading to a Peclet number of 7.59×10^{-3}. The Peclet numbers for the three layers are detailed in Table 4-1.

Table 4-1 Calculated lateral Peclet numbers for the three layers with lateral flow in the Model 1 simulation.

	Upper Gravel	Sand	Lower Gravel
Theoretical Maximum	5.58	8.20×10^{-3}	22.3
Model	5.58	7.59×10^{-3}	1.12

Vertical flow was limited only by the hydraulic conductivity of each of the layers. The anisotropy reduced the vertical saturated hydraulic conductivity of the upper gravel and sand layers by 25%. Thus, the maximum discharge for the upper gravel layer was 7.50×10^{-5} m/s, while the maximum for the sand was 7.50×10^{-8} m/s. No anisotropy was applied to the lower gravel layer and the vertical hydraulic conductivity was the same as the lateral, 1.00×10^{-4} m/s. The maximum Peclet numbers are shown in Table 4-2. The vertical water unit flux through the cover profile tended to be smaller than the lateral discharges. The upper gravel averaged approximately 2.60×10^{-6} m/s vertical flow during the snowmelt period, resulting in a Peclet number of 2.18. The sand layer reached the saturated vertical hydraulic conductivity for a period during the snowmelt, giving a Peclet number of 9.23×10^{-2}. The discharge in the lower gravel was two orders of magnitude lower than the maximum value at 3.20×10^{-7} m/s, resulting in a Peclet number of 1.07.

Table 4-2 Calculated vertical Peclet numbers for the three layers with vertical flow in the Model 1 simulation.

	Upper Gravel	Sand	Lower Gravel
Theoretical Maximum	62.8	9.23×10^{-2}	335
Model	2.18	9.23×10^{-2}	1.07

The gravel layers have the greatest potential for lateral convection to influence the thaw of frozen soil, especially the upper gravel, where large lateral flows occurred. Lateral convection, however, is not likely to play a role in the thaw of the sand layer, as the Peclet number is well below 1.

4.4.2 Model 2: Shallow Slope

The shallow slope model was designed to encourage lateral diversion by the frozen layer like the steep slope model, but the shallower slope also encourages more vertical flow through the soil profile. This slope model explored the role of vertical flow and vertical convection in thawing the frozen soil.

Thaw of the upper gravel layer occurred by the 119th day of the simulation. Thaw was uniform throughout the layer and progressed at a rate of 7.5 mm/hour. No zero-curtain developed within the upper gravel and all regions proceeded quickly through 0 °C and into positive temperatures (Figure 4.18). Thaw near the interface of the upper gravel with the sand slowed to less than 1 mm/hour.

The sand layer thawed relatively uniformly throughout the slope. The thaw rate, however, was considerably slower through the sand than through the upper gravel. Sand has lower thermal and hydraulic conductivities, lowering the ability of the soil to transmit heat through both conduction and convection. The sand thawed at a rate of 1.7 mm/hour at the middle and top of the slope and 1.6 mm/hour at the toe of the slope. Unlike the upper gravel, a zero-curtain developed in the sand layer. At the base of the layer at all regions,

the soil remained at 0 °C for approximately 4 days before sharply increasing, as shown in Figure 4.19.

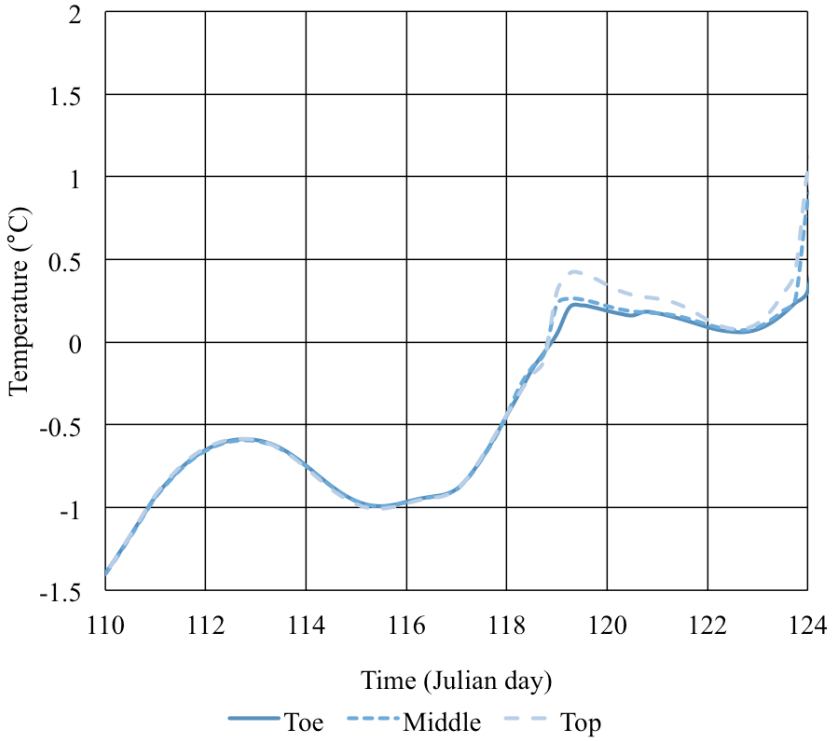

Figure 4.18 Temperatures at the bottom of the upper gravel at the top, middle and toe of the Model 2 slope during the thaw period.

The base of the lower gravel layer barely froze, reaching a minimum temperature of -0.25 °C, while the freezing front did not progress into the silt layer. The lower gravel layer did not thaw completely until the 147th day. Like the sand layer, a zero-curtain developed within the lower gravel layer. At the base of the layer, the soil remained isothermal at 0 °C for 2-3 days before thawing and increasing to positive temperatures. Thaw through the layer occurred at an average rate of 4.0 mm/hour. The silt layer froze from the bottom to about the middle of the layer. This frozen interface was not influenced by the infiltration of snowmelt or other precipitation and remained frozen for the duration of the simulation.

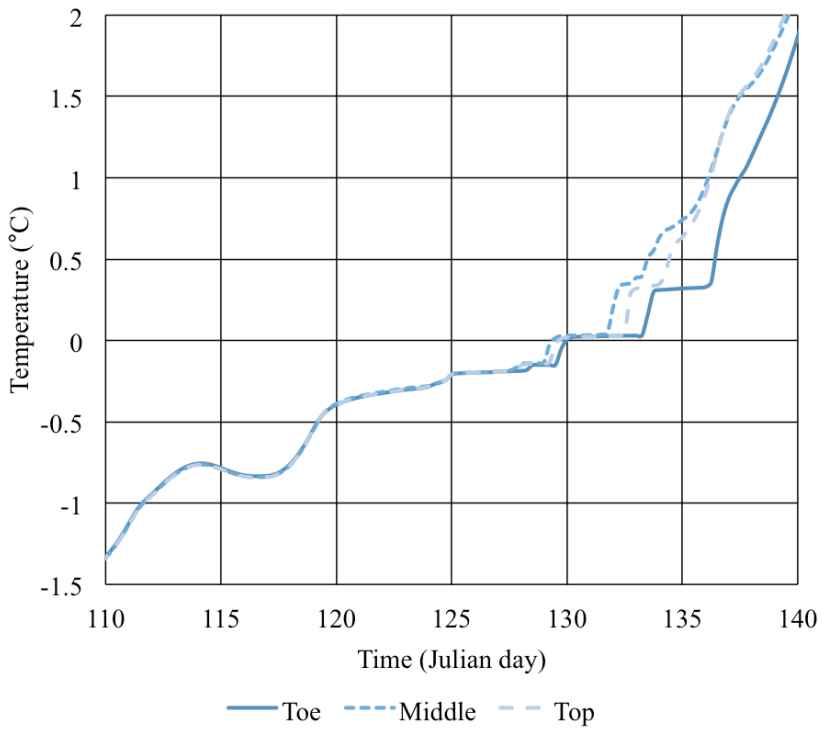

Figure 4.19 Temperatures at the base of the sand layer at the top, middle and toe of the Model 2 slope.

The volumetric water content of the upper gravel rose to elevated levels of saturation for a period of approximately 10 days following snowmelt (Figure 4.20). The water content at the top of the slope did not reach the level of saturation of the middle or toe of the slope. The elevated levels of saturation persisted until the end of snowmelt, after which drainage began. The top of the slope begins to drain about a day before the middle and toe. After thaw, the layer is able to drain, causing the water content to decline.

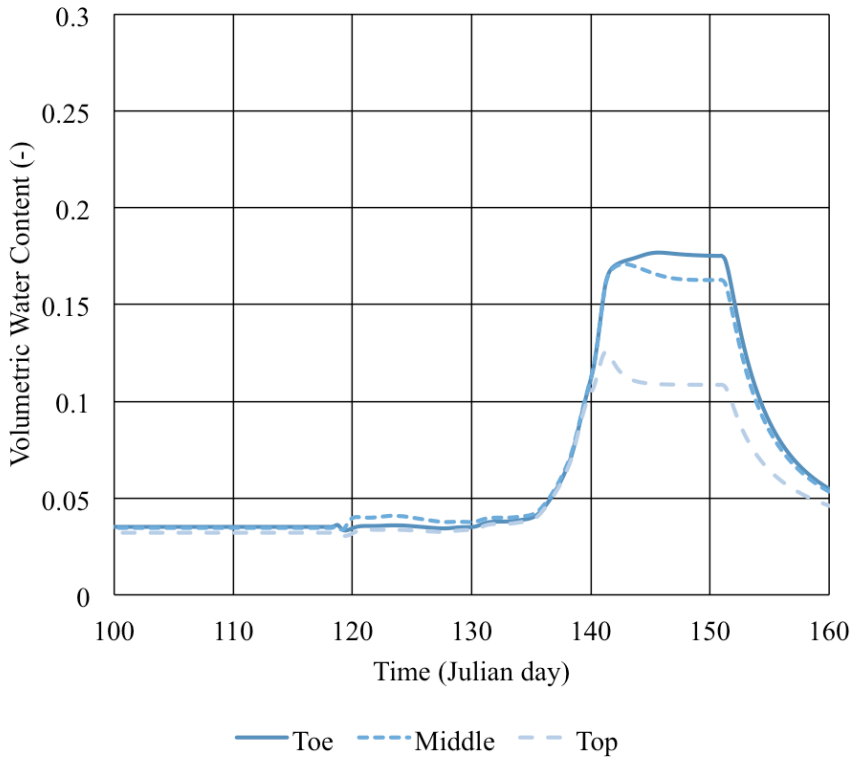

Figure 4.20 The volumetric water content of the upper gravel layer at the top, middle and toe of the Model 2 slope.

The sand layer experienced an increase in water content starting after the 140th day, with the toe and middle of the slope reaching saturation by the 146th day (Figure 4.21). The top of the slope did not reach saturation. The sand remained at or near saturation until the 153rd day and then began to slowly decline. The water content declined to near pre-snowmelt levels over the summer, increasing with large summer precipitation events before declining to pre-melt levels in the fall.

The water content in the lower gravel layer did not reach saturation during the simulation. A slight increase in water content over residual levels was observed starting on the 150th day, but quickly drained. Over the summer, only the largest precipitation event influenced the water content of the lower gravel layer.

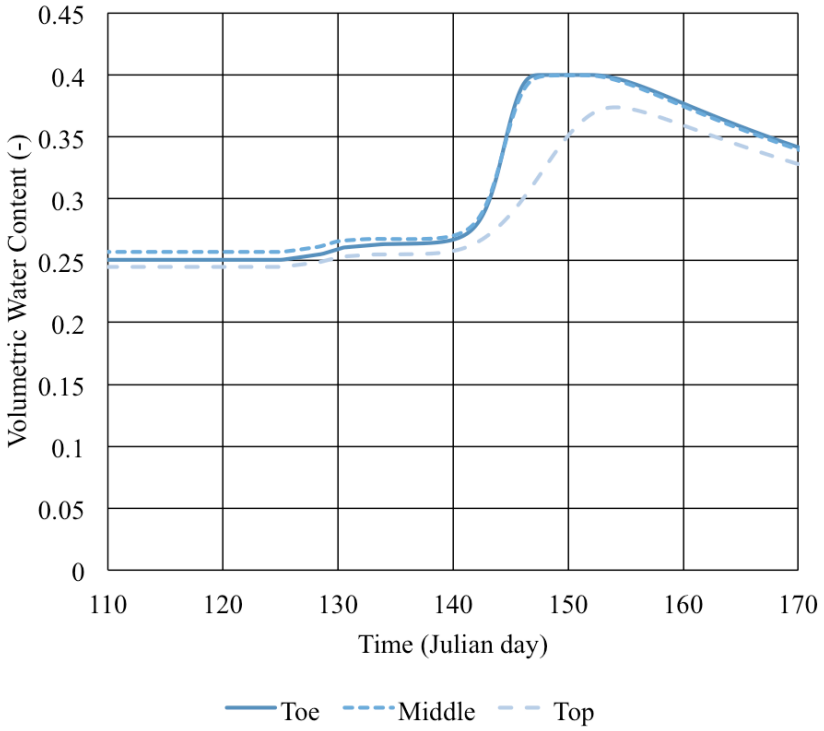

Figure 4.21 The volumetric water content of the sand layer at the top, middle and toe of the Model 2 slope.

Water flow within the model domain occurred as both lateral and vertical flow, but the majority of water flow through the upper gravel layer was vertical. In the sand layer, water flow out of the layer was mainly vertical flow into the lower gravel with limited flow out of the toe of the slope. Due to the high saturation levels near the base of the upper gravel, some lateral water flow in the sand flowed back into the gravel at the toe before exiting the domain. The two layers together experienced a large flow event out of the toe after the end of the snowmelt period at about the 180th day, as shown in Figure 4.22. During the spring freshet period the sand and upper gravel layers laterally diverted approximately 79% of infiltrating meltwater. By the end of the year, after the summer precipitation events, approximately 97% of precipitation had percolated into the lower gravel, resulting in failure of the cover system. The majority of water in the lower gravel

layer exited out of the toe. More flow occurred through the gravel layers than through the sand due to their larger hydraulic conductivity.

The vertical specific discharges reflect the large amount of vertical flow, with the upper gravel layer being an order of magnitude larger than the sand layer. Both the upper and lower gravel had a gravitational maximum specific discharge of 1.00×10^{-4} m/s. This resulted in a maximum Peclet number of 84 for the upper gravel and 335 for the lower gravel. The Peclet number for the lower gravel is larger than the upper gravel due to its increased thickness. The sand had a maximum specific discharge of 1.00×10^{-7} m/s, resulting in a maximum Peclet number of 0.12. Vertical Peclet numbers for all three layers are shown in Table 4-3.

Table 4-3 Calculated vertical Peclet numbers for the three layers with vertical flow in the Model 2 simulation.

	Upper Gravel	Sand	Lower Gravel
Theoretical Maximum	83.7	0.123	335
Model	1.81	0.123	1.57

The vertical specific discharge measured through the upper gravel layer during the snowmelt period was 2.02×10^{-6} m/s. This led to a calculated Peclet number of 1.81, less than the maximum value, but still in the range where convection should be dominating. Flow through the sand layer was reduced to the hydraulic conductivity, or 1.00×10^{-7} m/s, resulting in a Peclet number that is the same as the maximum value. Within the lower gravel, water flow peaked at a value of 4.70×10^{-7} m/s. The calculated Peclet number for the lower gravel was 1.57 during that time period.

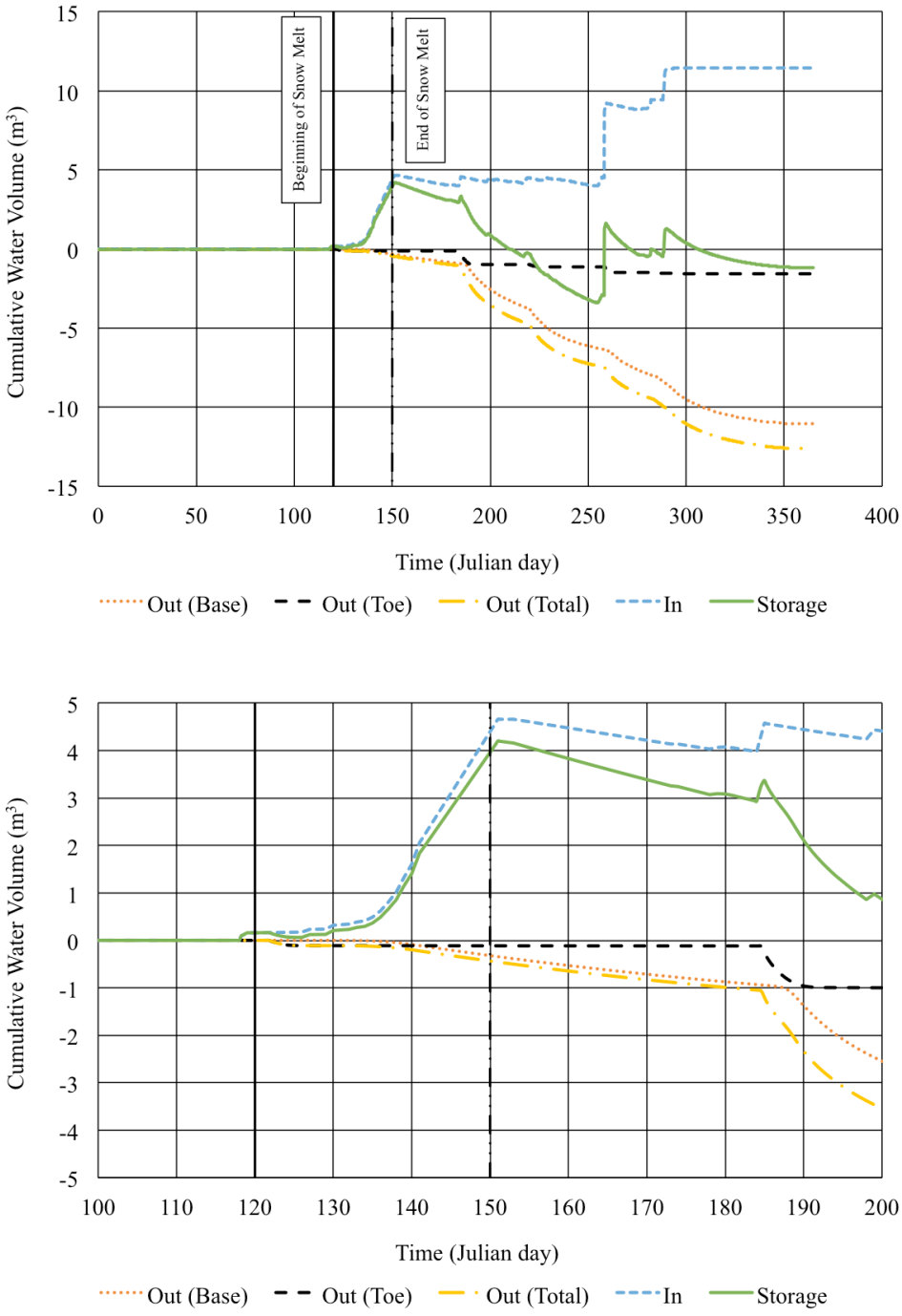

Figure 4.22 The cumulative water volumes entering and exiting the upper gravel and sand layers, along with the change in storage, in the Model 2 slope (top). A close up during spring freshet is shown in the bottom graph.

Lateral flow through the upper gravel occurred at an average rate of 4.80×10^{-6} m/s during the snowmelt infiltration period, leading to a Peclet number of 1.34 (Table 4-4). The gravitational maximum for the upper gravel was 1.00×10^{-5} m/s, an order of magnitude lower than the hydraulic conductivity, due to the gradient of the slope. The gravitational maximum specific discharge of the other layers were equally effected, all being one order of magnitude lower than the saturated hydraulic conductivity. The gravitational maximum Peclet number of the upper gravel was calculated as 2.79. The sand layer had a gravitational maximum Peclet number of 4.10×10^{-3} using a specific discharge of 1.00×10^{-8} m/s. The simulation produced a specific discharge of 4.90×10^{-7} m/s, a value larger than the gravitational maximum, indicating water flow was occurring in saturated conditions and as a result of pressure gradients beyond gravity. The sand had a Peclet number of 2.01×10^{-1}, larger than the max value, but far below the value at which convection is a significant driver of heat transfer.

The lower gravel did not experience water flow at pressures greater than those created by gravity alone. The maximum discharge under gravity was 1.00×10^{-5} m/s, leading to a Peclet number of 11.2. Flow within the model averaged 2.40×10^{-7} m/s, resulting in a Peclet number of 0.27.

Table 4-4 Calculated lateral Peclet numbers for the three layers with lateral flow in the Model 2 simulation.

	Upper Gravel	Sand	Lower Gravel
Gravitational Maximum	2.79	4.10×10^{-3}	11.2
Model	1.34	2.01×10^{-1}	0.27

Vertical convective heat transfer within the model has the greatest potential to influence the thaw of the model domain due to the increased specific discharges that can occur as a result of the vertical flow.

4.4.3 Model 3: Slope with Depression

In this simulation a bench with a depression was added to the middle of the flattest slope. The depression disrupted the flow of water and allowed it to pond. This simulation focused on the effect the ponded water would have on the thaw of the frozen soil underneath the depression, relative to the other regions.

The volumetric water content began increasing on the 137th day and reached saturation in the depression on the 140th day. The other regions did not reach saturation and began to drain on the 149th day. The depression remained saturated until the 153rd day at the interface of the upper gravel and the sand. After the beginning of drainage, the depression remained at higher levels of saturation than the other regions, as shown in Figure 4.23.

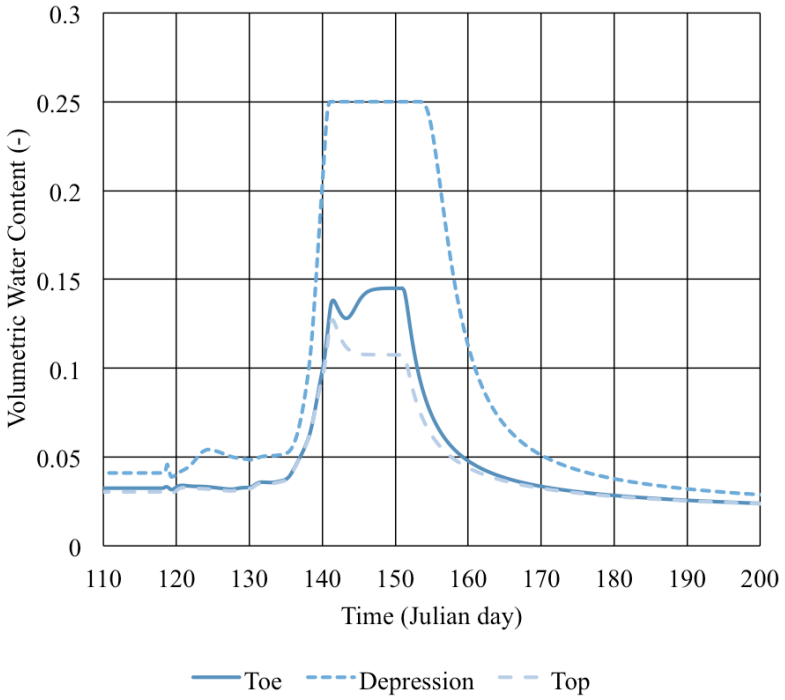

Figure 4.23 The volumetric water content at the interface between the upper gravel and sand layers at the top, depression and toe of the Model 3 slope.

The increased water content resulted in an increased thermal conductivity, but decreased thermal diffusivity in the depression relative to the other regions of the slope. The thermal conductivity declines after the soil thaws, as ice has a higher thermal conductivity than liquid water. The thermal conductivity and diffusivity were uniform throughout the slope until the water content began to increase. The toe and top of the slope saw modest increases in thermal conductivity, while the depression experienced a large increase due to the large increase in volumetric water content, peaking at a value of 2.70 J s^{-1} m^{-1} K^{-1}. As the water content decreased after the 150th day, the thermal conductivity followed. The thermal conductivity of the upper gravel and sand interface is shown in Figure 4.24. The thermal diffusivity decreased in the depression during the same time period from a value of approximately 1.14 x 10^{-6} m^2/s to approximately 1.10 x 10^{-6} m^2/s (Figure 4.25), due to an increase in the volumetric heat capacity as a result of the increase in water content.

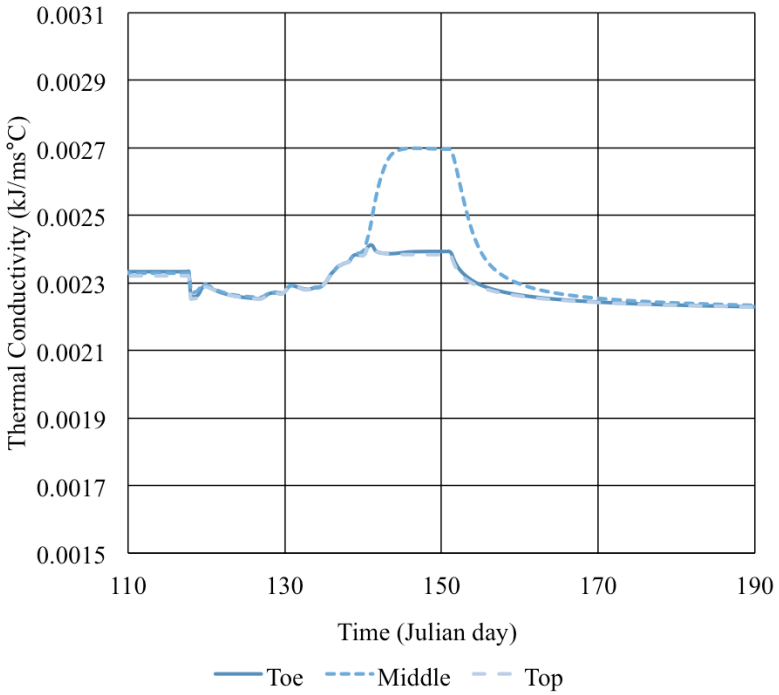

Figure 4.24 The thermal conductivity of the upper gravel and sand interface at the top, depression and toe of the Model 3 slope.

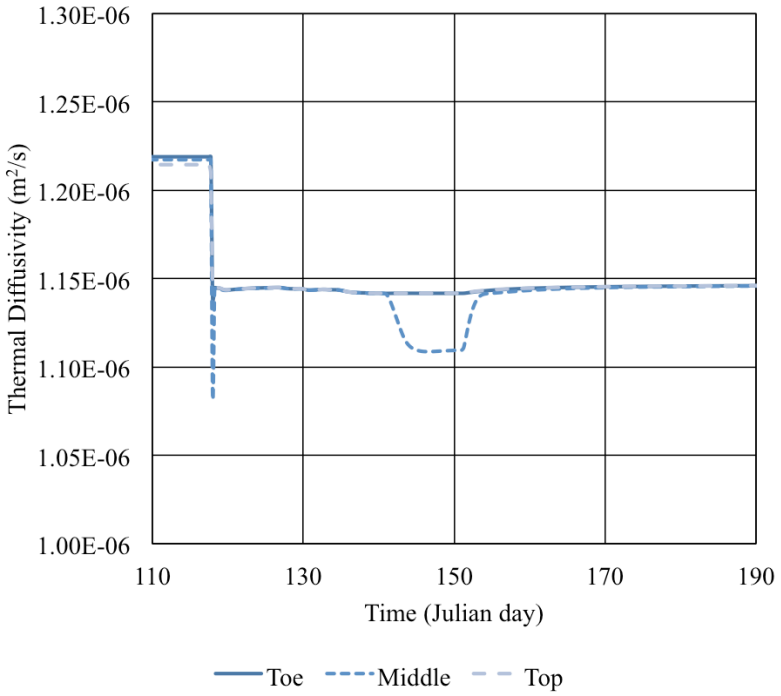

Figure 4.25 The thermal diffusivity of the upper gravel and sand interface at the top, depression and toe of the Model 3 slope.

Thaw of the upper gravel occurred before the large increase in water content and thermal conductivity occurred and was therefore not influenced by the increase. Thaw at the upper gravel-sand interface occurred on the 119th day in in all regions of the slope. A zero-curtain developed that lasted for 5 days, as shown in Figure 4.26. Thaw through the layer occurred at a rate of 7.5 mm/hour.

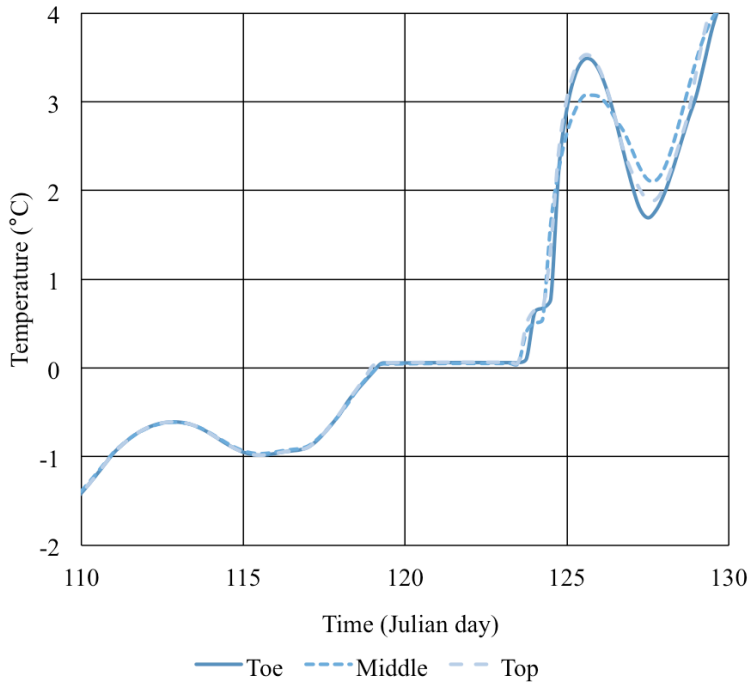

Figure 4.26 Temperature at the base of the upper gravel at the top, depression and toe of the Model 3 slope.

The depression had a subsurface expression in the upper gravel that did not extend to the other layers. The sand layer began increasing in water content around the same time as the upper gravel layer. The depression began to increase in water content before the other regions and reached saturation 5 days before the toe of the slope (Figure 4.27) and maintained saturated conditions for 5 days after the water content at the toe began to decline. The top of the slope never reached saturation, achieving 95% saturation before declining.

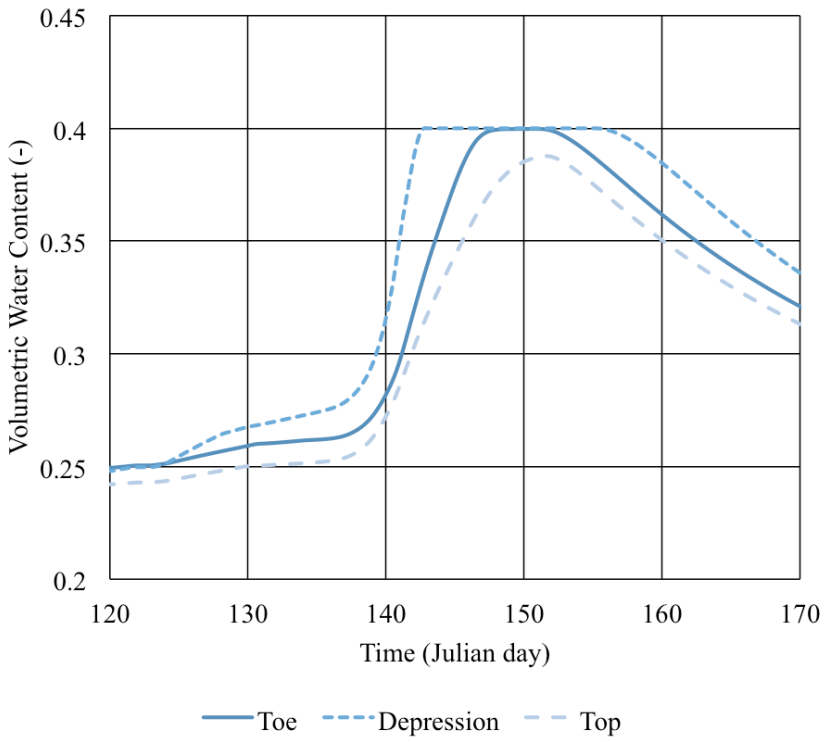

Figure 4.27 The volumetric water content of the sand layer in the Model 3 slope.

An increase in the thermal energy transfer through the depression in the upper gravel due to increased surface energy led to accelerated thaw under the depression in the sand and increased heat flux through the sand (Figure 4.28). Thaw of the sand layer under the depression occurred several days prior to thaw at the top and toe (Figure 4.29). Thaw through the sand under the depression occurred at a rate of 4.5 mm/hour, while the top thawed at 2.5 mm/hour and the toe thawed at 1.4 mm/hour. The toe and top of the slope, however, remained at the zero-curtain for 4 to 5 days, while the depression remained at 0 °C for only 2 days. The difference in thaw time can be attributed to the increased thaw in the upper gravel.

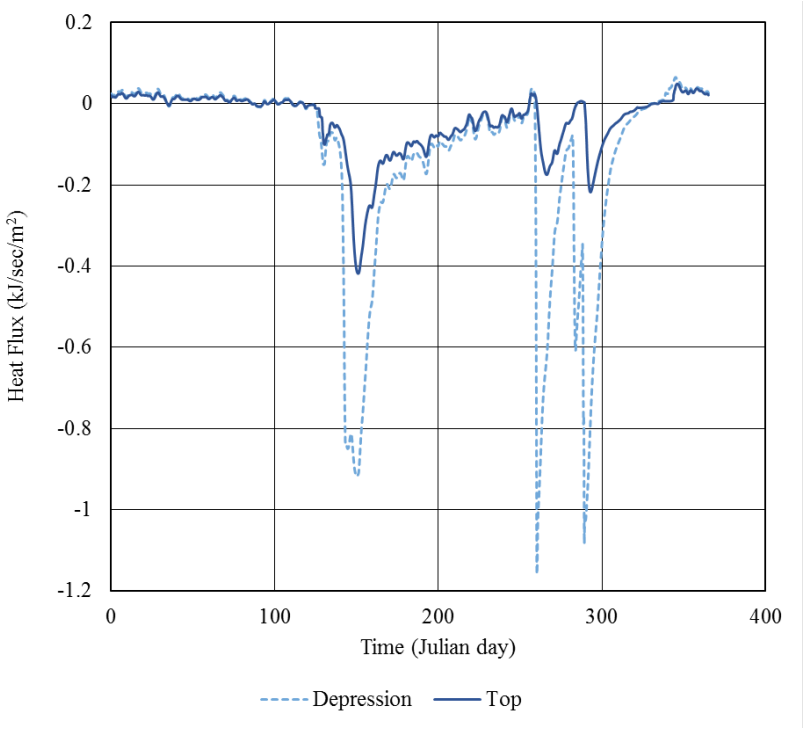

Figure 4.28 Heat flux through the sand layer under the depression and at the top of the slope.

The same pattern of the water content under the depression increasing prior to the other regions of the slope was also observed in the lower gravel layer. However, unlike the sand layer, the layer did not reach saturation. Water flow into the lower gravel layer from the sand was mainly diverted laterally downslope by the low hydraulic conductivity silt layer below. The lower metre of the lower gravel layer barely reached 25% saturation during the snowmelt event. The thermal conductivity of the lower gravel also increased under the depression due to the increased water content. Thaw progressed through gravel under the depression at a rate of 3.9 mm/hour. The top thawed at a rate of 3.6 mm/hour, while the toe experienced the highest thaw rate at 4.7 mm/hour.

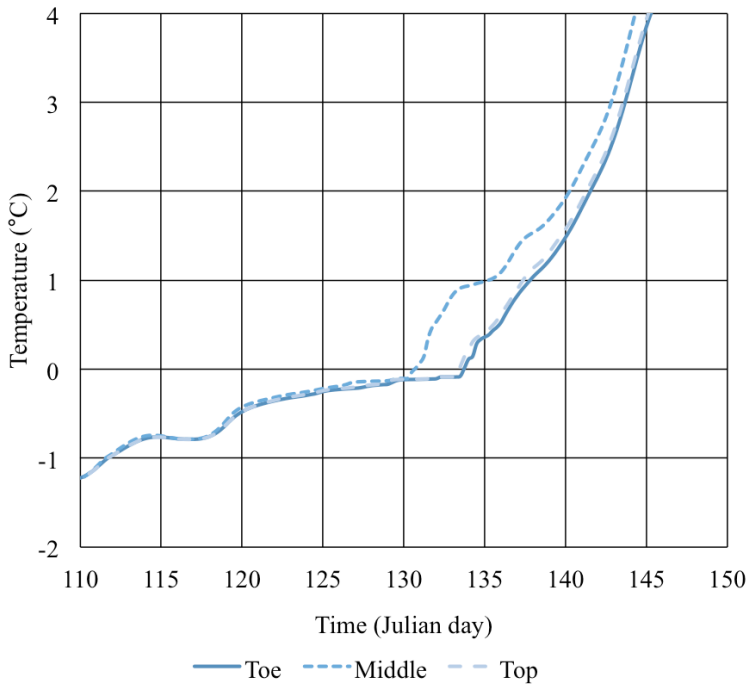

Figure 4.29 Temperature at the base of the sand at the top, depression and toe of the Model 3 slope.

Water flow through the upper gravel and sand layer was mainly vertical. During the snowmelt event, flow out the base of the two layers was approximately equal to flow out of the toe (Figure 4.30). After the snowmelt event, very little water exited the model domain through the toe of the upper gravel or sand layers, except during large summer precipitation events. The majority of water, approximately 93% by the end of the year, exited through the base of the sand layer into the lower gravel layer. Water flow through the lower gravel layer was mainly lateral flow, with the majority of water exiting through the toe of the slope and very little percolating through to the silt below (Figure 4.31).

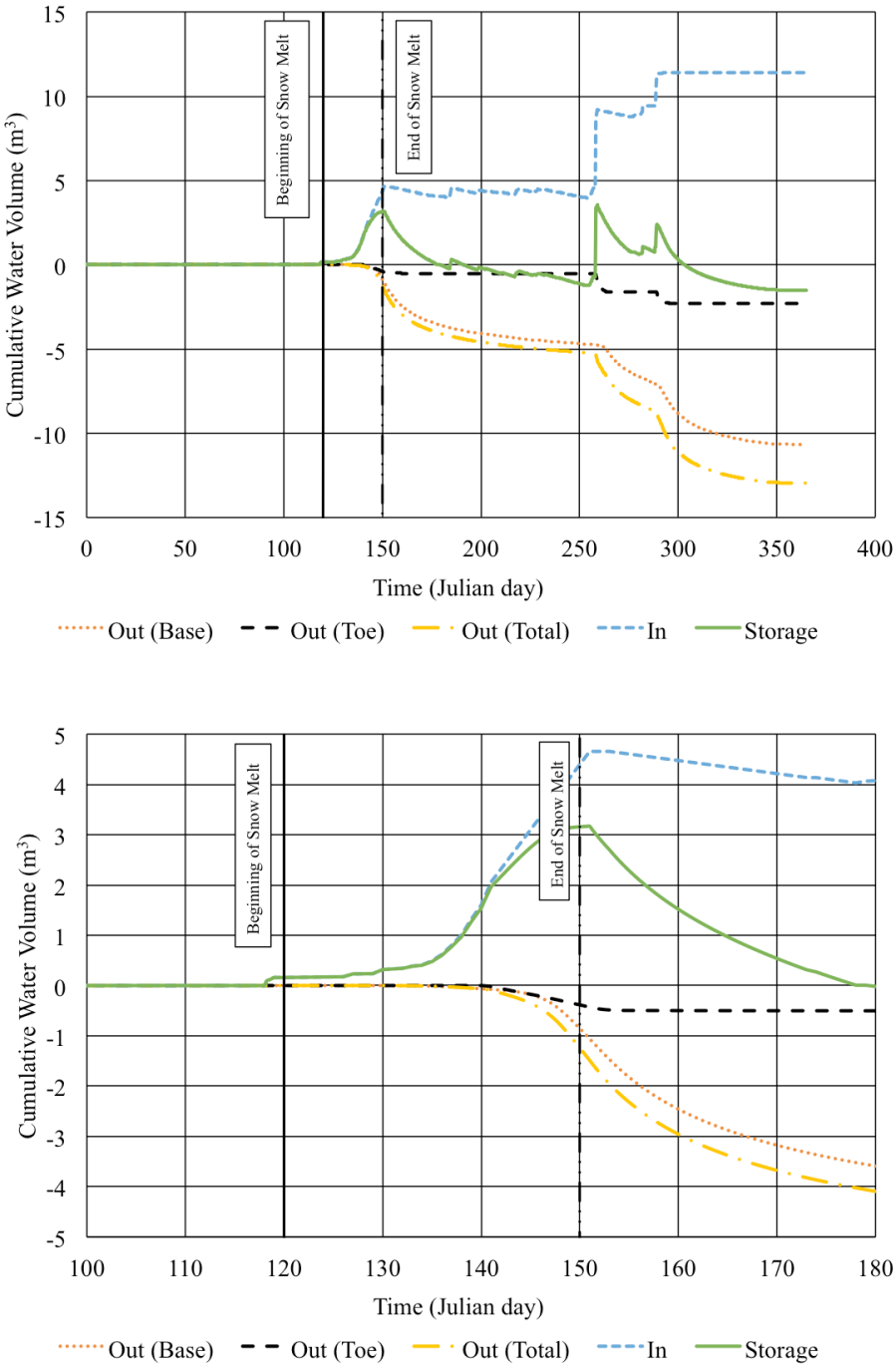

Figure 4.30 The cumulative water volumes entering and exiting the upper gravel and sand layers, along with the change in storage, in the Model 3 slope (top). A close up during the spring freshet is shown in the bottom graph.

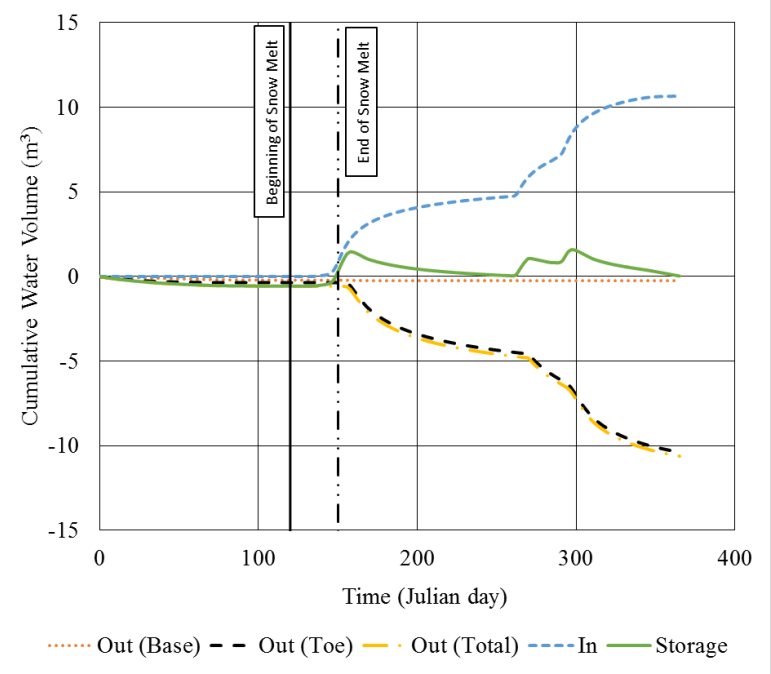

Figure 4.31 The cumulative water volumes entering and exiting the lower gravel layer, along with the change in storage, in the Model 3 slope.

4.5 Discussion

The three model domains illustrate the potential for failure of a SFCBD due to heat transfer associated with water flow. The first model domain, the steep slope model, encouraged lateral downslope flow due to frozen ground and a high slope gradient. This model setup had a larger potential for lateral convection dominated heat transfer. The shallow slope model also encouraged lateral flow, but experienced more vertical flow, which increased the potential for vertical convection. The third model featured a bench with a depression to encourage ponding and increase the conduction. The increased surface energy and water content of the depression promoted increased energy transfer through the soil. The soil under the depression thawed at an accelerated rate, resulting in preferential percolation. The three models diverted a varying portion of snowmelt infiltration, dependent on the design, as a result of the frozen soil, but illustrate three potential failure modes.

Lateral water flow within the steep slope model occurred mainly in the upper gravel. The elevated saturation reached during the snowmelt period encouraged water flow within the upper gravel rather than in the sand due to the higher hydraulic conductivity. At lower saturation levels, water flow will occur in the sand layer due to the higher unsaturated hydraulic conductivity (Figure 4.4). The water flow in the upper gravel occurred above the frozen soil, but was concentrated near the base of the layer following thaw. The lower hydraulic conductivity of the sand slowed percolation, increasing the water content at the base of the gravel and encouraging more lateral flow. This lateral water flow carried heat through lateral convection.

During the spring snowmelt period, the Peclet number, determined using the specific discharge, was equivalent to the gravitational maximum of 5.58. Flow occurred under near saturated conditions and convection was the dominant heat transfer mechanism. The thaw rate at the toe and middle of the slope was greater than the thaw rate at the top of the slope, in contrast to the Wolf Creek simulations. Water flow increased toward the toe, adding additional thermal energy, resulting in increased thaw (Figure 4.32). In contrast, the Wolf Creek simulations experienced greater thaw at the top than at the toe, which was determined to be a result of differences in initial ice content and thaw occurring through conduction rather than lateral convection.

Vertical flow also occurred through the upper gravel, but at a rate slower than the lateral flow. The reduction in vertical flow can be attributed to the frozen soil and the vertical anisotropy. Theoretically, if enough water flowed vertically through the upper gravel layer, vertical convection could dominate the vertical heat transfer. The vertical flow was not as great as the hydraulic conductivity, resulting in a Peclet number of 2.18, but still above the threshold where convection begins to dominate.

The shallow slope model failed to prevent large amounts of percolation through the cover system. While the frozen layer did divert some of the melt water, flow through the base of the sand and upper gravel layer was always larger than the amount of flow through the toe of the slope. The vertical water flow carried heat from the surface into the slope, increasing thaw of the frozen soil. The upper gravel layer did not reach saturation, but did

experience a large increase in water content. The duration of elevated saturation during the initial snowmelt showed lateral flow was occurring. At the 134th day, the water content of all three regions began to increase, corresponding to the increase in the snowmelt infiltration flux. As expected with lateral downslope flow, the toe reaches the highest saturation, followed by the middle and the top. The lateral water transfer causes an increase in the water content at the toe, but a decrease at the top.

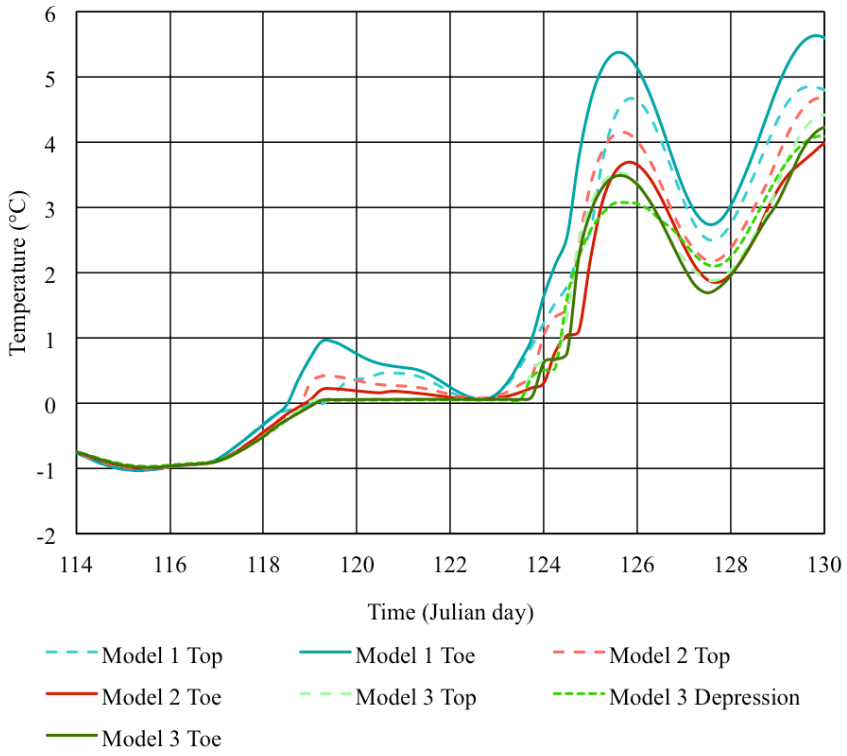

Figure 4.32 Comparison of temperatures at the base of the upper gravel in the three SFCBD models around the time of thaw.

The upper gravel in all models thawed at the same rate, with the exception of the top of the steep slope model, which had a slower thaw rate (Figure 4.32). The uniform thaw through the upper gravel of all models shows that, despite the large Peclet numbers, conduction altered the thaw rate through the upper gravel. If lateral convection were a larger contributor to thaw in the models, it would be expected that the toe would experience greater thaw rates than the upper portions of the slope. The steep slope model

did have higher thaw rates at the middle and toe of the slope than at the top (Figure 4.32), suggesting that lateral convection may have played some role in increasing thaw. The majority of lateral water flow in the upper gravel occurred at the base of the layer, above the interface with the sand layer. Lateral convection may not have played a large role in thaw of the upper gravel, but may have contributed to thaw in the sand.

The greatest energy transfer was through the upper gravel and sand under the depression (Figure 4.28). Water flow from the top of the slope flowed downslope and was captured by the depression. Such a depression could form as a result of erosion, preferential consolidation, animals or vegetation. The increased water content and surface energy due to ponding in the depression increased the heat transfer through conduction in that region of the soil, increasing the thaw rate below.

The lower hydraulic conductivity of the steep slope sand layer resulted in lower flows within the highly saturated sand, both vertical and lateral. Average lateral flow through the layer produced a Peclet number of only 7.59×10^{-3}. The measured specific discharge associated with this Peclet number was only slightly below the gravitational maximum value, indicating that flow was occurring under near saturated conditions. Vertical flow through the sand layer occurred at the saturated hydraulic conductivity. This produced a Peclet number of 9.23×10^{-2}. The vertical Peclet number was thus an order of magnitude higher than the lateral Peclet number. Both Peclet numbers were well below one, resulting in a conduction dominated heat transfer regime within the sand layer. Convection within the sand is therefore unlikely to play an important role in thawing the sand. However, lateral convection at the base of the upper gravel is likely to play a role in the thaw of the sand layer. In the steep slope model, the thaw rate in the sand increased with distance down the slope, with the toe experiencing the greatest thaw rates (Figure 4.33). As the flows within the sand layer are not great enough to generate convection to influence the thaw rate, the difference in thaw rate can be attributed to the extra heat contributed by lateral convection at the base of the upper gravel.

A zero-curtain that lasted for several days developed in the sand layer (Figure 4.33). Refreezing within the soil releases latent heat, which rapidly brings the soil to 0 °C (Kane

et al. 2001). Latent heat absorption by the surrounding soil reduces the overall warming effect, leading to isothermal conditions, or a zero-curtain window. The lower thermal conductivity of the sand and the higher ice content likely increased the zero-curtain effect, as observed by Carey and Woo (1998). A lack of external thermal energy added through convection within the sand layer may have also contributed to the extended zero-curtain window.

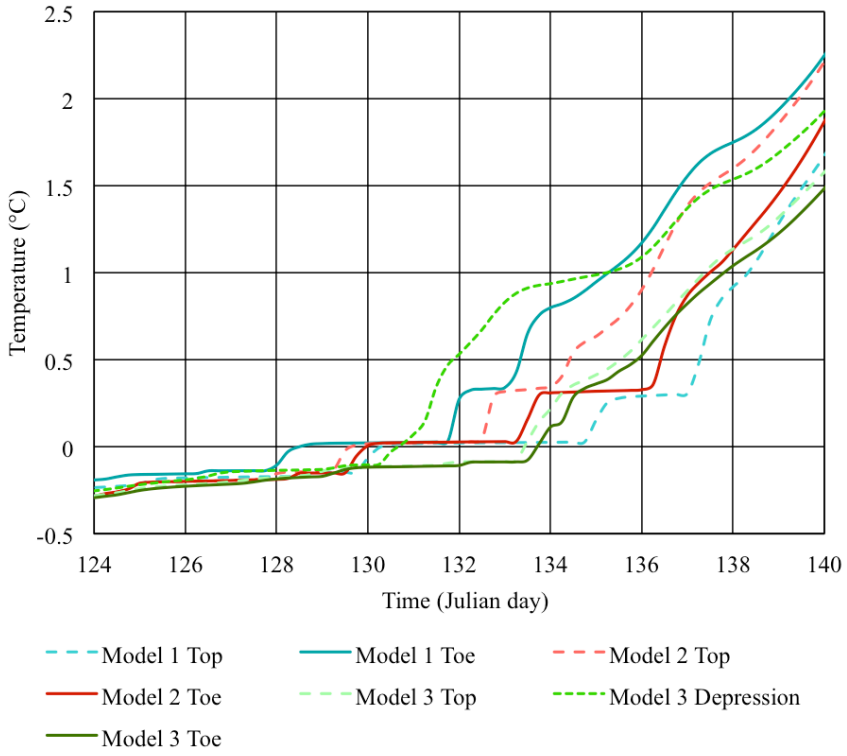

Figure 4.33 Comparison of temperatures in the sand in the three SFCBD models around the time of thaw.

The zero-curtain also developed in the sand layer of the shallow slope model, but did not last as long (Figure 4.33), indicating the increased vertical convection through the shallow slope sand layer may have had some effect on thaw. The vertical Peclet number for the shallow slope sand layer was only 0.123, while the lateral Peclet number 0.201. Both values are less than 1, signifying an environment dominated by conduction. Despite

the increase in vertical convection in the shallow slope over the steep slope, conduction remains dominant.

The sand layer in the depression model experienced an increased rate of thaw compared to the two other models. A zero-curtain also developed, but did not last as long as in the other simulations. At the base of the layer, the zero-curtain lasted only 2 days, which was several days shorter than in the two other models. Vertical flow through the sand of the depression model was at the same rate as the shallow slope model, limiting the influence of convection. The thermal conductivity of the upper gravel layer at the depression experienced a greater increase than either the shallow or steep slope models due to the higher water content. The increased water content also increased the volumetric heat capacity, lowering the thermal diffusivity. The higher surface energy transfer that occurred due to the increased water content in the depression increased the thermal energy transfer via conduction to the sand layer, increasing the thaw rate and decreasing the zero-curtain window.

The lower gravel layer barely froze, with the base of the layer only reaching just below zero in the shallow slope model at around the 35^{th} day and not until the 75^{th} day in the steep slope model. Freezing reached the base of the depression model by the 60^{th} day. Thaw through the layer occurred at same rate through all three models, at an average rate of 4.0 mm/hour. The vertical water flux through the layer in all simulations produced a Peclet number greater than 1. The steep slope model had a vertical Peclet number of 1.07, indicating that convection and conduction were relatively equal. The shallow slope had greater vertical flows through the layer, resulting in a Peclet number of 1.57, which indicates vertical convection should be dominating.

The numerical model does not allow different kinds of heat to be tracked separately. Therefore, no distinction can be made between sensible heat conducted or convected from the surface and latent heat generated through refreezing within the soil profile. Zhao et al. (1997) found that after a certain time, once quasi-steady state is reached, it is latent heat released during refreezing that supplies the energy required to increase soil temperatures, and not sensible heat conducted from the surface. Within the SFCBD

models, quasi-steady state is not reached due to the changes in infiltration rate. The applicability of these findings is limited, but does suggest that a large portion of the thermal energy required to increase soil temperatures comes from latent heat. Zhao et al. (1997) further suggests that the heat is transferred downwards via conduction and convection. The formulation of the Peclet number given by Kane et al. (2001), and used in this research, does not account for the transfer of latent heat, only the transfer of sensible heat. Kane et al. (2001) suggests that, under conditions of water infiltrating into sub-zero temperature soils, the accompanying release of latent heat could increase the role of convection by an order of magnitude. The simulations included the release and transfer of latent heat, but the calculated Peclet numbers may be underestimating the influence of convection.

The saturation level of the upper gravel and sand played a major role in determining the success of the SFCBD in diverting water. In initial versions of the SFCBD models, the two layers were at lower initial water contents. Upon the start of snowmelt infiltration, the water content did not reach a suitable level to promote lateral flow and the majority of water flow was vertical through the layers. In the current models, the initial water contents were set through the spin up years, allowing the water content to reach steady state year over year. The steep slope provided conditions for lateral flow and was able to laterally divert most of the snowmelt. The shallow slope, even at high saturations, had extensive vertical flow in addition to lateral flow. In both models, flow through the sand was mainly vertical, even when the sand was at or near saturation. Some lateral flow through the sand would flow to the toe before flowing upwards into the highly saturated, high hydraulic conductivity gravel before leaving the domain.

The only difference between the steep slope model and the shallow slope model was the gradient of the slope. The steeper slope, at a slope gradient of 0.2, outperformed the shallower, 0.1 gradient slope in terms of water diversion. The greater slope angle increased the gravity gradient, allowing the slope to rely less on hydraulic pressures to generate flow. The feasibility of achieving such a steep slope over actual mine waste could present other challenges, in both construction and in operation. A shallower

gradient slope is capable of lateral diversion, as shown by the shallow slope model, but would need to be investigated further on a site-by-site basis.

The thickness of the layers is also important in determining the success of a SFCBD cover system. In initial SFCBD cover models, the thickness of the upper gravel in the depression model was reduced to encourage saturation and ponding. A thicker layer at the same snowmelt infiltration rates reduced ponding by increasing the storage in the upper layer, while allowing more water into the lower layer before saturation (i.e. ponding). To encourage lateral flow within the upper gravel, a saturated or nearly saturated zone needs to develop at the base of the upper gravel. With a thicker upper layer, the storage increases, as does the delay in water reaching the base of the layer.

An increase in the thickness of the sand layer would likely increase the time required to thaw, further encouraging lateral flow above the frozen soil. However, a thicker sand layer would require more water to maintain the elevated levels of saturation required for the cover to perform as a capillary barrier and to generate the ice content necessary in the fall/winter to prevent infiltration in the spring.

The slope length of the simulations was limited by the constraints of the numerical model to 30 m. In reality, cover systems can be much longer than the simulated slope length. It is not expected for an increased length of the slope to detrimentally impact the performance of the cover system in terms of thermal energy heat transfer. Natural analogues that feature a frozen layer diverting snowmelt infiltration that are 500-1200 m in length have been observed (Carey and Woo 2001a). Increased slope lengths may experience increases in the specific discharges within the layers due to the additional water and extra travel distance. A slight increase in the importance of convection may accompany the increase in flow rates. However, the specific discharges in the upper gravel and sand of the simulations already approached the upper limit of flow in the simulations. Therefore, only a slight increase in the convective energy transfer is thought to be possible.

The hydraulic conductivity controls the amount of water that can flow through a material. An increase in the hydraulic conductivity of the upper sand would allow more water to

flow through the layer. The higher discharge rates would increase the role of convection, both lateral and vertical, as more heat could be carried with the water. Flow is limited not by the hydraulic conductivity however, but by the availability of water. Therefore, an increase in the hydraulic conductivity may not result in an increase in convection. In a SFCBD system, where inflow into the system is limited to the snowmelt, the thermal energy transfer results are likely to be the same as those explored in the simulations, even when the hydraulic conductivity of the upper gravel is increased.

Changes in thermal properties may alter the role of convection within the soil layers. Increasing the thermal diffusivity would effectively increase the conduction, lowering the influence of convection and reducing the Peclet number. Decreasing the thermal diffusivity would increase the relative influence of convection by decreasing the conductive heat transfer. These effects would likely be minor given the typical ranges of thermal properties that tend to be in the same order of magnitude, relative to hydraulic properties, which can vary over orders of magnitude.

The hydraulic conductivity provides the greatest control on determining the success or failure of a SFCBD cover system. While other properties tend to be similar between various materials, the hydraulic conductivity can vary by orders of magnitude. It also determines the amount of flow that can occur within a layer, thereby influencing the ability of the material to shed water and altering the thermal energy transfer regime. The basic design of a SFCBD cover relies on the difference in hydraulic conductivity between the two layers to maximize snowmelt runoff, making it one of the greatest properties of interest in a SFCBD cover design. Factoring in the control on the thermal energy transfer within the soil, it becomes the most important property to consider. It can, to an extent, be controlled through the average grain size of the material and could be reduced by crushing the material into smaller grains.

Of the three geometries simulated, the first model domain, the steep slope, provides the best example of a functioning SFCBD cover system. Despite the increased thaw due to lateral convection, the slope successfully diverted the bulk of the meltwater during the spring freshet. Practicality of construction and operation of such a geometry would have

to be determined on a site by site basis. Ultimately, all model domains failed to divert the majority of infiltrating waters when the summer performance is taken into account. Further study into capillary barriers and the influence of freezing and thawing on performance is recommended.

The shallow slope model was able to divert snowmelt laterally, but experienced larger vertical flow into the lower gravel layer, resulting in a failure of the cover system. Altering the slope geometry, either in increasing the slope gradient or the thickness of the sand layer, may prevent the large amounts of vertical percolation.

The depression model would not be an ideal design for a SFCBD cover. The depression allowed water to pond, resulting in accelerated thaw and preferential infiltration and percolation. This is a scenario that should be avoided in designing a SFCBD cover. Ponding surface water can also increase the surface radiation capture, further increasing the accelerated thaw (Hayashi et al. 2003).

The vertical convection of the shallow slope model and the increased conduction of the depression model showed the highest thaw rates and likely present the greatest threats to the success of a SFCBD cover system.

5 CONCLUSIONS AND RECOMMENDATIONS

5.1 Conclusions

The research into the thermal design considerations of a seasonally frozen capillary barrier diversion cover system explored the effect of coupled water and heat flow on the performance of a SFCBD cover. The cover is designed to incorporate the seasonal freezing that occurs in cold regions, with the proven design of capillary barrier covers. A textural difference between the lower coarser textured material and the middle 'finer' textured material promotes elevated levels of saturation within the finer layer. Freezing of this layer creates a barrier to flow during the spring snowmelt. The upper 'coarser' layer provides a medium through which the meltwater can be laterally diverted downslope. Once spring thaw and runoff has finished, the cover will use the capillary barrier to prevent further percolation into the mine waste/tailings below.

The research was accomplished using the numerical modelling suite GeoStudio in several phases. The first phase benchmarked and compared the TEMP/W and SEEP/W products of the GeoStudio suite with analytical solutions and other numerical models. The benchmarks showed the capabilities of TEMP/W and SEEP/W to model the various processes involved in a SFCBD cover. The second phase modelled several case studies to explore the roles of convection and conduction in thaw using examples from the literature. Lateral convection was investigated through simulating the Wolf Creek basin in the Yukon. Vertical convection was examined through simulations to replicate and extend the column tests performed by Watanabe et al. (2013). Ponding and increases in conduction leading to preferential thaw were studied by simulating the phenomenon proposed by Hayashi et al. (2003). The final phase applied the knowledge gained in the previous phases to illustrative SFCBD cover simulations. These models incorporated the

climate data for the Giant Mine in the Northwest Territories, along with idealized material properties. The models illustrate several different geometries, each with a possible failure mode due to thermal conditions.

There were two main objectives directing this research. The SFCBD cover system provides a new approach to mine reclamation in cold regions and needed to be investigated numerically before laboratory or field studies could be carried out. The first objective of this research was to further understand and determine the impact of the different thermal energy transfer process on the performance of a frozen barrier layer.

The Wolf Creek case study revealed that lateral convection has the potential to dominate the thermal heat transfer within the soil when large fluxes of water occur. Under climatic snowmelt conditions however, the role of convection is reduced and the Peclet number suggests conduction dominates the thermal heat transfer regime within the organic-rich soil. The mineral soil of both slopes showed that in a mineral soil, whether low hydraulic conductivity, like the north slope, or relatively high, like the west slope, the potential for convection is limited.

Further investigation through the steep slope SFCBD illustrative model confirmed lateral convection can occur and influence the thaw of the frozen soil. Increased thaw rates at the middle and toe of the slope were observed in the sand layer as a result of convective heat transfer with water flow at the base of the upper gravel. The Peclet number, a measure of the relative importance of convection and conduction, showed that convection dominated within the upper gravel layer. The frozen soil was able to divert large amounts of snowmelt, with lateral flow accounting for the majority, or at least equal amount, of water flow through the upper gravel and sand until the 200th day, well after thaw was complete (Table 5-1).

Table 5-1 Percentage of precipitation percolating through the upper gravel and sand into the lower gravel during the spring freshet and the entire year.

	Spring Freshet	Full Year
Steep Slope Model	19%	70%
Shallow Slope Model	21%	97%
Depression Model	86%	93%

The influence of vertical convection was not as straightforward as lateral convection. The column case study showed higher Peclet numbers at higher discharges, but lower thaw rates. This is likely the result of increased water flows creating more ice due to refreezing, while stripping and carrying away the accompanying latent heat and counteracting conduction from the bottom of the column. It was the lowest initial water content and lowest water flow that showed the largest thaw rates. The low ice content decreased thaw times, while the slower water flow allowed more heat to remain and contribute to thaw.

The shallow slope SFCBD illustrative model experienced high vertical flows in the upper gravel resulted in a Peclet number greater than one. However, like the other SFCBD models, the upper gravel had thawed via conduction prior to the simulation of the majority of snowmelt infiltration and percolation due to the inability to model the snowpack on the surface. Some water was diverted laterally and the lateral Peclet number suggests lateral and vertical convection are almost equal. There was, however, no increase in thaw rates at the toe compared to the top as was observed in the steep slope model. Vertical Infiltration and percolating water carried sensible heat from the surface and latent heat from refreezing to the thawing front, stabilizing the thaw rate at all regions. The shallow slope model diverted approximately 79% of infiltrating water during the spring freshet, but over the entire year, failed to divert the majority of precipitation, with 97% percolating through to the lower gravel (Table 5-1).

The sand layer in both the steep slope and shallow slope model did not appear to be greatly influenced by convection within the layer, either lateral or vertical. Thaw through the sand occurred mainly as conduction, due to the low hydraulic conductivity of the sand. With a lower thermal conductivity and without the influence of internal convection,

thaw of the sand layer was significantly reduced. However, thaw of the sand in the steep slope model increased with lateral distance down the slope, suggesting that lateral convection within the upper gravel influenced thaw of the underlying sand layer.

Ponding of water increased the conduction due to the increase in energy transfer that resulted from the increased water content. Both the case study model and the SFCBD model showed increased thaw under the depression after water had collected in the depression. Due to the increased thaw, infiltration and percolation under the depression occurred prior to thaw in the other regions of the slope. During the spring freshet and over the entire year, the depression model failed to divert the majority of precipitation. Approximately 86% of meltwater and approximately 93% of total precipitation percolated into the lower gravel (Table 5-1).

From all of these simulations, it can be seen that there is not one single dominant heat transfer mechanism in frozen soil. Lateral convection will likely dominate in sloped coarse soils with high hydraulic conductivities. Without the development of a saturated zone, large flow rates will not be achieved and the influence of lateral convection will drop. Vertical convection can occur when large amounts of water flow are not diverted, but instead percolate vertically. Vertical convection can cause greater thaw rates than lateral convection and will affect the slope equally in the absence of heterogeneity. Conduction will always occur and will dominate the thermal energy transfer in the absence of water flow. In a finer layer with a lower hydraulic conductivity, conduction is likely to always be the dominant heat transfer process. Water is unable to reach suitable flow rates to allow convection to dominate. Where a finer layer is overlain by a coarser layer, lateral convection within the coarser layer can influence the thaw of the finer layer.

The second objective of this research was to determine the feasibility of a SFCBD cover system at a representative mine site using available, ideal materials and the climatic conditions of the site. Some of the critical properties that could determine the success or failure of a SFCBD cover were also to be identified in this research.

The Giant Mine in Yellowknife, NWT was used as the representative mine in this study. Climate data from the region was used to construct the boundary conditions of the

simulations. Materials were idealized versions of borrow materials available at or near the site.

The illustrative SFCBD cover models suggest a SFCBD cover would be feasible for a location such as the Giant Mine given the availability of proper materials. The climatic conditions of such a location are sufficiently cold for the freezing front to reach the base of the sand and extend into the lower gravel layer. Other regions in the north would likely have similar or colder conditions and be able to support a SFCBD cover.

The hydraulic conductivity of the materials was determined to be one of the critical properties exhibiting a large control on the performance of the cover. The hydraulic conductivity controls the amount of water that can flow through the material. The sand and gravel used were ideal materials for the design, but not necessarily available at all mine sites. The SFCBD cover design does not require the use of sand and gravel, as in the simulations, but relies on the difference in texture between the layers. While water transfer within a coarse material tends to be limited by the availability of water and not the hydraulic conductivity, finer layers are more susceptible to changes in hydraulic conductivity. The finer layer in a SFCBD cover is designed to remain at elevated levels of saturation, where the hydraulic conductivity becomes the limiting factor to flow. Flow through a lower hydraulic conductivity layer tends to be vertical, as was observed in the sand layer of all SFCBD simulations.

The cover design relies on the difference between the water retention curves and hydraulic conductivity functions of the coarser and finer materials to retain the elevated saturation within the finer layer and promote lateral water flow above the finer layer. Changes in the hydraulic conductivities of the layers may increase the amount of water shed laterally by the sand layer, but could also alter the relationship such that maintaining elevated saturation within the sand layer becomes more difficult.

The hydraulic conductivity also plays a large role in determining the extent to which convection dominates the thermal energy transfer. Larger hydraulic conductivities allow greater discharges, which carry more heat and increase the Peclet number, as observed in the upper gravel. When hydraulic conductivities are low, conduction will likely dominate,

even under saturated conditions, as was the case in the sand. The influence of hydraulic conductivity on the thermal energy transfer within a soil, coupled with the control on water flow, gives the hydraulic conductivity great influence on the performance of a SFCBD cover.

The degree of saturation within the sand and upper gravel layer is also a critical property. The design relies on the elevated saturation of the sand layer to prevent ingress of water into the mine waste. The saturation level in a SFCBD cover is controlled by the water retention curves and the hydraulic conductivity functions. Capillary forces maintain the elevated saturation of the sand layer at higher matric suctions. The hydraulic conductivity of the lower gravel decreases below that of the sand at high matric suctions, thus promoting flow in the sand.

At low initial water contents, initial test simulations showed mainly vertical water flow through the cover. The matric suction was high, reducing the hydraulic conductivity and prompting the water to take the 'path of least resistance' vertically through the upper gravel to reach the sand layer. During the current models, the initial water content was increased and lateral downslope flow occurred. The increased initial water content allowed a zone of saturation or near saturation to develop at the base of the upper gravel, increasing the hydraulic conductivity and promoting preferential lateral flow. The initial water content and the saturation are thus important considerations in the design of a SFCBD cover.

The slope geometry was also found to influence the overall performance of a SFCBD cover system. The gradient of the slope exerted a large control on the ability of the slope to create lateral downslope flow. The steep slope model was able to shed more water laterally than the shallow slope model due to its higher slope gradient. The feasibility of a high slope gradient would have to be assessed on a site by site basis. A shallower slope gradient could be implemented and succeed, but other slope properties may have to change to ensure success.

The SFCBD cover system design presents a new opportunity to re-evaluate mine waste reclamation. Current practice takes designs and ideas that were developed for temperate

climates and applies them to northern, cold climate mines without necessarily taking into account the effects of the cold climate. The SFCBD cover incorporates the cold climate and the materials typically available at a northern mine into the design and utilizes them to maximize snowmelt runoff. The simulations carried out in this research have shown the SFCBD cover system is a viable alternative to the current practice and worth pursuing further.

5.2 Recommendations

Several gaps in understanding were encountered during the course of the research. These gaps could not be filled through the current research and further work is recommended. It is advised that laboratory and field studies, along with heterogeneity and site specific modelling be performed to further the understanding of thermal energy transport and determine the suitability of a SFCBD for specific locations. Additional modelling should be undertaken prior to the completion of lab and field studies.

5.2.1 Laboratory and Field Studies

The current research was limited to numerical modelling only. Field and laboratory data was incorporated through the case studies, but was limited in applicability. Laboratory and field data covering tests of the actual SFCBD design are needed before the SFCBD design could be adopted. Laboratory studies would allow the thermal energy transfer on a smaller scale to be investigated.

Simple laboratory studies could be carried out to validate some of the findings of this research and further the understanding of water flow over frozen soil. A scale model of a SFCBD cover, instrumented to capture temperature changes, water content and other relevant data, along with controlled water influxes, could be used to investigate heat flow with water through the cover. A conservative, coloured tracer and a camera could be used to track and record water flow, while a thermal imaging camera could be used to track and record heat flow.

Laboratory studies could also be used to study the effect of heterogeneity on the thermal energy transfer and frozen soil. Macropores could be replicated, along with patches of increased or decreased hydraulic conductivity. Several freeze-thaw cycles could be replicated to determine their impact on the material's hydraulic conductivity and other properties. The development of erosional features could also be investigated in a controlled environment.

Once the laboratory studies have been complete, small cover trials could be built at representative mines. These small-scale field studies would allow the cover to be tested under real field conditions before being employed at real scales. Water content and temperature sensors would be required to track the flow of heat and water within the cover trial. Flumes would be able to calculate the amount of runoff diverted by the cover, determining the success of the cover. Once cover trials are complete, a full-scale SFCBD cover could be built.

5.2.2 Heterogeneity Modelling

Heterogeneity adds a layer of complexity that was beyond the scope of this research. It may, however, have a large impact on the performance of a SFCBD cover system. Heterogeneity of the hydraulic conductivity would cause some water to flow faster or slower than the average, which could alter the thermal energy transfer. Screening of the soil materials would help reduce heterogeneity within the soil, but modelling of various heterogeneity possibilities should still be undertaken.

Macropores are one type of heterogeneity that could significantly alter the thermal energy transfer regime within the soil. Macropores due to vegetation or wildlife could create pathways for water to bypass the cover system. They would also introduce preferential flow into the cover, which could increase the thermal energy transfer and result in preferential thaw.

Soil piping could have similar effects, creating preferential flow paths within the soil layers, allowing water to flow faster than the hydraulic conductivity and increasing the

convection occurring. The current models assumed sheet flow within the slopes. Piping and other preferential flow paths would alter the thermal energy transfer by providing conduits of high water flow, increasing the local role of convection.

Other erosional features could develop as a result of the diverted water flow. As shown by the current research, an erosional feature such as a depression, will cause increased conduction and thaw, leading to preferential infiltration and percolation. Erosional modelling would help predict where erosional features may develop and how they could be prevented. Linking the subsurface models to a surface water model could also provide useful insight about surface water flow and erosion, while also allowing the energy balance to be closed.

It is suggested that future modelling take into account soil heterogeneity and examine its impacts on thermal energy transfer within the soil. Soil piping and other erosional features also need to be taken into consideration before a SFCBD cover can be built.

5.2.3 Site Specific Modelling

It is also recommended that, along with laboratory and field studies and heterogeneity modelling, site specific modelling be completed. Each potential site has a different climate that may impact the design in different ways. It is also important to incorporate the actual properties of the materials available on site. Different material properties may necessitate changes in the design of the cover.

Climate change should also be taken into account in site-specific modelling. Changes in temperature and precipitation due to climate change will influence the performance of a SFCBD cover system. Design changes may be required to accommodate change in climate.

The aspect of the slope is another important site-specific property that would affect the performance of the cover. Different slope aspects receive different amounts of solar radiation, which would increase or decrease the amount of energy available to melt the

snow and thaw the soil. North slopes receive the least amount of energy and often have lingering snow and frozen soil after the disappearance of snow and thaw of the frozen soil on slopes facing a different aspect. The aspect of the slope therefore needs to be taken into account, as the shortened or extended snowmelt and thaw period could affect the overall performance of the cover.

REFERENCES

Andersland, O.B., and Ladanyi, B. 1994. An Introduction to Frozen Ground Engineering. Chapman and Hall, New York, New York.

Anderson, D.M., and Tice, A.R. 1973. Predicting unfrozen water contents in frozen soils from surface area measurements. J. Terramechanics **10**.

Anderson, M.P. 2005. Heat as a ground water tracer. Ground Water **43**: 951–68. doi: 10.1111/j.1745-6584.2005.00052.x.

Baker, J.M., and Spaans, E.J.A. 1997. Mechanics or meltwater movement above and within soil. *In* International Symposium on Physics, Chemistry, and Ecology of Seasonally Frozen Soils, Fairbanks, Alaska, June 10-12, 1997. *Edited by* I.K. Iskandar, E.A. Wright, J.K. Radke, B.S. Sharratt, P.H. Groenevelt, and L.D. Hinzman. U.S. Army Cold Regions Research and Engineering Laboratory, Hanover, NH. pp. 31–36.

Bayard, D., Stähli, M., Parriaux, A., and Flühler, H. 2005. The influence of seasonally frozen soil on the snowmelt runoff at two Alpine sites in southern Switzerland. J. Hydrol. **309**: 66–84. doi: 10.1016/j.jhydrol.2004.11.012.

Bredehoeft, J.D., and Papadopulos, I.S. 1965. Rates of vertical groundwater movement estimated from the Earth's thermal profile. Water Resour. Res. **1**.

Carey, S.K., and Woo, M. 1998. Snowmelt hydrology of two subarctic slopes, southern Yukon, Canada. Nord. Hydrol. **29**: 331–346.

Carey, S.K., and Woo, M. 1999. Hydrology of two slopes in subarctic Yukon, Canada. Hydrol. Process. **13**: 2549–2562.

Carey, S.K., and Woo, M. 2001a. Slope runoff processes and flow generation in a subarctic, subalpine catchment. J. Hydrol. **253**: 110–129.

Carey, S.K., and Woo, M. 2001b. Spatial variability of hillslope water balance, Wolf Creek basin, subarctic Yukon. Hydrol. Process. **15**: 3113–3132. doi: 10.1002/hyp.319.

Carey, S.K., and Woo, M. 2005. Freezing of subarctic hillslopes, Wolf Creek Basin, Yukon, Canada. Arctic, Antarct. Alp. Res. **37**: 1–10. doi: 10.1657/1523-0430(2005)037[0001:FOSHWC]2.0.CO;2.

Daanen, R.P., Misra, D., and Epstein, H. 2007. Active-Layer Hydrology in Nonsorted Circle Ecosystems of the Arctic Tundra. Vadose Zo. J. **6**: 694. doi: 10.2136/vzj2006.0173.

Dall'Amico, M., Endrizzi, S., Gruber, S., and Rigon, R. 2011. A robust and energy-conserving model of freezing variably-saturated soil. Cryosph. **5**: 469–484. doi: 10.5194/tc-5-469-2011.

Davis, S.N., and DeWiest, R.J.M. 1966. Hydrogeology. John Wiley & Sons, Inc., New York, New York.

Dingman, S.L. 2008. Physical Hydrology. *In* Second Edi. Waveland Press, Inc., Long Grove, IL.

Domenico, P.A., and Schwartz, F.W. 1990. Physical and Chemical Hydrogeology. Wiley, New York, New York.

Environment Canada. 2010. Canadian Climate Normals 1981-2010 - Yellowknife A.

Environment Canada. 2012. Daily Data Report for 2012 - Yellowknife A. Environment Canada, Yellowknife, NT.

Farouki, O.T. 1981. Thermal properties of soils. *In* CRREL Monograph 81-1. U.S. Army Cold Regions Research and Engineering Laboratory, Hanover, NH.

Ferguson, G. 2015. Screening for Heat Transport by Groundwater in Closed Geothermal Systems. Groundwater **53**: 503–506. doi: 10.1111/gwat.12162.

Fetter, C.W. 1999. Contamintant Hydrogeology. *In* Second Edi. Waveland Press, Inc., Long Grove, IL.

Fetter, C.W. 2001. Applied Hydrogeology. *In* Fourth Edi. Prentice Hall, Upper Saddle River, NJ.

Flerchinger, G.N. 2000. The Simultaneous Heat and Water (SHAW) Model: Technical Documentation. Northwest Watershed Research Center, USDA Agricultural Research Service, Technical Report NWRC 2000-09, Boise, Idaho.

Fredlund, D.G., and Rahardjo, H. 1993. Soil Mechanics for Unsaturated Soils. John Wiley & Sons, Inc., New York, New York.

Freeze, R.A., and Cherry, J.A. 1979. Groundwater. Prentice Hall, Upper Saddle River, NJ.

van Genuchten, M.T. 1980. A Closed-form Equation for Predicting the Hydraulic Conductivity of Unsaturated Soils. Soil Sci. Soc. Am. J. **44**: 892–898.

GEO-SLOPE International Ltd. 2012. 1D Infiltration into Dry Soil: Benchmark.

GEO-SLOPE International Ltd. 2014. GeoStudio.

Golder Associates Ltd. 2004. Giant Mine Borrow Investigation.

Granger, R.J., Gray, D.M., and Dyck, G.E. 1984. Snowmelt infiltration to frozen Prairie soils. Can. J. Earth Sci. **21**: 669–677. doi: 10.1139/e84-073.

Grasby, S.E., Majorowicz, J., and McCune, G. 2013. Geothermal energy potential for northern communities. doi: 10.4095/292840.

Gray, D.M., Landine, P.G., and Granger, R.J. 1985. Simulating infiltration into frozen Prairie soils in streamflow models. Can. J. Earth Sci. **22**: 464–472.

Hansson, K., Simunek, J., Mizoguchi, M., Lundin, L.-C., and Th. van Genuchten, M. 2004. Water flow and heat transport in frozen soil: Numerical solution and freeze-thaw applications. Vadose Zo. J. **704**: 693–704.

Harlan, R. 1973. Analysis of coupled heat-fluid transport in partially frozen soil. Water Resour. Res. **9**: 1314–1323.

Hayashi, M., van der Kamp, G., and Schmidt, R. 2003. Focused infiltration of snowmelt water in partially frozen soil under small depressions. J. Hydrol. **270**: 214–229. doi: 10.1016/S0022-1694(02)00287-1.

INAC. 2010. Northern Contaminated Sites Program, Progress Report 2005-2010. Indian and Northern Affairs Canada, Ottawa, ON.

Iwata, Y., Hayashi, M., and Hirota, T. 2008. Comparison of Snowmelt Infiltration under Different Soil-Freezing Conditions Influenced by Snow Cover. Vadose Zo. J. **7**: 79. doi: 10.2136/vzj2007.0089.

Iwata, Y., Hayashi, M., Suzuki, S., Hirota, T., and Hasegawa, S. 2010. Effects of snow cover on soil freezing, water movement, and snowmelt infiltration: A paired plot experiment. Water Resour. Res. **46**. doi: 10.1029/2009WR008070.

Jansson, P.-E., and Karlberg, L. 2004. Coupled heat and mass transfer model for soil-plant-atmosphere systems. Royal Institute of Technology, Department of Civil and Environmental Engineering, Stockholm.

Johansen, O. 1977. Thermal Conductivity of Soils. *In* Draft Translation 637. U.S. Army Cold Regions Research and Engineering Laboratory, Hanover, NH.

Johnston, G.H., Ladanyi, B., Morgenstern, N.R., and Penner, E. 1981. Engineering characteristics of frorzen and thawing soils. *In* Permafrost: Engineering design and construction. *Edited by* G.H. Johnston. Wiley, Toronto, Ontario. pp. 73–147.

Jury, W.A., and Horton, R. 2004. Soil Physics. *In* Sixth Edit. John Wiley & Sons, Inc., Hoboken, New Jersey, USA.

van der Kamp, G., and Bachu, S. 1989. Use of dimensional analysis in the study of thermal effects of various hydrogeological regimes. *In* Geophysical Monograph Series. *Edited by* A.E. Beck, G. Garven, and L. Stegena. AGU, Washington, D. C. pp. 23–28. doi: doi:10.1029/GM047p0023.

van der Kamp, G., and Hayashi, M. 1998. The groundwater recharge function of small wetlands in the semi-arid northern prairies. Gt. Plains Res. **8**: 39–56.

van der Kamp, G., Hayashi, M., and Gallen, D. 2003. Comparing the hydrology of grassed and cultivated catchments in the semi-arid Canadian prairies. Hydrol. Process. **17**: 559–575. doi: 10.1002/hyp.1157.

Kane, D.L. 1980. Snowmelt infiltration into seasonally frozen soils. Cold Reg. Sci. Technol. **3**: 153–161.

Kane, D.L., and Chacho, E.F. 1990. Frozen ground effects on infiltration and runoff. *In* Cold Regions Hydrology and Hydraulics. *Edited by* W.L. Ryan and R.D. Crissman. American Society of Civil Engineers, New York, New York. pp. 259–300.

Kane, D.L., Hinkel, K.M., Goering, D.J., Hinzman, L.D., and Outcalt, S.I. 2001. Non-conductive heat transfer associated with frozen soils. Glob. Planet. Change **29**: 275–292.

Kane, D.L., and Stein, J. 1983. Water movement into seasonally frozen soils. Water Resour. Res. **19**: 1547–1557. doi: 10.1029/WR019i006p01547.

Klene, A.E., Nelson, F.E., Shiklomanov, N.I., and Hinkel, K.M. 2001. The N-Factor in Natural Landscapes: Variability of Air and Soil-Surface Temperatures, Kuparuk, River Basin , Alaska, U.S.A. Arctic, Antarct. Alp. Res. **33**: 140–148.

Klock, G.O. 1972. Snowmelt Temperature Influence on Infiltration and Soil Water

Retention. J. Soil Water Conserv. **27**: 12–14.

Krahn, J. 2004a. Thermal Modeling with TEMP/W: An Engineering Methodology. GEO-SLOPE International Ltd., Calgary, Alberta.

Krahn, J. 2004b. Seepage Modeling with SEEP/W: An Engineering Methodology. GEO-SLOPE International Ltd., Calgary, Alberta.

Lunardini, V. 1991. Heat Transfer with Freezing and Thawing. Elsevier, New York, New York.

Lunardini, V. 1998. Effect of convective heat transfer on thawing of frozen soil. *In* Proceedings of the 7th International Conference on Permafrost. Canada: Yellowknife. *Edited by* A.G. Lewkowicz and M. Allard. Universite Laval, Centre d'etudes nordiques, Collection Nordicana No 55. pp. 689–695.

Marsh, P. 1990. Snow Hydrology. *In* Northern Hydrology: Canadian Perspectives. *Edited by* T.D. Prowse and C.S.L. Ommanney. Environment Canada, Saskatoon, Saskatchewan. p. 308.

MathWorks. 2010. MATLAB. Natick, Massachusetts.

McKenzie, J.M., Voss, C.I., and Siegel, D.I. 2007. Groundwater flow with energy transport and water–ice phase change: Numerical simulations, benchmarks, and application to freezing in peat bogs. Adv. Water Resour. **30**: 966–983. doi: 10.1016/j.advwatres.2006.08.008.

MEND 1.61.5c. 2012. Cold Regions Cover System Design Technical Guidance Document.

Morris, C., and Stormont, J. 1997. Capillary barriers and subtitle D covers: estimating equivalency. J. Environ. Eng. **3**: 3–10.

Munroe, J.S., and Bockheim, J.G. 2001. Soil Development in Low-Arctic Tundra of the Northern Brooks Range, Alaska, U.S.A. Arctic, Antarct. Alp. Res. **33**: 78. doi: 10.2307/1552280.

Nixon, J.F. 1975. The Role of Convective Heat Transport in the Thawing of Frozen Soils. Can. Geotech. J. **12**: 425–429. doi: 10.1139/t75-046.

Nixon, J.F., and McRoberts, E.C. 1973. A Study of Some Factors Affecting the Thawing of Frozen Soils. Can. Geotech. J. **10**: 439–452.

Oldenburg, C.M., and Pruess, K. 1998. Layered Thermohaline Convection in Hypersaline Geothermal Systems. Transp. Porous Media **33**: 29–63.

Painter, S.L. 2011. Three-phase numerical model of water migration in partially frozen geological media: model formulation, validation, and applications. Comput. Geosci. **15**: 69–85. doi: 10.1007/s10596-010-9197-z.

Pollack, H.N., Hurter, S.J., and Johnson, R. 1993. Heat flow from the Earth's interior: Analysis of the global data set. Rev. Geophys. **31**: 267–280.

Quinton, W.L., Bemrose, R.K., Zhang, Y., and Carey, S.K. 2009. The influence of spatial variability in snowmelt and active layer thaw on hillslope drainage for an alpine tundra hillslope. Hydrol. Process. **23**: 2628–2639. doi: 10.1002/hyp.

Ross, B. 1990. The Diversion Capacity of Capillary Barriers. Water Resour. Res. **26**: 2625–2629.

Rykaart, M., and Hockley, D. 2010. Cold Regions Cover Research - Phase 2 Mend Report 1.61.5b.

Sauty, J.-P. 1980. An analysis of hydrodispersive transfer in aquifers. Water Resour. Res. **16**: 145–158.

Schwartz, F.W., and Zhang, H. 2003. Fundamentals of Ground Water. John Wiley & Sons, Inc., New York, New York.

Shirazi, T., Allen, D.M., Quinton, W.L., and Pomeroy, J.W. 2009. Estimating soil thaw energy in sub-Alpine tundra at the hillslope scale, Wolf Creek, Yukon Territory, Canada. Hydrol. Res. **40**. doi: 10.2166/nh.2009.043.

Smerdon, J.E., Pollack, H.N., Cermak, V., Enz, J.W., Kresl, M., Safanda, J., and Wehmiller, J.F. 2004. Air-ground temperature coupling and subsurface propagation of annual temperature signals. J. Geophys. Res. **109**. doi: 10.1029/2004JD005056.

Smerdon, J.E., Pollack, H.N., Enz, J.W., and Lewis, M.J. 2003. Conduction-dominated heat transport of the annual temperature signal in soil. J. Geophys. Res. **108**. doi: 10.1029/2002JB002351.

SRK Consulting. 2007. Giant Mine Remediation Plan. Yellowknife, NT.

SRK Consulting. 2010. Giant Mine Tailings Cover Trials 2010 Data Summary. Yellowknife, NT.

Stähli, M. 2006. Freezing and thawing phenomena in soils. *In* Encyclopedia of Hydrological Sciences. *Edited by* M.G. Anderson and J.J. McDonnell. Wiley, Chichester, England.

Stähli, M., Jansson, P., and Lundin, L. 1999. Soil moisture redistribution and infiltration in frozen sandy soils. Water Resour. Res. **35**: 95–103.

Steeves, J., and Amos, M. 2013. Determining the retardation factor of a thermal plume through laboratory experiments. : 1–6.

Steeves, J.T., Barbour, S.L., Ferguson, G., and Carey, S.K. 2016. Heat transfer within frozen slopes in subarctic Yukon, Canada. Environ. Geotech.

Stormont, J., and Morris, C. 1997. Unsaturated drainage layers for diversion of infiltrating water. J. Irrig. Drain. Eng. **123**: 364–366.

Tedrow, J.C.F., and Cantlon, J.E. 1958. Concepts of soil formation and classification in Arctic regions. Arctic **11**: 166–179.

Voss, C.I., and Provost, A.M. 2010. SUTRA A Model for Saturated-Unsaturated Variable-Density Ground-Water Flow with Solute or Energy Transport. U.S. Geological Survey, Water-Resources Investigations Report 02-4231, Reston, Virginia.

Warrick, A.W., Lomen, D.O., and Yates, S.R. 1985. A generalized solution to infiltration. Soil Sci. Soc. Am. J. **49**: 34–38.

Watanabe, K., Kito, T., Dun, S., Wu, J.Q., Greer, R.C., and Flury, M. 2013. Water

Infiltration into a Frozen Soil with Simultaneous Melting of the Frozen Layer. Vadose Zo. J. **12**. doi: 10.2136/vzj2011.0188.

White, M.D., and Oostrom, M. 2000. STOMP Subsurface Transport Over Multiple Phases Version 2.0 Theory Guide. Pacific Northwest National Laboratory, Richland, Washington.

Zhao, L., Gray, D.M., and Male, D.H. 1997. Numerical analysis of simultaneous heat and mass transfer during infiltration into frozen ground. J. Hydrol. **200**: 345–363.

APPENDIX: MODEL BENCHMARKING

A.1 Introduction

The different components of GeoStudio that were used, SEEP/W and TEMP/W, were tested independently and together as a coupled package. Benchmarks in one and two dimensions, saturated and unsaturated flow, along with conduction and convection were performed in SEEP/W and TEMP/W independently and coupled together.

This section describes the background and methodology of the various tests, along with the results. These benchmarks provide the basis for the research, as they verify the ability of the numerical model to accurately model the processes involved. Therefore, it is important to examine the results of these benchmarks prior to the completion of the remainder of the work.

A.2 One-Dimensional Transient Unsaturated Flow

A.2.1 Introduction

Unsaturated flow is a key process involved in the design of a SFCBD cover system. Flow through the cover system is expected to occur under unsaturated conditions. The ability of SEEP/W to model unsaturated conditions accurately needed to be assessed. Several benchmarking analyses have been performed by GEO-SLOPE and are available on their website, including a comparison to the semi-analytical solution of Warrick et al. (1985) to infiltration into an unsaturated soil profile (GEO-SLOPE International Ltd 2012).

The analysis undertaken in the current research compared SEEP/W to the Warrick solution, as in the example file, but also to the numerical solution of HYDRUS-1D. The analysis was performed following the procedure and soil outlined in Warrick et al. (1985). The semi-analytical solution was computed using the tables and equations given and the computational program MATLAB (MathWorks 2010). This solution is not a full analytical solution, and as a result, gives only three points on the water retention curve.

A.2.2 Model Setup

A.2.2.1 Domain

The analysis consisted of infiltration into a one meter high column. The Warrick solution is truly one-dimensional, but a two-dimensional column was used. The column width of 0.2 m enabled the results to be visualized. It is assumed that only vertical, one-dimensional flow will occur in the column and that no lateral, two-dimensional flow will occur. The analysis was run for 13 hours as a transient analysis.

A.2.2.2 Material Properties

The soil in the simulation was modelled after the Hypothetical Loam Soil used as an example in Warrick et al. (1985). The soil had a saturated hydraulic conductivity of 6×10^{-6} m/s. The hydraulic conductivity function was estimated using the van Genuchten method (van Genuchten 1980).

The water retention curve was estimated using the van Genuchten equation (van Genuchten 1980) and a saturated water content of 0.45, a residual water content of 0.1 and the hydraulic conductivity function. The alpha value was set to 9.8 kPa and the *n* value was 2. The soil was set to an initial water content of 0.17.

A.2.2.3 Boundary Conditions

The initial head conditions within the column were set to a pressure head of -7.29 m to achieve the desired initial water content. The top boundary was set to zero pressure to represent an unlimited source of water for infiltration while the lower boundary was set to a pressure head of -7.29 m. The boundary conditions created a hydraulic gradient within the soil that encouraged infiltration.

A.2.3 Results and Discussion

The simulated water content profiles from SEEP/W were compared to the points calculated using the semi-analytical solution for two different times (Figure A.1). The graph shows good agreement between the SEEP/W analysis results and the semi-analytical solution.

The results from SEEP/W and the Warrick solution were also compared to the results from HYDRUS-1D (Figure A.1). The HYDRUS results match the SEEP/W results almost exactly. Both numerical models show good agreement to the analytical solution, especially at the early time. The analytical model predicts the wetting front to have progressed slightly further into the column than the numerical models after 5 hours. However, the overall match between the numerical and analytical models is good.

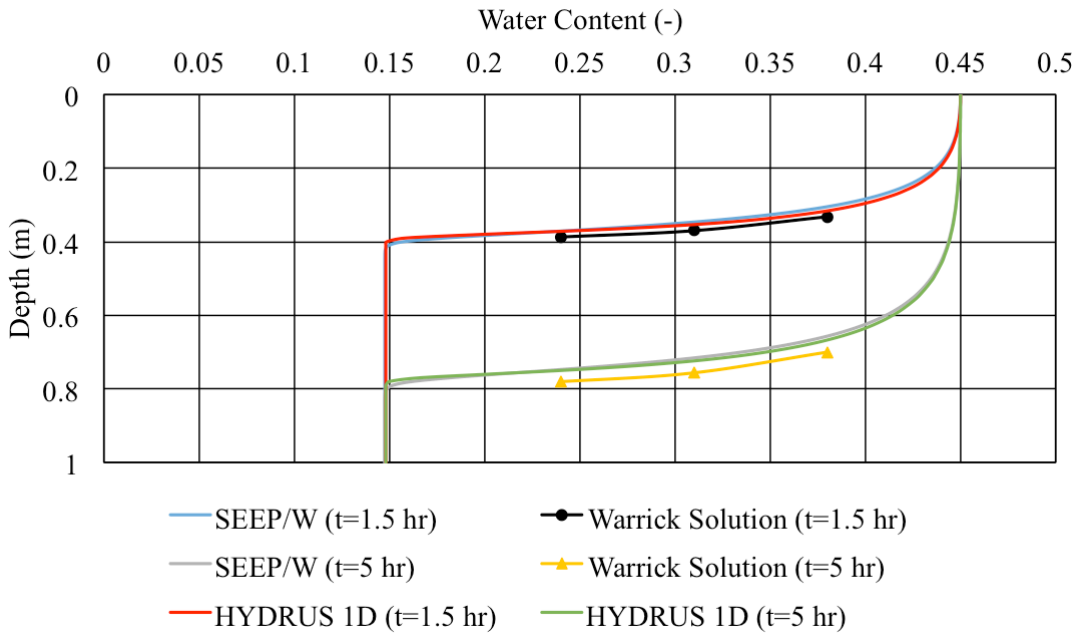

Figure A.1 Volumetric water content profile as generated by SEEP/W, the semi-analytical solution of Warrick et al. (1985) and HYDRUS-1D at t=1.5 hours and t=5 hours.

A.3 One-Dimensional Transient Thermal Conduction with Thawing

A.3.1 Introduction

The transfer of heat through conduction in a frozen soil is one of the key thermal processes being investigated in this research. A comparison to the Neumann solution for freezing and thawing benchmarked TEMP/W for 1D conduction. The Neumann solution (Nixon and McRoberts 1973, Andersland and Ladanyi 1994) can be used to predict the depth to which freezing or thawing occurs, depending on the initial conditions. The

thawing version of the Neumann solution was chosen to compare to TEMP/W, as thawing will be the main process of interest in further research. There are two equations that describe thaw of a frozen soil. The equations differ in their application of the temperature distribution in the thawed zone. Both equations assume that the soil properties are homogenous and independent of the temperate in the soil, that latent heat is released at 0 °C and both ignore the temperature of the frozen zone.

The first method uses a step temperature distribution in the thawed soil and can be found by the equation (Nixon and McRoberts 1973, Andersland and Ladanyi 1994):

$$X = \alpha\sqrt{t} \tag{A.1}$$

where X is the thaw depth, t is the elapsed time and α is a constant defined as (Nixon and McRoberts 1973, Andersland and Ladanyi 1994):

$$\alpha = 2\sqrt{\alpha_u}\left(\frac{Ste}{2}\right)^{1/2}\left(1 - \frac{Ste}{8}\right) \tag{A.2}$$

where α_u is the thermal diffusivity and Ste represents the Stefan number. The Stefan number is the ratio of sensible heat to latent heat and is defined as (Nixon and McRoberts 1973, Andersland and Ladanyi 1994):

$$Ste = \frac{c_u T_s}{L} \tag{A.3}$$

where c_u is the volumetric heat capacity, T_s is the surface temperature and L is the latent heat.

The second method uses a linear temperature distribution in the thawed zone and can be found by the equation (Nixon and McRoberts 1973, Andersland and Ladanyi 1994):

$$X = \sqrt{\frac{2k_u T_s}{L}}\sqrt{t} \tag{A.4}$$

where k_u is the thermal conductivity. Both equations were compared to the results of the TEMP/W analysis.

A.3.2 Model Setup

A.3.2.1 Domain

The simulation was undertaken on a 10 meter high, 0.5 m wide column of clay. The analysis was constructed as a TEMP/W transient analysis and was run for 300 days.

A.3.2.2 Material Properties

Clay was used as the material in the column and was simulated using the Simplified Thermal material model. It had an unfrozen volumetric heat capacity of 2300 kJ m^{-3} °C^{-1} and a frozen volumetric heat capacity of 1900 kJ m^{-3} °C^{-1}. The frozen and unfrozen thermal conductivity were the same at 165 kJ day^{-1} m^{-1} °C^{-1}. The thermal properties of the soil were taken from Andersland and Ladanyi (1994).

A.3.2.3 Boundary Conditions

The initial temperature within the column was set to -10 °C to simulate frozen soil conditions. The upper boundary condition increased to 1 °C at the start of the transient analysis to initiate heat flow and thawing of the column downwards from the top. The bottom boundary was held constant at -10 °C for the duration of the simulation.

A.3.3 Results and Discussion

The Neumann equations were implemented in a MATLAB script (MathWorks 2010) and plotted against the results of TEMP/W (Figure A.2). The two Neumann methods produced identical results, as seen by the overlapping plots in Figure A.2. The TEMP/W analysis follows the Neumann solution quite closely, indicating the numerical model is capable of accurately modelling thermal conduction and freeze/thaw.

The two Neumann equations make simplifying assumptions about the temperature and thermal conductivity. These assumptions could account for the small difference that develops between the analytical solution and the numerical solution at later times. These differences are quite small, however, and likely would not affect the overall result.

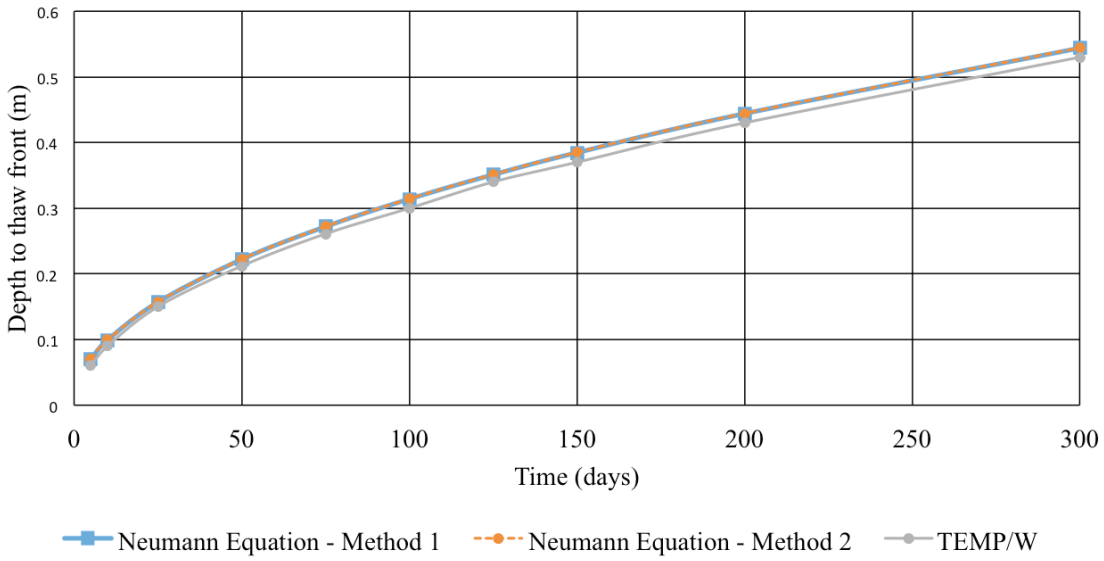

Figure A.2 The depth to thaw front as predicted by the two methods that employ the Neumann equation and TEMP/W.

A.4 One-Dimensional Saturated Coupled Heat and Water Flow

A.4.1 Introduction

The forced convection of thermal energy can be simulated with GeoStudio by the coupling of TEMP/W and SEEP/W. The model also includes the ability to reduce the hydraulic conductivity of the soil as freezing occurs. In order to evaluate forced convection alone, the model was first used to simulate heat transfer without freezing.

Steeves and Amos (2013) conducted a series of controlled column experiments to demonstrate forced convection of heat. In these experiments, a heated pulse of saline water was injected into a column filled with coarse-grained sand. The experiments were conducted at three different flow rates. The tests from the highest and lowest flow rates were modelled in GeoStudio and the data from the thermocouple at the top of the column was used for comparison. Steeves and Amos (2013) also used a contaminant transport analytical model to describe their results (Sauty 1980, Fetter 1999). The heat injection was treated as an instantaneous slug injection into a one-dimensional flow field and modelled as relative concentration. The analytical model was also included in the comparison.

A.4.2 Model Setup

A.4.2.1 Domain

The simulation domain was setup to match the column upon which the tests had been carried out. The column was 26.8 cm high and had a radius of 5.1 cm. The model represented a two-dimensional slice through the centre of the column. The hot water was added to the column for a limited time in a pulse before the column was flushed with tap water, requiring the simulation to be broken up into several nested analyses.

A.4.2.2 Material Properties

The material in the column was a commercially available, coarse-grained, angular sand. The sand had a porosity of 0.431 and a saturated hydraulic conductivity of 1.5×10^{-4} m/s. Thermal properties were not measured, but were estimated using typical properties of sand. The sand had a saturated thermal conductivity of 3.26 J s^{-1} m^{-1} $°C^{-1}$ and a dry thermal conductivity of 2.11 J s^{-1} m^{-1} $°C^{-1}$. The saturated volumetric water content was determined as the product of the density and specific heat of the fluid-sand mix (Domenico and Schwartz 1990) and was found to be 3910 kJ m^{-3} $°C^{-1}$.

A.4.2.3 Boundary Conditions

The model replicated the conditions of the column experiments. Two different inflows were modelled based on the influxes into the column. A low flux of 5.8 cm^3/s (5.8×10^{-6} m^3/s) was first simulated, followed by a high flux of 10.1 cm^3/s (1.01×10^{-5} m^3/s).

The initial temperature of the column was set to the temperature of 13.8 °C, the temperature of the tap water used to flush the column. As the heat was injected in a pulse, the first analysis had a lower boundary temperature of 50.8 °C and no set upper temperature boundary. The second analysis simulated the flushing of the column with tap water, so the bottom temperature boundary was returned to 13.8 °C.

A.4.3 Results and Discussion

Figure A.3 shows the experimental data and the analytical model, along with the results from the GeoStudio analyses. GeoStudio was able to accurately simulate the movement

of heat through the column by advection at both flow rates. It was also able to predict the dispersion, or spreading, of the heat due to the different flow rates, but was not as good of a match as the analytical model.

The simulated arrival of the thermal peak was approximately 10 seconds later than that observed in the experiment or in the analytical model. There were also differences between the simulation and the observations towards the end of the simulation period with the simulated results returning more rapidly to the original temperature than observed. The TEMP/W results for the higher flow rate were a closer match to the observed data and the analytical model, but underestimated the dispersion. The differences between the numerical model and the observations and analytical model is likely due to the thermal properties used. Unlike the hydraulic properties, the thermal properties of the sand were not determined experimentally. Instead, they were based on literature values of typical sand. The estimated properties did not have a large influence on the analytical model, as only the volumetric heat capacity was incorporated. The analytical model also used only a singular value of the volumetric heat capacity and not a function, as in the numerical model.

An underestimation of the saturated thermal conductivity would increase the time required to reach temperature equilibrium between the soil grains and the water, delaying the arrival of the peak. At lower fluxes, the role of convection is reduced and conduction is increased. The underestimated thermal conductivity and delay in thermal peak arrival would be more pronounced at the lower fluxes, as observed in this benchmarking example. Overall, there is a good match between the experimental, analytical and numerical results.

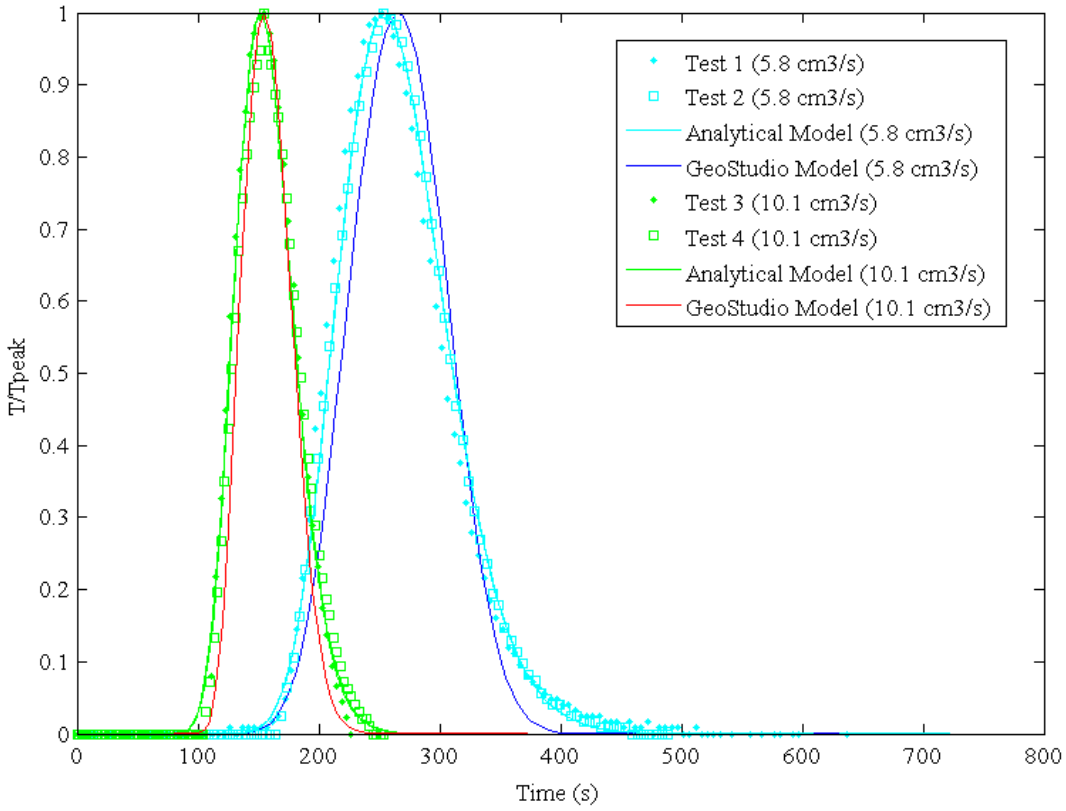

Figure A.3 Comparison between the experiments and analytical model of Steeves and Amos (2013) and the GeoStudio models. Good agreement is shown between the GeoStudio models and the experiments in the timing of the plume arrival and dispersion.

A.5 Two-Dimensional Saturated Coupled Heat and Water Flow

A.5.1 Introduction

The ability of TEMP/W and SEEP/W to model advective energy transfer in two dimensions with freezing was evaluated by comparing the GeoStudio models to the results for a modelling exercise conducted with SUTRA-ICE (McKenzie et al. 2007). The simulation modelled groundwater flow around a frozen barrier wall, similar to what might be constructed to form a seepage barrier.

A.5.2 Model Setup

A.5.2.1 Domain

The model domain was a region 50 metres long and 10 metres wide. The wall was 5 metres high by 0.5 metres wide and was placed 20 m from the upstream end of the domain. A schematic of the domain is shown in Figure 6 of McKenzie et al. (2007). The analysis was run for 800 days.

A.5.2.2 Material Properties

The soil properties were the same as those given in Table 2 of McKenzie et al. (2007). The soil had a saturated hydraulic conductivity of 1.14×10^{-8} m/s and a saturated volumetric water content of 0.1. The thermal conductivity of the soil was 3.5 J s^{-1} m^{-1} $°C^{-1}$. The volumetric heat capacity was defined as 2184 kJ m^{-3} $°C^{-1}$. All water was assumed to freeze at a temperature of 0 °C.

A.5.2.3 Boundary Conditions

The entire domain, with the exception of the frozen wall had an initial temperature of 5 °C. The wall was kept frozen by setting a constant temperature of -5 °C. The temperature of the left hand side of the model, where water was flowing into the domain, was set to 5 °C. Hydraulic head conditions on the left and right hand side were used to match the flow conditions of the SUTRA-ICE simulation. The left side was set to a hydraulic head of 1.0 m and the right side was set to 0.5 m. No temperature or hydraulic boundary conditions were set to the top and bottom boundaries, resulting in no flow conditions.

A.5.3 Results and Discussion

The flowing water diverted around the wall and cooled, resulting in an expansion of the frozen zone downstream of the frozen wall. Figure A.4 compares the flow field (velocity vectors) and temperature contours obtained from the GeoStudio simulation to those presented by McKenzie et al. (2007) for an elapsed time of 800 days. The two simulations are similar. Although the extent of the frozen layer was not explicitly given in McKenzie et al. (2007), the zero degree isotherm shown in Figure A.4 was obtained by

overlaying the water saturation result over the temperature result and outlining the crossover.

The frozen wall expands upstream and downstream of the wall. Expansion of the wall downstream is greater than upstream as the flowing water is forced around the barrier, but still brings heat to the upstream end of the wall, preventing large expansion. Downstream, the water has been forced to flow around the wall, creating a region of low flow and low temperature directly behind the wall, allowing the wall to expand. The restricted area of flow creates higher velocities toward the top of the simulation, which carry more heat, leaving the region behind the wall cooler.

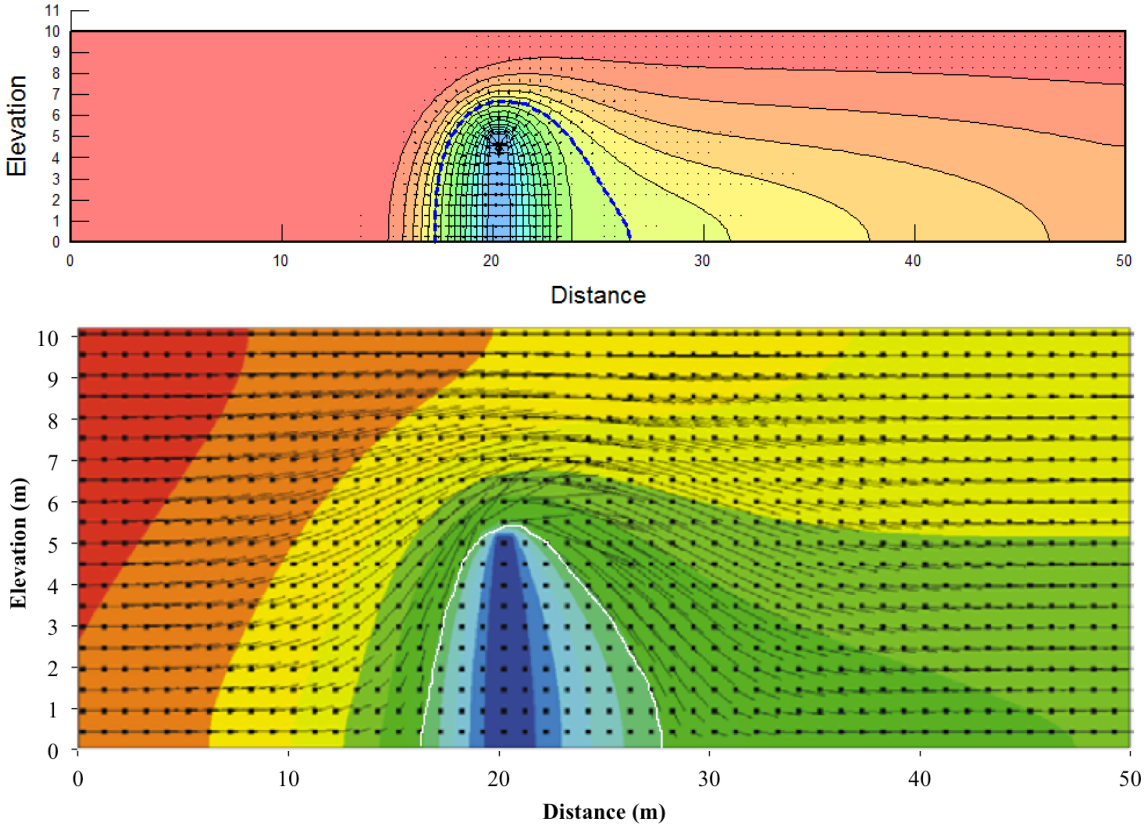

Figure A.4 Comparison of the coupled GeoStudio analysis (top) to the results of McKenzie et al. (2007) (bottom) after 800 days. The results show a good match between the extent and shape of frozen barrier.

A.6 Two-Dimensional Ground Freezing

A.6.1 Introduction

Ground stabilization is often undertaken through the use of ground freezing. Freezing pipes are inserted into the ground and low temperature brines are circulated through these pipes to promote freezing of the adjacent soil. In the absence of groundwater flow, the zero degree isotherm, which represents the edge of the frozen soil, spreads out radially from the freeze pipe and the frozen zones merge to form a continuous frozen wall. When ground freezing is undertaken within a region of active groundwater flow however, the soil columns may not merge, due to the additional heat brought in with the flowing water and the inability of the freeze pipes to remove heat from the flowing water at a sufficient rate. The merging of the frozen zones is dependent on the rate of groundwater flow. It is generally accepted that at a velocity of greater than 1 m/day, the soil columns will not merge (Andersland and Ladanyi 1994). An estimation of the velocity at which the soil columns will not merge for a particular soil type can be found from Equation 6.1-1 in Andersland and Ladanyi (1994).

A.6.2 Model Setup

A.6.2.1 Domain

The simulation of the frozen earth cofferdam was completed using a domain of 5 m by 8 m. The freeze pipes were arranged in a semi-circular fashion within the domain, spaced 1 metre apart, to create a circular frozen earth cofferdam. The freeze pipes had a diameter of 76 mm. The analysis was completed in plan view of the domain.

A.6.2.2 Material Properties

A gravelly sand with a hydraulic conductivity of 1×10^{-3} m/s and a porosity of 23% was specified. The water retention curve was estimated based on the porosity and the material texture. The frozen thermal conductivity of the sand was estimated to be 3.2 W m^{-1} $°C^{-1}$ and the thermal conductivity function was estimated using the water retention curve and a material mineral thermal conductivity of 0.6 J s^{-1} m^{-1} $°C^{-1}$. The volumetric heat capacity was determined using the de Vries method and the water retention curve. The unfrozen water content function was determined using texture.

A.6.2.3 Boundary Conditions

The ground temperature was set to 10 °C, while the heat flux at the freeze pipes was set such that the exterior of the freeze pipes was approximately -20 °C. Using Equation 6.1-1 of Andersland and Ladanyi (1994), the critical groundwater velocity for which the freezing soil columns will not merge for this example is 0.85 m/day.

Two separate simulations were conducted with GeoStudio: one with a groundwater flow velocity of around 0.85 m/day and another with a velocity of approximately 0.2 m/day, lower than 0.85 m/day. Hydraulic gradients were created by setting the hydraulic head conditions on the left and right side of the domain. By increasing or decreasing the hydraulic gradient, the desired velocity could be achieved.

With the higher velocity, the heat flux at the freeze pipes had to be double that of the lower velocity to maintain the -20 °C surface temperature. 500 J s^{-1} m^{-2} of energy had to be removed from the freeze pipes at the 0.85 m/day water velocity, while only 250 J s^{-1} m^{-2} of energy had to be removed from the lower velocity (~0.2 m/day). The analyses were also run with a constant -20 °C boundary condition on the freeze pipes for comparison.

A.6.3 Results and Discussion

At the 0.85 m/day flow rate, the freezing soil columns do not merge, even after 1 year (Figure A.5A). At the ~0.2 m/day flow rate, the columns begin to merge after only 15 days (Figure A.5B). The constant temperature boundary condition analyses produced very similar results, with the high flow rate not being able to merge and the low flow rate merging within 15 days. Figure A.6 shows the time required for the columns to merge as a function of the flow rate. As the flow rate approaches the critical value, the time required to merge the frozen columns increase exponentially before becoming asymptotic at the critical value. At the critical value, the columns do not merge, regardless of the time given.

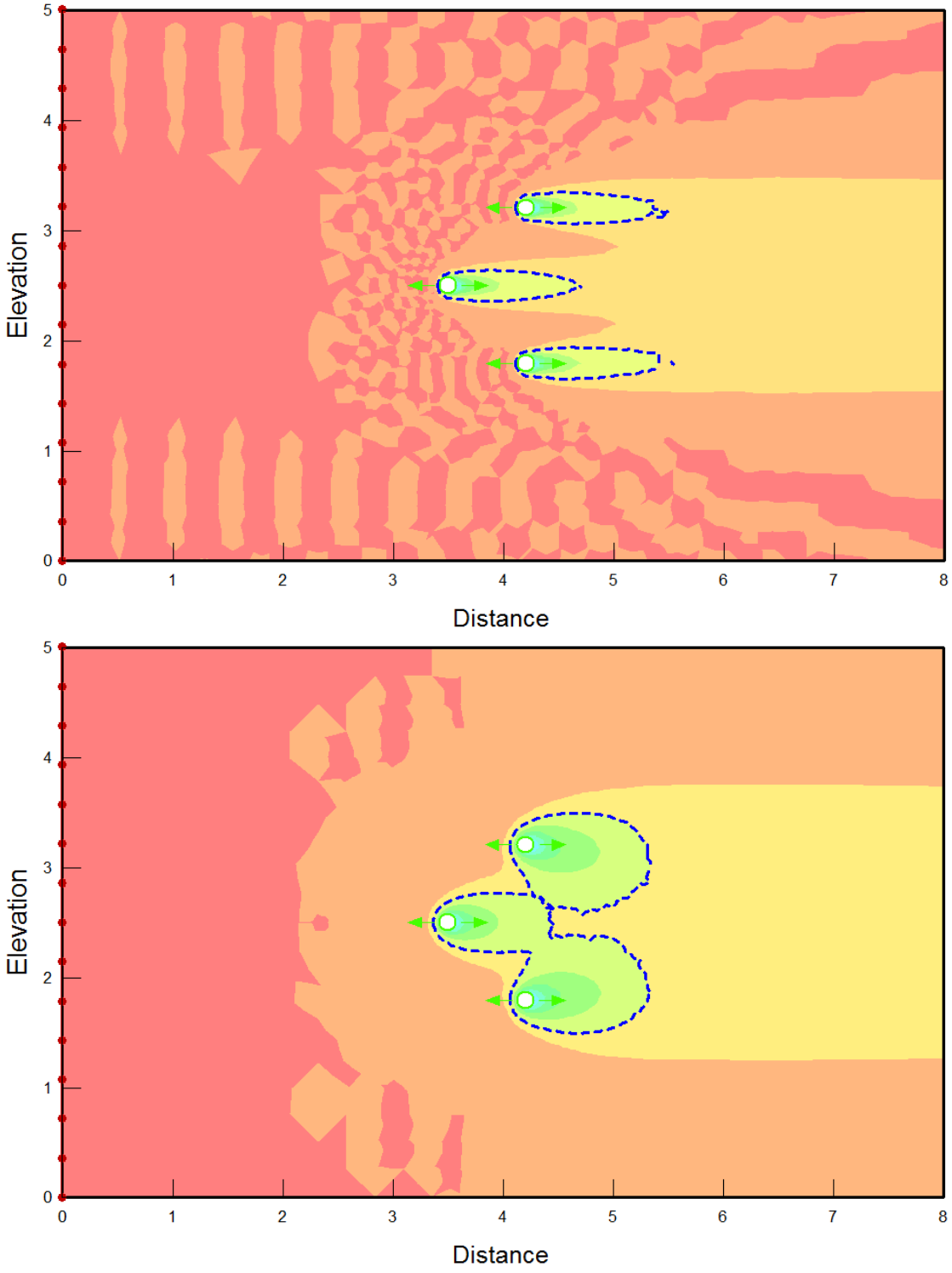

Figure A.5 A) Result of freeze pipe analysis after 1 year with a water velocity of 0.85 m/day. The water is moving too fast for the freeze pipes to effectively strip the heat from the flowing water, preventing the freezing soil columns from merging. This velocity is consistent with the critical velocity. B) Result of freeze pipe analysis after 15 days with a water velocity of approximately 0.2 m/day. The freezing soil columns are able to merge, forming a continuous frozen earth cofferdam.

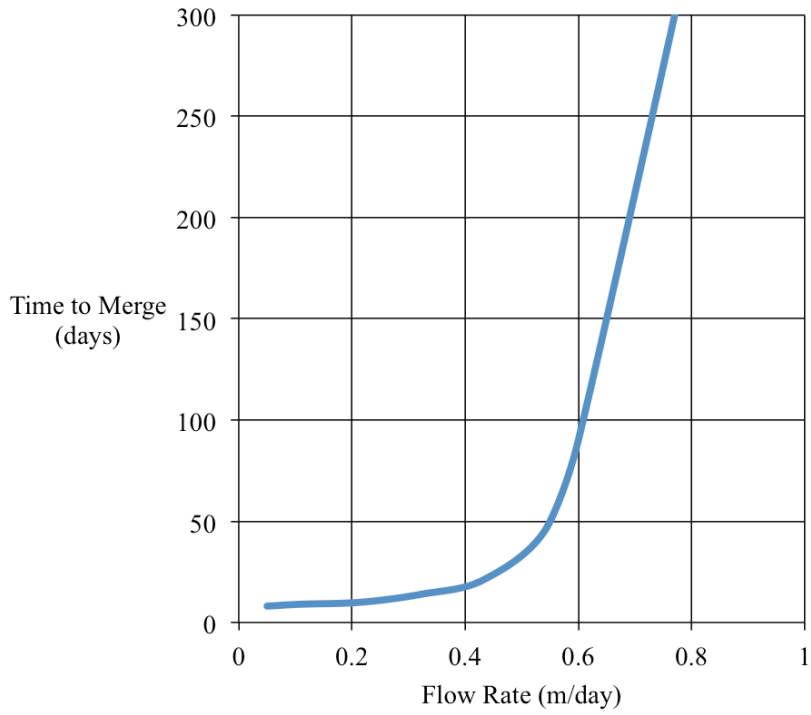

Figure A.6 The time required for the freezing pipes to merge increases exponentially with increasing flow rate. As the flow rate approaches 0.85 m/day, the time required goes to infinity, indicating that the critical groundwater velocity has been reached and no merging will occur.

A.7 One-Dimensional Unsaturated Coupled Heat and Water Flow

A.7.1 Introduction

The previous examples demonstrate the ability of the model to simulate flow through unsaturated soil as well as coupled heat and water flow, with freezing, within saturated soils. This example evaluates the ability of the model to simulate infiltration and groundwater flow processes within frozen, unsaturated soil profiles. When infiltration into frozen ground occurs, the infiltrating water carries heat with it through advection. This additional heat influences the extent and position of the frozen layer.

This phenomenon was investigated using the frozen soil column experiments of Watanabe et al. (2013). One of these experiments was simulated using GeoStudio to test

the ability to model one-dimensional unsaturated coupled heat and water flow in a frozen system.

A.7.2 Model Setup

A.7.2.1 Domain

The model was set to replicate the columns used by Watanabe et al. (2013). The column was 35 cm in height and 7.8 cm in diameter. The same domain was used for the vertical convection simulations of Chapter 3 and is described in more detail in Section 3.2.2.1

A.7.2.2 Material Properties

The material was based on the Volcanic Ash A horizon used in the column experiments. A water retention curve and hydraulic conductivity function were estimated using the van Genuchten method (van Genuchten 1980). A saturated hydraulic conductivity of 2.3×10^{-6} m/s and a saturated water content of 0.617 were used. The estimated water retention curve and hydraulic conductivity function are shown in Figure 3.2. More details of the hydraulic property estimates are contained in Section 3.2.2.2

Thermal properties were estimated with literature values and the estimating tools within GeoStudio. The Johansen method (Johansen 1977) was used to find the thermal conductivity function, as shown in Figure 3.3. The saturated thermal conductivity was approximately 0.7 J m^{-1} s^{-1} $°C^{-1}$. The volumetric heat capacity function is shown in Figure 3.4. The unfrozen volumetric heat capacity was 3.65×10^{6} J m^{-3} $°C^{-1}$ and the frozen volumetric heat capacity was 1.80×10^{6} J m^{-3} $°C^{-1}$. The unfrozen water content function was based on soil texture and is shown in Figure 3.5.

A.7.2.3 Boundary Conditions

The highest initial water content column was simulated with an initial water content of 0.46. The column had an initial equilibrium of 3.5 °C before being allowed to freeze from the top for 48 hours by applying a constant temperature of -6.2 °C while maintaining the bottom boundary condition at a temperature of 2 °C. This caused a freezing front to develop in the column that progressed downwards from the upper boundary. During the freezing stage, the top and bottom boundaries were set to zero water flux conditions. After 48 hours of freezing, a water flux at the surface simulated infiltration, while water

exited the domain at the bottom of the column. The top and bottom boundaries were returned to 3.5 °C.

A.7.3 Results and Discussion

The movement of the infiltrating water into the column was tracked by measuring changes in the volumetric water content of the soil. Watanabe et al. (2013) showed that the volumetric water content decreases sharply through the frozen layer and that thaw is influenced by the advective flux of energy carried with the infiltrating water.

The simulation was able to recreate the pattern of thaw and infiltrating water movement within the soil column although the results were different from the observations reported by Watanabe et al. (2013). The soil warmed quicker in the simulation than the experiment (Figure A.7). The rise in temperature at the top of the column was not instantaneous in the experiment as it was in the simulation. A slower increase in the temperature at the top would reduce the heat added to the column and reduce the temperature within the column relative to an instantaneous temperature change.

The experimental results showed a sharp difference between the water content above and below the wetting front at the base of the frozen layer (Figure A.8). The wetting front in the simulation was more gradual and not always at the base of the frozen layer. Greater percolation into the frozen layer was observed in the experiment; however, the overall percolation trend of delayed infiltration due to the frozen layer was observed in both the observed data and the simulation.

The three phases observed by Watanabe et al. (2013) are evident in the simulation results. Initially, little water is able to infiltrate into the column due to the presence of the ice layer; however, as the upper portion of the column began to reach 0 ºC, ice and water can coexist within the pores and infiltration began to increase. This leads to heat transport into the column by both advection as well as conduction. After approximately 24 hours, the temperature is near 0 ºC and the wetting front has almost reached the bottom of the frozen layer, after which infiltration and drainage through the column proceeds at nearly the same rate as it would for an unfrozen column.

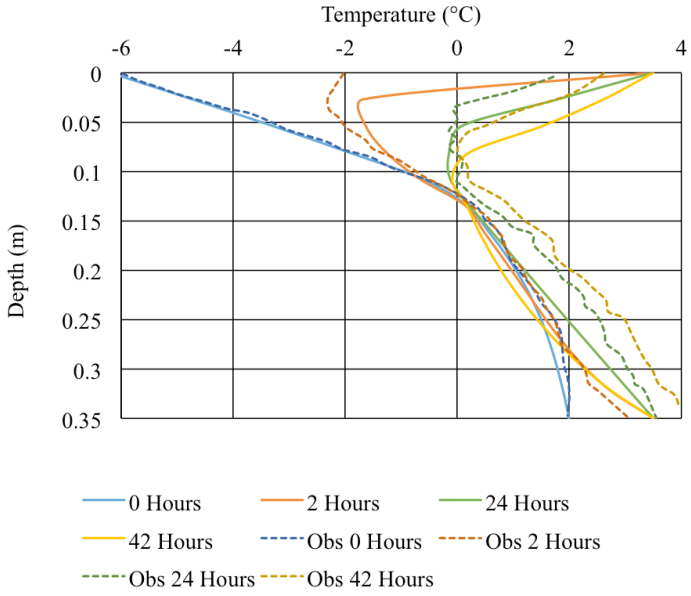

Figure A.7 The temperature profiles of the simulation and experimental column. The solid lines represent the simulation results while the dashed lines represent the results of Watanabe et al. (2013).

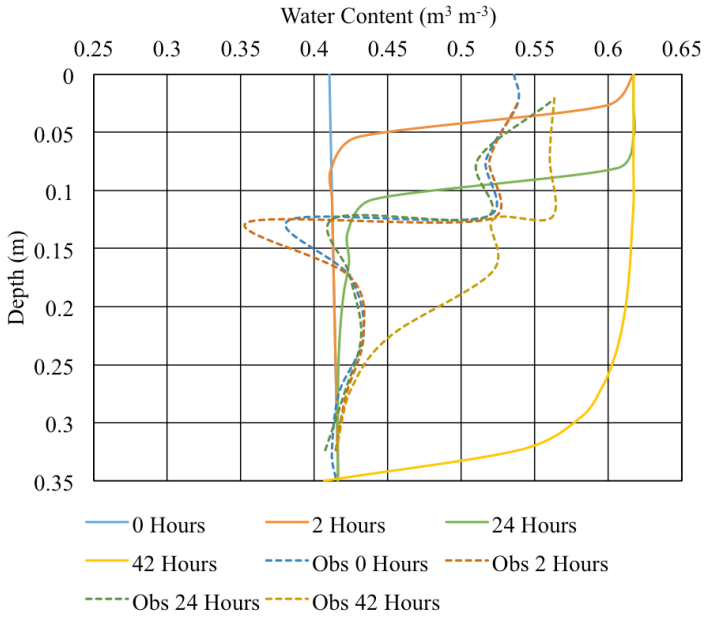

Figure A.8 The water content profiles of the simulation and experimental columns. The solid lines represent the simulation results and the dashed lines represent the experimental results of Watanabe et al. (2013).